Investigation of Bipolar Charge Distribution of Pharmaceutical Dry Powder Aerosols using the Phase Doppler Anemometry System

Radu Beleca

A thesis submitted for the degree of

Doctor of Philosophy (PhD)

Brunel University

Centre for Electronic Systems Research

School of Engineering and Design

March 2012

Abstract

Electrostatic properties of formulation component materials and blends play an important role in dry powder inhalation (DPI) products, and that valid measurement of charge distribution will lead to more precise control of powder behavior in DPI manufacturing processes. Ultra-fine powders are known to be bipolarly charged, have non-spherical shapes and tend to be highly cohesive. Real time, non-invasive techniques need to be developed to obtain a precise and accurate time-history characteristic of electrically charged powders as they aerosolize from a DPI product, and how this measure relates to materials behavior throughout the various steps of a manufacturing process i.e. from drug micronisation, blending with lactose, through to filling dose units. A novel non-invasive technique for simultaneous measurement of size and charge of pharmaceutical powders is considered which employs the Phase Doppler Anemometry (PDA) system. Previous research demonstrated the advantages of this technique in measuring the bipolar charge distribution on a population of particles. These findings led to significant improvements in understanding performance of dry powder formulations, manufacturing processes and development of new platforms for inhaled drug delivery.

The main aim of this research is to perform an investigation of electrostatic properties of pharmaceutical dry aerosols using the PDA system. The PDA technique was used to track the motion of charged particles in the presence of an electric field. The magnitude as well as the polarity of the particle charge can be obtained by solving the equation of particle motion in DC and AC fields combined with the simultaneous measurement of its size and velocity. The results show the capability of the technique to allow real-time size and charge distribution in the control of dry powder attributes that are critical to fully understanding manufacturing design space.

The data obtained from initial investigations of electrical properties of pharmaceutical powders and bipolar charge measurements was used to perform an in-depth study of electrostatic properties of pharmaceutical aerosols dispensed by dry powder inhaler (DPI) devices. The delivery of a drug to the lungs can only be achieved by a combination of inhaler device and drug formulation which is capable of producing an aerosol of an aerodynamic diameter smaller than 5 μm and of appropriate charge. The aerosols generated by these devices are often bipolarly charged and can influence specific site deposition in human lung.

By controlling the electrostatic charge generated by tribielectrification, it may be possible to achieve the desired drug deposition in the airways. Bipolary charged dispensed ultrafine particles are inhaled through the extrathoracic and tracheobronchial airways down into the alveolar region. Anatomically realistic respiratory airways and computation fluid dynamics (CFD) models have been created to study airflow structures and predict aerosol deposition within the human respiratory system using visible human data sets, human casts and morphometric data. Many theoretical studies of charged aerosol deposition in human respiratory systems have been developed, however getting real time, non-intrusive data of bipolar charge levels on aerosols dispensed from DPI's within the human respiratory system represents a challenging issue.

This research project presents a simplified human upper airway model which combined with the modified Phase Doppler Anemometry (PDA) system is able to provide real time bipolar charge distributions of aerosols delivered from several commercially available DPI devices. A three dimensional (3D) reconstruction of the upper respiratory system was performed from two dimensional (2D) images obtained from computerized tomography (CT), magnetic resonance imaging (MRI) and cryosectioned images available from Visible Human Server data set (Ecole Polytechnique Fédérale de Lausanne). The resulting dimensions of the model were consistent with morphometric data from the literature from which the simplified upper airway model consisting of two connected segments, i.e., the oral airways from the mouth to trachea (Generation G0), was created. The findings of this study provided a better understanding of the interaction between specific active ingredients and DPI devices. These results may be used in designing future generation DPI devices and a better understanding of aerosol transport and deposition efficiency within the human airways.

Dedication

To my grandmother Cristina who inspired me, who believed in me, who always encouraged me to accomplish my dreams and never to forget service above self as the secret of life, can be known only by those who seek it, serve it, live it.

"Labor improbus omnia vincit, per aspera ad-astra."

Acknowledgments

First I would like to greatly thank my supervisors Prof. Wamadeva Balachandran and Dr. Maysam Abbod for the opportunity to undertake this PhD research project and for their guidance and continuous support. Their patience, understanding and continuous encouragement helped me overcome all difficulties and look confident towards the future.

My appreciation extends to the Engineering and Physical Sciences Research Council team for their invaluable technical and financial support for this project together with the TSI Inc. assistance and service.

Special acknowledgments go towards Mr. Paul Miller and the Pfizer team, UK for their involvement, financial and scientific assistance during my experimental work and to TEVA Pharmaceuticals, Ireland for their significant contribution towards completion of my PhD thesis.

I would like to thank Brunel University for all the training and support it provides for its research students making it indeed a world-class university.

Finally, I thank my mom Emilia and aunt Maria for their love, sacrifice and continuous support throughout all these years. I wouldn't have achieved all this without them.

Contents

List of Figures

List of Symbols

Symbol	Name	Unit
α	Lactose monohydrate	-
τ_p	Relaxation time	s
d_p	Particle diameter	m
ρ_p	Particle density	-
η	Air viscosity	kg/(m·s),
E	Electrical field	V m^{-1}
V_p	Particle velocity	m/s
U	Applied voltage	V
r_2, r_1	Radii of circular electrodes	mm
r	Radial position	-
v_f	Velocity	m/s
λ_p	Mobility of the charged particle	-
m_p	Mass of the particle	kg
r_p	Particle radius	mm
q_p	Charge on a particle	C
Q/m	Charge to mass ratio	q/kg
a	Particle acceleration	m/s^2
C_d	Aerodynamic drag coefficient	-
dN/dt	Particle count rate	Particle/s
d_x	Measurement Volume Diameter in x direction	m
d_y	Measurement Volume Diameter in y direction	m
d_z	Measurement Volume Diameter in z direction	m
d_f	Beam waist diameter	m
d_m	Beam diameter	m

f_D	Doppler frequency	Hz
f_{drive}	Drive frequency of the excitation field	Hz
f_L	Focal length in the front lens	m
f_s	Sampling frequency	Hz
M	Number of fringes	-
$n_{particle}$	Particle refractive index	-
n_{rel}	Relative refractive index	-
R_e	Reynolds number	-
V_x	Particle velocity in x direction	m/s
V_y	Particle velocity in y direction	m/s
λ	Wavelength of the laser beam	nm
μ_m	Electrical mobility of the particle	m^2/Vs
φ	Scattering angle	deg
Ψ	Elevation angle	deg
v	Angle between the velocity vector and velocity component in Y direction	deg
ω_D	Doppler frequency	Rad/s

List of Nomenclature

COPD	Chronic obstructive pulmonary disease
WHO	World Health Organization
MDI	Metered-dose inhaler
DPI	Dry powder inhaler
CFCs	Chloroflourocarbons
HFCs	Hydroflourocarbons
pMDI	pressured Metered-dose inhaler
IFR	Internal flow rate
H	Head region
TB	Tracheobronchial region
A	Alveolar region
LDV	Laser Doppler Velocimetry
FPF	Fine particle fraction
API	Active pharmaceutical ingredient
ELPI	Electrical Low Pressure Impactor
E-SPART	Electrical Single Particle Aerodynamic Relaxation Time Analyzer
ESRG	Electronic Systems Research Group
PDA	Phase Doppler Anemometry
BCMS	Bipolar Charge Measurement Systems
HPLC	High-performance liquid chromatography
ToF	Time-of-flight
CI	Cascade Impactor
MSLI	Multi-stage liquid impinger
TI	Twin Impinger
LD	Laser diffractometry
SEM	Scanning Electron Microscopy
ICC	Ion current control

DUSA	Dosage Unit Sampling Apparatus
RH	Humidity
JCI	John Chubb Instruments
CFD	Computation fluid dynamics
CT	Computer Tomography
MRI	Magnetic resonance imaging
EPFL	Ecole Polytechnique Fédérale de Lausanne
BU	Brunel University
VHP	Visible Human Project
CAD	Computer-aided design
RANS	Reynolds Average Navier-Stokes
DNS	Direct numerical simulations
LES	Large Eddy simulation
PIV	Particle Image Velocimetry

Chapter 1

Introduction

1.1 General introduction

Allergic diseases are increasing in prevalence worldwide and are now the most frequent reasons patients seek medical care (World Health Organization Office for Europe, 2007; Pawankar et al., 2008). Recent reviews suggest that the prevalence of allergic diseases is increasing throughout Europe and is no longer restricted to specific seasons or environments. Allergies are also becoming more complex, and patients frequently have multiple allergic disorders. Even the less severe allergic diseases can have a major adverse effect on the health of hundreds of millions of patients and diminish quality of life and work productivity. Allergy is a major problem for the 21st century, and this problem is predicted to worsen as this century moves forward. Allergy represents an immune programming error. Immunoglobulin E is normally protective against many parasites, but can also cause the release of histamine and other chemical mediators on exposure to otherwise benign proteins present in airborne pollen, molds, animal danders and food.

Chronic respiratory diseases are chronic diseases of the airways and other structures of the lung. Some of the most common are asthma, chronic obstructive pulmonary disease (COPD), respiratory allergies, occupational lung diseases and pulmonary hypertension. The most important risk factors for preventable chronic respiratory diseases are: Tobacco smoking; Indoor air pollution; Outdoor pollution; Allergens; Occupational risks and vulnerability.

Asthma is one of the most common and increasingly prevalent chronic diseases in the world, and children are particularly susceptible to it. World Health Organization (WHO) states that according with their estimates 300 million people suffer from asthma and 255 000 people died of asthma in 2005. Asthma is an inflammatory disorder of the bronchial airways produced by allergies, viral respiratory infections and airborne irritants, while genetic factors predispose to develop asthma. Symptoms vary from person to person and can be mild, moderate or severe. Currently, there is no known cure for asthma. It's a chronic condition that requires monitoring and control over a lifetime. If left uncontrolled, asthma can put severe

limits on daily activities and is sometimes fatal. The economic cost of asthma is very significant in terms of both direct and indirect medical costs.

As the number of persons susceptible of various allergic disorders increases, the demand for drug delivery systems increases by over 10 per cent a year, reaching $132bn in US by 2012 with growth driven by injectable biologic dugs, according to a new study by the Freedonia Group.

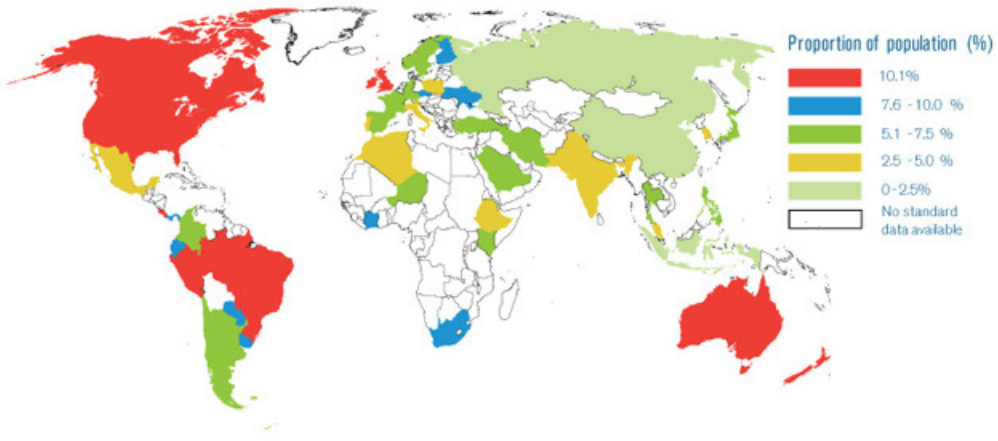

Fig. 1.1. World Map of Prevalence of Clinical Asthma. Over 10% of western society populations are afflicted with asthma (source: AIM Therapeutics Inc. 2008).

The report suggests that oral delivery methods will continue to dominate the sector, with increased patient demand for alternatives to injection-based medications and significant advances in transmucosal and oral disintegration technologies producing a sustained 7 per cent annual growth rate over the period. Only the US market for asthma drugs exceeded $10bn (€7.8bn) in 2005 and it is expected that by 2013 the global pulmonary delivery market will reach $40bn reflecting consumer expectations of simple drug delivery mechanisms to replace injections and pills according to the reports released by various pharmaceutical companies (Psivida Corp., Skyepharma, 2008).

Asthma patterns vary throughout the world, considerable increases in both the prevalence of asthma and its severity have occurred globally over recent decades (Figure 1.1). Asthma is etiologically complex, with numerous contributing factors and interactive effects within the causal web, many of which are modified by climate. The changing global climate compounds this complexity. Specific hypotheses relating asthma to climate change

must be developed and rigorously tested (Beggs & Bambrik, 2005). Early diagnosis and appropriate treatment lead to much better disease control and outcomes.

When someone has asthma symptoms, it means that the flow of air is blocked as it passes in and out of the lungs. This happens because the lining of the airways becomes inflamed (irritated, reddened and swollen), narrowing the airways and causing more mucous production. Mucous secretions block the airways, and the more inflamed the airway, the more sensitive the airway becomes – perpetuating more symptoms. If inflammation of the airway is not treated, the muscles that surround the airways can become sensitive, twitch, tighten and contract excessively, causing the airway to narrow even more. This is referred to as bronchospasm and makes it increasingly difficult to breathe (Farzan, 1978; Barnes et al., 1994; AIM Therapeutics Inc, 2008).

Since 1950s the delivery of drugs to the respiratory tract has become an increasingly important and effective therapeutic method for treating a variety of pulmonary disorders, including asthma, cystic fibrosis or chronic bronchitis (Noakes 2002; Kulon, 2003; Labirish & Dolovich, 2003). Systemic drug delivery using inhalation aerosols presents requirements and challenges. To be well absorbed from the lung, a compound needs to be delivered to the alveolar region and recent high technology inhaler systems have allowed increased efficiency of drug administration to the deep lung. Inhalation aerosols have been used for therapy of lung pathologies for thousands of years but have been developed for systemic therapeutic applications only since the 1990s (Anderson, 2005). This recent interest in systemic absorption from the lung results from the increasing number of drugs with a proteinous nature, the quest for their noninvasive administration as well as the recent comprehensive understanding of particle deposition within the respiratory systems (Vanveber, 2005).

Inhalation represents an attractive, rapid and patient-friendly route for the delivery of systemically acting drugs, as well for drugs that are designed to act locally on the lungs themselves. Aerosol medications have a number of advantages over oral administration, including the use of less drug to achieve the same therapeutic benefit, a reduction in the likelihood of systemic side effects, and a more rapid onset of action (Carveth & Kanner, 1999). Developing an efficient and effective portable inhalation system for medicinal use provides a greater challenge than most other drug delivery forms, requiring a complex integration of formulation and device technologies (Morton & Staniforth, 2006).

The development of modern inhalation devices can be divided into three different categories, the refinement of the nebulizer and the evolution of two types of compact portable devices, the metered-dose inhaler (MDI) and the dry powder inhaler (DPI) (Figure 1.2). MDIs deliver only a small fraction of the drug dose to the lung. Typically only 10-20% of the emitted dose is deposited in the lung (Carveth & Kanner, 1999; Labiris & Dolovich, 2003).

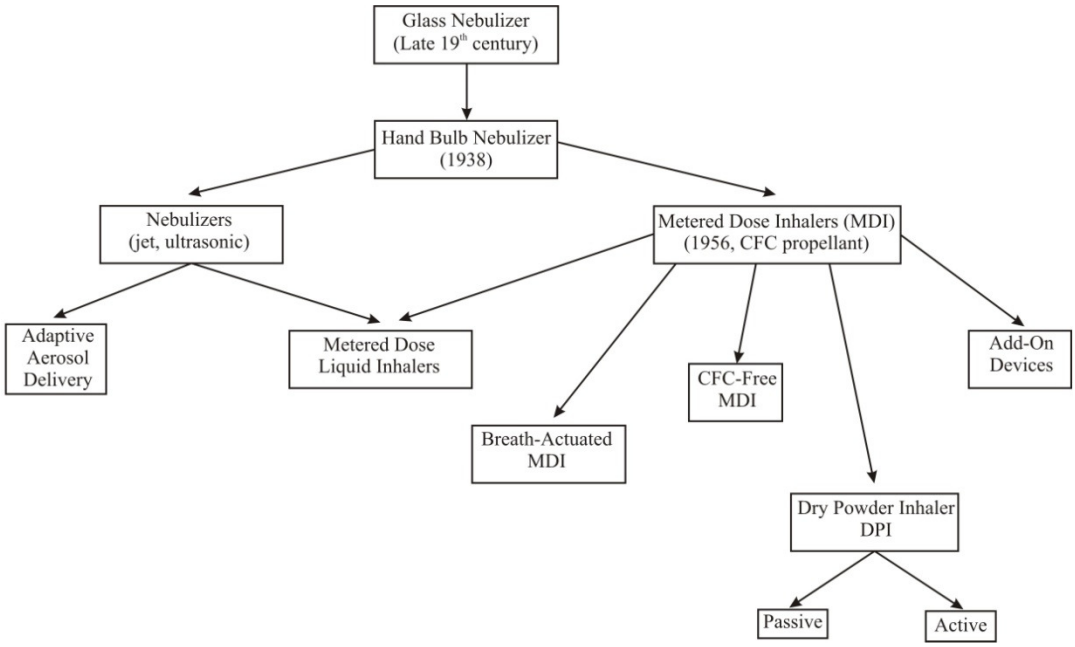

Fig. 1.2. Evolution of pulmonary delivery devices (Labiris & Dolovich, 2003, Anderson 2005).

The high velocity and large particle size of the spray causes approximately 50-80% of the drug aerosol to impact in the oropharyngeal region (Fig. 1.3). Lung deposition varies among the different DPIs, approximately 12-40% of the emitted dose is delivered to the lungs with 20-25% of the drug being retained within the device (Labiris & Dolovich, 2003; Pitcairn et al., 1997; Young et al., 2007). In a study performed by Davis et al. using gamma-scintigraphy to evaluate the lung deposition of a drug using MDIs, 75% of the dose was deposited in the oropharynx, only 11% was deposited in the lungs. Figure 1.3 shows the scintigraphic image of lung and oropharyngeal deposition of the radiolabelled particles following the aerosol inhalation from metered dose inhaler. As stated above only a small fraction of aerosol is deposited in the lungs, while the rest deposits in the extrathoracic and upper airways, and will be swallowed and subsequently absorbed in the gastrointestinal tract (Kulon, 2003).

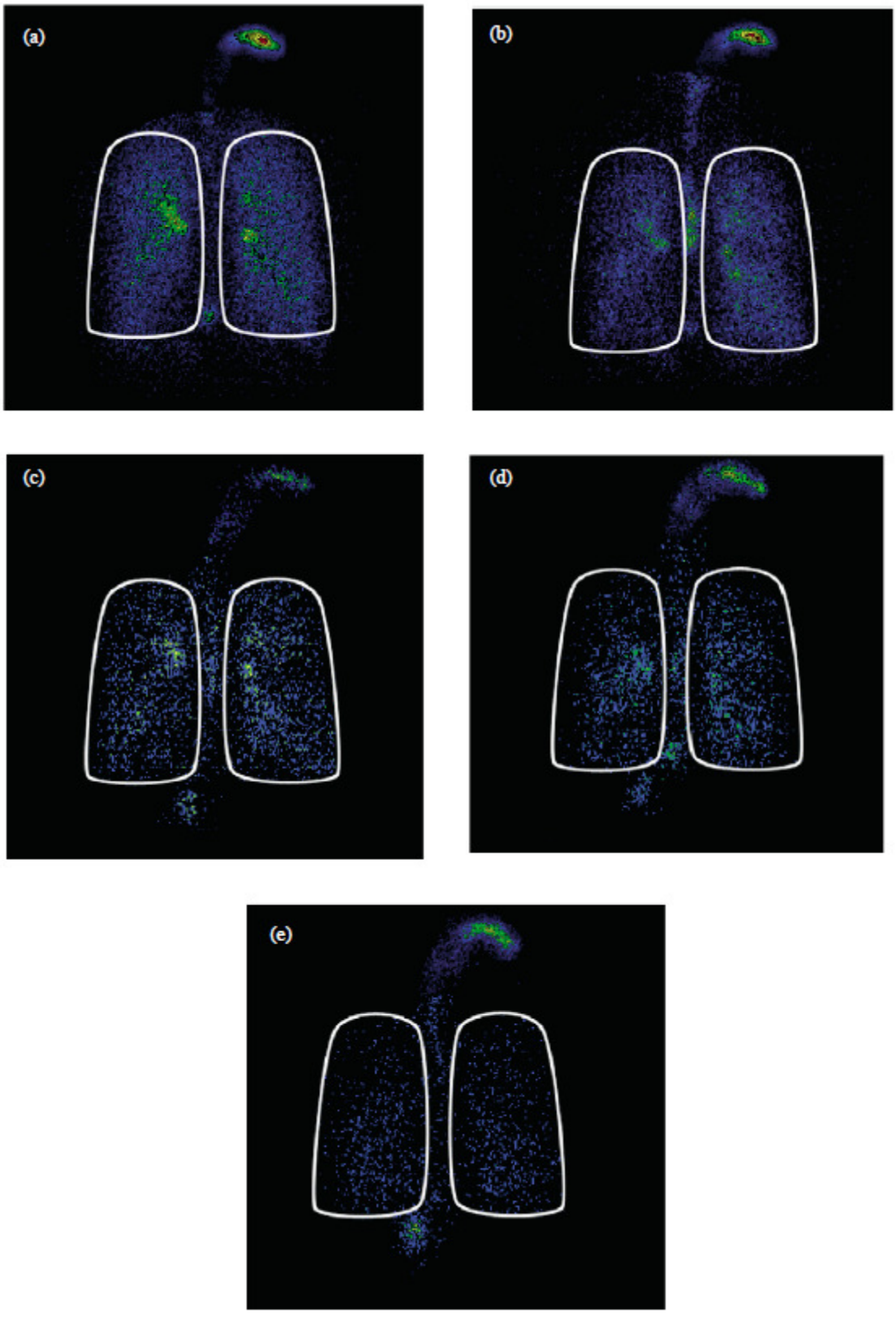

Fig. 1.3. Scintigraphic image showing lung and oropharyngeal deposition of the radiolabelled particles delivered from Airmax™ at (a) 60 $lmin^{-1}$ (b) 30 $lmin^{-1}$;Turbuhaler® at (c)60 $lmin^{-1}$ (d) 30 $lmin^{-1}$ and (e) a pMDI at 30 $lmin^{-1}$. (Hirst et al., 2002).

The modern dry powder inhalers offer the advantage of greater efficiency without the use of environmentally harmful propellants, and frequently without the use of additives. A brief reflection is required to understand the need for impeccable toxicology from any propellant gas used, whatever compound is chosen as propellant, it will make up more than 99% of the inhaled dose. The selection criteria for a substance to become a candidate for the duty of propellant has always been very demanding, some of the key requirements were: benign toxicology, boiling point, solvency, non-flammability and density. In 1987 a protocol was signed in Montreal to demise the chloroflourocarbons (CFCs) and other compounds used as propellants which were capable to deliver chlorine into stratosphere and perturb the natural ozone creation/destruction cycle (Molina & Rowland, 1975). This has proved to be a process far more challenging than originally envisaged, and especially the MDI industry which had originally been the case with the development of CFCs, will make a complete transition to other types of propellants such as hydroflourocarbons (HFCs) by 2007-2010 (Peart & Byron, 1999; Noakes, 2002).

To move away from the use of chlorofluorocarbon propellants, together with an increasing realisation of the difficulties that many patients experience in using pressurized MDIs correctly, has stimulated increased interest in the development of dry powder systems for drug delivery to the lungs (Davis et al., 1992). Formulating dry powders for inhalation involves either micronization via jet milling, precipitation, freeze-drying or spray-drying using various excipients, such as lipids and polymers, or carrier systems like lactose. At present, marketed dry powder inhalers contain either the drug alone or mixed with a bulk carrier, usually lactose (α – lactose monohydrate). Lactose is one of three sugars (the other being glucose and mannitol) allowed as carriers by the Food and Drug Administration (Labiris & Dolovich, 2003), and has an established safety profile improving the flow properties of the formulation necessary for reproducible filling and promoting dosing accuracy.

It is now recognized that it is not enough just to have inhalation therapy available for prescribing: physicians and other healthcare providers need a basic understanding of aerosol science, inhaled formulations, delivery devices, and bioequivalence of products to prescribe these therapies optimally. Targeted delivery of drug molecules to organs or special sites is one of the most challenging research areas in pharmaceutical sciences. Optimization of the whole system (drug, drug formulation and device) is necessary for the development of inhalation therapies and the therapeutic effect depends upon the dose deposited past the

oropharyngeal region into the central or peripheral airways and its distribution uniform or non-uniform within the lung. Successful delivery of inhaled particles along the respiratory tract depends mostly on particle characteristics such as: size, shape and density, hygrosopicity and electrical charge (Wilson, 1947; Yu, 1977; Balachandran et al., 1991; Bailey, 1997), anatomy of the respiratory system, the formulation and reproducibility in dose uniformity together with breathing conditions such as inhalation flow rate, breath-holding pause and exhalation flow rate. Studies provided compelling evidence that the electrical charge can affect the particles dispersion characteristic and significantly alter particles respiratory deposition. Generation of pharmaceutical aerosols by commonly used drug delivery devices such as nebulizers, pressurized metered dose inhalers (MDIs), and dry powder inhalers (DPIs) very often results in charged aerosols. Charge also occurs during powder manufacturing and handling operations, including mixing and milling. Mixing is the most important step in drug manufacturing process where the homogeneity and physical stability is achieved. The success of this step is related directly to the physical and chemical properties of the constituent particles: size distribution, shape, density, surface roughness and electrical properties which determine the charge transfer especially at the interactions between the particles and equipment surfaces (Engers et al., 2007).

In general many pharmaceutical aerosols, whether produced by nebulisation of liquids or dispersion of bulk powders, not only acquires a significant level of electrostatic charge but also exist in a bipolar state (Balachandran et al., 1991; Mazumder et al., 2004).

The mechanism of the charge production in delivery devices has been neither well characterised nor understood. One reason for our present poor understanding of the electrostatic charge generation process within the drug delivery systems is the complex fluid dynamics in these devices coupled with the effect of the excipients, such as surfactants, on particle properties. Second reason is the lack of systematic experimental studies as well as measurement equipment suitable for characterization of bipolar charge of rapidly evolving aerosols produced by these devices. Despite the large number of charge measurement techniques (Brown, 1997; Flagan, 1998) and instruments (Mazumder et al., 1991) none of them is without serious disadvantages and practical limitations from the specific point of view of their application to the measurement of bipolar charge on pharmaceutical aerosols generated by drug dispensers (Kulon, 2003).

1.2 Drug Delivery Devices

Pulmonary drug delivery is an important research area which impacts the treatment of illnesses such as asthma, chronic obstructive pulmonary disease (COPD) and cystic fibrosis. Inhalation gives the most direct access to drug target using the lung as a gateway for systematic drug delivery. In the treatment of obstructive respiratory diseases, pulmonary delivery can minimize systemic side effects, provide rapid response and minimize the required dose since the drug is delivered directly to the conducting zone of the lungs. Inhalation is an attractive option for systemic therapies because the respiratory region (mainly alveoli) of the lung provides an enormous surface area (80/100 m^2/adult) and a highly permeable membrane for absorption of medication into the blood. It is a needle-free delivery system capable of administering a variety of therapeutic substances. Large protein molecules which degrade in the harsh gastrointestinal conditions and are eliminated by the first-pass metabolism in the liver can be delivered via the pulmonary route if deposited in the respiratory zone of the lungs. Although, over the years, the need for better clinical therapies and improved performance of the inhalers have led to several innovations and new designs in the respiratory drug delivery field the fundamental operation principles of these three the most popular types of inhalers have remained virtually unchanged. The detailed discussion of the mechanics of different inhalers as well as advantages and disadvantages of different drug delivery techniques can be found in the large amount of literature available on this subject (Clark, 1995; Pedersen, 1996; Fink, 2000; Terzano, 2001; Smith, 2003; Zhu, Daniher, Islam, 2008). Devices used to deliver aerosolized therapeutic agents are based on one of three platforms; pressured metered-dose inhaler (pMDI), nebulizer and dry powder systems (DPIs). These inhalers types are based either on atomization of liquids, solutions, suspensions or the dispersion of dry powders. The criteria for an ideal medical inhaler are: reliability, reproducibility, accuracy, small particle size (1-5 μm), simple to use and handle, multiple dose capability, resistance to bacterial contamination, durability, cost effectiveness, product stability. The oldest of these is the pneumatic nebulizer. The nebulizer uses an external power source to break up aqueous drug solutions. In the mid 1950s the pressurized metered dose inhaler (pMDI) joined the nebulizer. The pMDI uses a propellant liquid as both its power source and the suspending, or dissolution, medium for the drug. Its inherent portability and perceived ease of use have made it the most popular form of inhalation delivery. In 1960s the

dry powder inhaler (DPI) was introduced, and it is using the energy supplied by the patient's inspiration to dispense and disperse a premetered of drug substance.

1.3 Dry Powder Inhalers

Dry powder inhalers were designed to eliminate the co-ordination difficulties associated with the MDI. Renewed interest in this delivery system has emanated from the urgency to eliminate CFC-containing MDIs (Peart and Byron, 1999; Noakes, 2002). There is a wide range of DPI devices on the market (Figure 1.4), from single-dose devices loaded by the patient (e.g. Aerolizer, Rotahaler) to multiunit dose devices provided in a blister pack (e.g. Diskhaler), multiple unit doses sealed in blisters on a strip which moves through the inhaler (e.g. Diskus) or reservoir- type (bulk powder) systems (e.g. Turbuhaler). Lung deposition varies among the different DPIs. Approximately 12–40% of the emitted dose is delivered to the lungs with 20–25% of the drug being retained within the device. Poor drug deposition with DPIs can be attributed to inefficient deaggregation of the fine drug particles from coarser carrier lactose particles or drug pellets. Slow inspiration flow rate (IFR), high humidity (Zhu, 2008) and rapid, large changes in temperature are known to effect drug

Fig. 1.4. DPI devices: (A) Aerolizer™, (B) Easyhaler™, (C) Turbohaler™, (D) Diskhaler™, (E) Novolizer™, (F) Rotahaler™, (G) Clickhaler™, (H) MAGhaler™, (I) Spinhaler™, (J) Handihaler™ (Islam, 2008).

deaggregation and hence the efficiency of pulmonary drug delivery with DPIs. With most DPIs, drug delivery to the lungs is augmented by fast inhalation. This is in contrast to the MDI, which requires slow inhalation and breath holding to enhance lung deposition of the drug. With DPIs, the drug aerosol is created by directing air through loose powder. Most particles from DPIs are too large to penetrate into the lungs due to large powder agglomerates or the presence of large carrier particles (e.g. lactose). Thus, dispersion of the powder into respirable particles depends on the creation of turbulent air flow in the powder container. The turbulent airstream causes the aggregates to break up into particles small enough to be carried into the lower airways and also to separate carrier from drug. Each DPI has a different air flow resistance that governs the required inspiratory effort. The higher the resistance of the device, the more difficult it is to generate an inspiratory flow great enough to achieve the maximum dose from the inhaler. However, deposition in the lung tends to be increased when using high-resistance inhalers (Labiris & Dolovich, 2003). Recent developments in DPI technology have focused on eliminating these problems. Active DPIs are being investigated that reduce the importance of a patient's inspiratory effort. By adding either a battery-driven propeller that aids in the dispersion of the powder or using compressed air to aerosolize the powder and converting it into a standing cloud in a holding chamber, the generation of a respirable aerosol becomes independent of a investigators from a variety of dry powder inhalers (DPIs) v*s.* the specific resistance of the DPI. The increase in deposition seen with the higher resistance devices may, in part, be a function of the degree to which these DPIs de-aggregate the powder dose in the device at the start of the inhalation manoeuvre, thus providing a finer aerosol for inhalation. However, DPIs in use today are breath actuated and are dependent on a patient's IFR of 30–130 l/min to achieve an aerosol within the respirable range. Dry powder inhaler devices are classified by dose type into single-unit dose, multi-dose reservoirs, and multi-unit dose, as illustrated schematically in Figure 1.5.

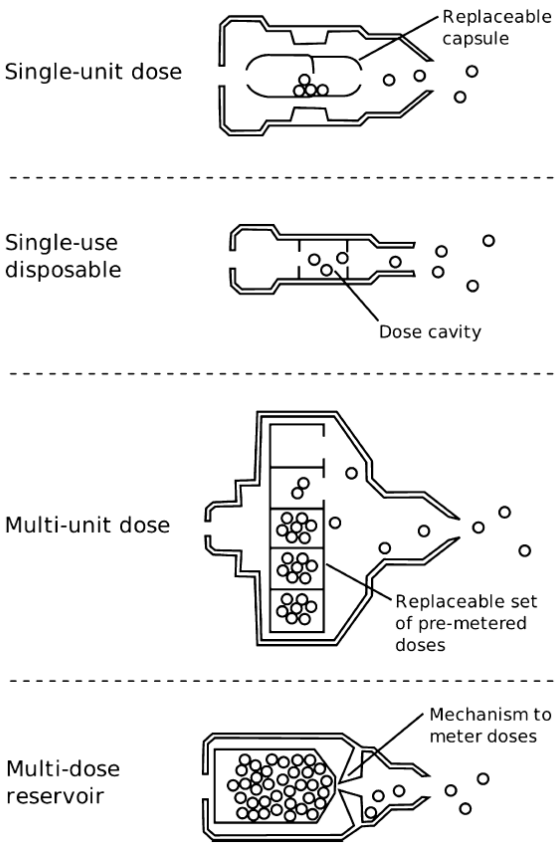

Fig. 1.5. Four dose design options available for Dry Powder Inhalers.

In a single-unit dose device, the drug is formulated as a micronized drug powder and carrier system and supplied in individual gelatine capsules, which are then inserted into the inhaler for a single dose and removed and discarded after use. There are two types of multi-dose devices, reservoir type devices and multi-unit dose devices. The multi-dose reservoir type device stores the formulation in bulk, and has a built in mechanism to meter individual doses from the bulk upon actuation. Newer devices of this type attempt to address issues such as reducing the flow rate dependent dose emission and of moisture ingress into the reservoir from patient exhalation or environmental humidity during the life of the product as these are common issues with the reservoir type device. The multi-unit dose device uses factory metered and sealed doses packaged in a manner that the device can hold multiple doses without having to reload. Typically, the packaging consists of replaceable disks or cartridges, or strips of foil-polymer blister packaging that may or may not be reloadable. This pre-packaged does have the advantage of being protected from the environment until use, and ensuring adequate control of dose uniformity. Consideration of patient compliance for device type is very important when selecting a device design. Table 1.1 summarizes some of the advantages and disadvantages of the inhaler devices presented.

Table 1.1. Advantages and Disadvantages of inhalation devices (Labirish&Dolovich, 2003).

Inhalation device	Advantages	Disadvantages
Nebulizers (jet & ultrasonic)	No specific inhalation technique or co-ordination required Aerosolizes most drug solutions Delivers large doses Suitable for infants and people too sick or physically unable to use other devices	Time consuming Bulky Non-portable Contents easily contaminated Relatively expensive Poor delivery efficiency Drug wastage Wide performance variation between different models and operating conditions
Pressurized metered dose inhalers (pMDI)	Compact Portable Multidose (approximately 200 doses) Inexpensive Sealed environment (no degradation of drug) Reproducible dosing	Inhalation technique and patient co-ordination required High oral deposition Maximum dose of 5 mg Limited range of drugs available
Dry powder inhalers (DPI)	Compact Portable Breath actuated Easy to use No hand-mouth co-ordination required	Respirable dose dependent on inspiratory flow rate Humidity may cause powders to aggregate and capsules to soften Dose lost if patient inadvertently exhales into the DPI Most DPIs contain lactose

1.4 Scope of the thesis

The main scope if this research project was to use, test and model a novel optical method of assesing the bipolar charge distribution of pharmaceutical dry powder aerosols disperssed by dry powder inhalers. The non-intrusive functional set-up is capable of measuring in real time size, speed and bipolar charge distribution of the pharmaceutical aerosols.

- To understand the complex inter-particle and particle-device interaction mechanisms.
- To test the electrical properties of pharmaceutical materials.
- To asses the delivery performance of new dry powder inhaler devices.

- To understand the principle of operation of the Phase Doppler Anemometer system, it's advantages and disatvantages compared to other measurement systems.
- To design appropriate modifications and extend PDA capabilities for bipolar charge measurement.
- To design and test a human mouth and throuat set-up for DPI testing using PDA system and model the electrodynamics in the measurement area.
- To compare PDA data with other similar optical techniques, leading to optimization of the system parameters and experimental procedures.

1.5 Outline of the Thesis

This thesis has been organized in 5 chapters.

Chapter 1 describes the importance of this research project in the fundamental undestanding of charge influence upon medication fabrication, development and delivery to human respiratory tract. Background information on the inhalation therapy is given. Next a description on the devices used for dry powder drug delivery is provided with the apporpiate literature review.

Chapter 2 presents a review of the different methodologies used for measuring the electrostatic charge of dry aerosols. It clarifies what is applicable and which are the best tools available today to measure bipoalr charge of pharmaceutical aerosols.

Chapter 3 is mainly concerned with fundamental inter-particle and particle-device charging mechanisms. Presents experimental procedures for pharamceutical powders electrical properties measurement and discusses the experimental set-up design which allows a more indepth study of DPI delivery performance with focus on electrostatic charge.

Chapter 4 focuses on undelying the principles of PDA. Next shows the modifications which are made so that the system can measure the bipolar charge levels of aerosols besides speed and size. Insists on the difficulty of DPI testing using this technique, providing a set of solutions which allow a better understanding on how bipolar charge influeces the aerosol dispertion by the DPI devices.

The thesis concludes with chapter 5 which summarizes the findings of this work, the inovations that were proposed for a more accurate measurement of bipolar charge distribution of aerosols from DPI devices and further research paths wihich could followed in the future

to improve and estabilsh the PDA technique as the best tool for non intrusive, real time measurement of size, speed and bipolar charge distribution of dry powder aerosols.

1.6 Conclusions

It is widely recognized that the incidence of allergies and allergic diseases is on the rise globally. Asthma is one of the most common and increasingly prevalent chronic diseases in the world, characterized by increased reactivity of the trachea and bronchi to various stimuli and manifested by widespread narrowing of the airways that change in severity either spontaneously or as a result of therapy. It's a disease with a periodic recurrence over many years, if not, for the patient's life and there is no actual curative treatment for it. -.

Many factors are involved in the delivery of a drug to its site of action and are considered under pharmacokinetics, whereas pharmacodynamics involves the mechanism of action of the drug, including its interaction with receptors or enzymes and the secondary events witch lead to the typical tissue responses.

Human respiratory system from the standpoint of respiratory deposition can be divided into three regions, each covering one or more anatomical zones. These regions differ markedly in structure, size, airflow pattern; function and sensitivity to deposited particles. The first is the head region (H), or extrathoracic region, which includes nose; mouth; pharynx and larynx. Inhaled air is warmed and humidified in this region. The second is the tracheobronchial region (TB), or conductive airways, which includes the airways from the larynx to the terminal bronchioles. This region resembles an inverted tree with a single trunk, the trachea, which subdivides into smaller and smaller airways. The third is the alveolar region (A), or pulmonary region, which includes the alveoli where gas exchange takes place. Once deposited, particles are retained in the lung for varying times depending on their chemical properties, their location within the lung, and the clearance mechanism involved.

It has been shown that the deposition of inhaled drug aerosol in the respiratory system is governed by inertial impaction, gravitational sedimentation, Brownian diffusion, interception and electrostatic forces . Electrostatic forces dominate the deposition particularly in the alveolar region and these forces can be divided into two different categories: space charge and image charge. Space charge seems to have more effect at the upper region of the respiratory tract, especially when the aerosol cloud is dense, while the image charge forces are dominant in the alveolar region. In addition to the improved deposition, static charge can

also be utilized in targeting the aerosol to the desired location of the respiratory tract. Charge on the pharmaceutical materials often arise, due to high surface resistivity of the materials which prevents the charge transferred in contact from leaking back. Charge retention can be reduced by lowering the resistivity by adding more moisture or some antistatic additive but often it is not advisable when pharmaceutically materials are concerned due to, e.g. stability.

Interparticulate or particle/substrate collisions lead to charge accumulation which is influenced by particle size and shape, nature and work function of the contacting materials, contact area and frequency, contact surface roughness and contamination and atmospheric humidity. Moisture, particulate contamination and method of cleaning of processing equipment during pharmaceutical manufacturing operations may influence the electrostatic behaviour of powders.

Withdrawal of atmospheric ozone depleting propellants and the development of biotechnology products that cannot be delivered by conventional routes of administration emphasize the need for improved inhaler design based on novel mechanisms or aerosol dispersion. Dry powders inhalers have become prominent alternatives to pressurized metered dose inhalers for pharmaceutical aerosol drug delivery since the ratification of the Montreal protocol in 1987 which describes the phase out of chlorofluorocarbons and eventual termination of use by 2010.

Powders which are used in DPIs are usually mixtures of small drug particles with an aerodynamic diameter <5µm and larger additive particles (63-150 µm). Particles of this size range, however, have high surface area to mass ratios, thus making them highly cohesive/adhesive and difficult to aerosolize. -. When a powder has more than one component, electrostatic charging becomes more difficult to understand. In addition to contacts with the inhaler surface, different particles also contact other particles and this may lead to very complicated bipolar charging processes . Drug and additive particles will charge with opposite polarity when they contact each other, and this may lead to reduced particle separation and weak performances. Small particles tend to adhere to the inhaler surface more than the larger ones which leads to increase number of contacts between adhered powder and the mixture . When a surface has been contaminated with a certain powder following contacts by the same material usually show reduced charge, because similar materials do not exchange charge to a high degree.

Materials which are used in DPIs as well as the size fraction of the powder have an effect on the triboelectrification process . Different plastics have different charging properties and these are influenced by colorants and other additives. Also the preparation and the amorphicity of the spray dried lactose in addition to DPIs structure has a significant effect in generating a specific amount of charge but the method used to measure the amount of charge does not give information about the bipolar charging which may be present especially when the emitted aerosol consists of different particles .

The control of triboelectric charging by DPIs plays an important role in the performance of inhalers, the monitoring of the aerosol charge gives essential information for the design and the formulation of the inhaler structures and materials. The electrostatic charge, if not dissipated, will influence the drug emission and dispersion at a later stage. Despite the widespread use of inhaled medications, our knowledge is limited regard to the optimal lung deposition, site for local therapeutic response, the factors that determine the absorption, clearance, and the role the bronchial circulations plays in the redistribution of the inhaled agents. Such understanding awaits further research.

1.7 List of Publications

A. Journal papers:

1. **Beleca, R.,** Abbod, M., Balachandran, W., Miller, P.R., 2010. "Investigation of Electrostatic Properties of Pharmaceutical Powders using Phase Doppler Anemometry," *IEEE Transactions on Industry Applications*, 46 (3), pp. 1181 - 1187.
2. **Beleca, R.,** Abbod, M., Balachandran, W., Ahern, J., Miller, P.R., 2010. Electrostatic Properties of DPI Dispensed Drug Aerosols in a Human Upper Airway Model. – *in process.*

B. Papers in conferences proceedings

1. **Beleca, R.,** Abbod, M., Balachandran, W., 2011. Bipolar charge measurement of dipolar spherical particles using Phase Doppler Anemometry. Proceedings of the 2011 Electrostatic Society of America Annual Meeting, Case Western Reserve University, Cleveland, Ohio, USA – *best paper award.*
2. **Beleca, R.**, Abod, M., Kulon, J., Balachandran, W., 2011. Bipolar charge distribution of dry powder aerosols using an optical technique. 13th Institute of Physics Conference on

Electrostatics – Electrostatics 2011, Bangor University, April 10-14, Bangor, Wales, UK – *best paper award*.

3. **Beleca R.,** Miao P., and Balachandran W., 2010. Experimental study on charging behavior of bio-fuels sprays generated by an annular electrostatic atomizer. In ILASS – Europe, 23rd Annual Conference on Liquid Atomization and Spray Systems, Brno, Czech Republic.
4. **Beleca, R.,** Abbod, M., Balachandran, W., Ahern, J., Miller, P.R., 2010. Electrostatic Properties of DPI Dispensed Drug Aerosols in a Human Upper Airway Model. Proceedings of the 2010 Electrostatic Society of America Annual Meeting, University of North Carolina at Charlotte, North Carolina, USA. 2010 – *best paper award*.
5. **Beleca, R.**, Abbod, M., Balachandran, W., Miller, P.R., 2010. Measurement of Bipolar Charge Distribution of Lactose Monohydrate using Phase Doppler Anemometry. Respiratory Drug Delivery Conference, April 25-29. Orlando, Florida, U.S.A. – *best poster award*.
6. **Beleca R.**, Abbod, M., Balachandran, W., Miller, P.R., "Investigation of Electrostatic Properties of Pharmaceutical Powders using Phase Doppler Anemometry," ESA 2009 Electrostatic Joint Conference, June 16-18, 2009, Boston University, Boston, USA – *best paper award*.

Chapter 2

Aerosol Charge Measurement Techniques

2.1 Introduction

The performance of dry powder aerosols for the delivery of drugs to the lungs has been studied extensively in the last decade. The behaviour of particles is the foundation on which dry powder inhaler (DPI) performance is built. Pharmaceutical powders are of great importance for oral dosage forms where particle behaviour is crucial to the processes involved in tablet and capsule manufacture and ultimately in their dissolution and drug availability (Engers et al., 2006). This interest extends to aerosol products that are highly dependent on the physico-chemical and performance characteristics of the particles that deliver drugs to the lungs. Aerosol particles are prepared in respirable sizes (<5 μm) and exibit unique properties based on the forces of interaction which are known to occur. The three most important parameters governing the behaviour of aerosol particles are their size, electric charge and shape. The first of these has been the subject of considerable study, especially when it plays an important part in defining where inhaled aerosol will deposit in the lower respiratory tract. This is because the lungs together with the airways have evolved to form a particle size-selective sampling system in which progressively finer particles are removed from the inhaled air-stream as they pass via the mouth, larynx and larger airways towards the alveolar spaces. Shape can be accounted for by broadening the definition of size so that several lengths are used to describe a particle rather than a single diameter (Brown, 1996). Electrical charge is a completely independent parameter. Its effects on pulmonary deposition may make it useful in medication. The simultaneous measurement of size and charge is necessary if the properties of particles are to be understood and their behaviour controlled.

There exist a considerable variety of different measurement techniques and instruments used to measure the electrical charge on aerosol particles (Fig. 2.1.). A comprehensive review of various measurement methods was presented by Brown and more recently by Flagan. One of the difficulties associated with the classification of all these methods, is related to finding the most representative criteria. Many methods demonstrate similar approach in measurement principles but differ in data collection or data analysis techniques. On the other hand different measurement principles are employed along with

similar instrument design. Taking into account these factors, the measurement techniques have been

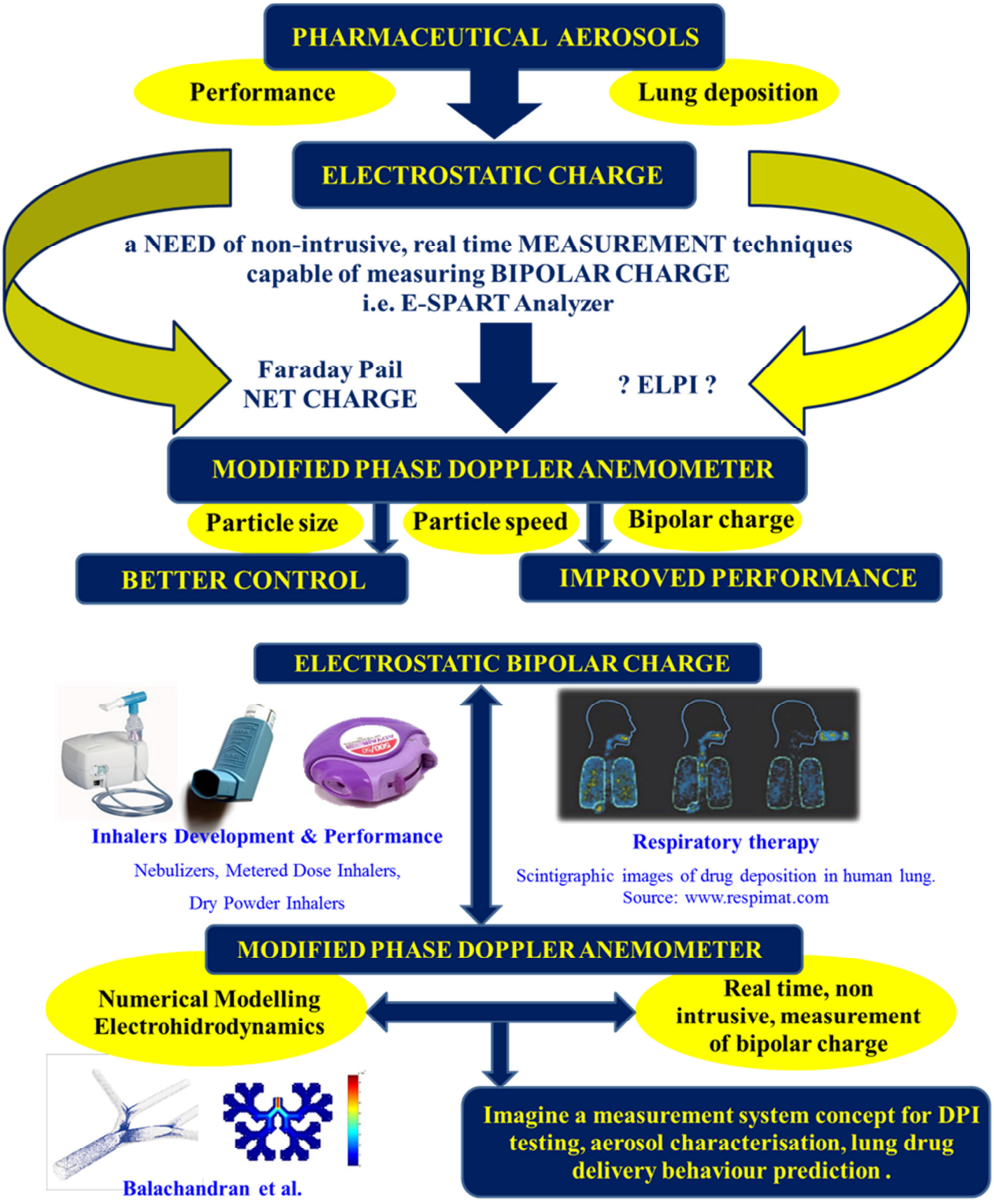

Fig. 2.1. Pharmaceutical powders bipolar charge measurement proposed solutions based on the pharmaceutical industry needs.

divided into two main categories, as shown in Figure 2.2, namely static and dynamic. The main criterion of this classification, have been suggested by Brown and is based on the fundamental principle by which the measurement is performed. If a given method requires the particle's response to the external electric field it is classified as dynamic otherwise it is static. As seen in Figure 2.2, the static methods have been further divided into two categories such as contact and non-contact methods. Contact methods require the particles to contact the conducting collector and give up their charge, while non-contact methods rely on the measurement of the induced signal as the particle travels in the vicinity of the measuring probe. The relationship between the induced signal and the particle charge is usually established as a function of the geometry of the charge-sensing electrode. However, it should be noted that this classification does not preclude the possibility where the induced signal is also present and measured using contact method or the occurrence of particle-electrode contact in non-contact techniques. The determining factor whether a given method is classified as contact or non-contact depends on how the majority of measurements are performed. The classic example when these two principles operate simultaneously can be found in the so-called Faraday pail method which is presented in Chapter 3. Dynamic methods require particle movement as a result of an external electric field. The particle electrical mobility can be measured either by means of direct observation of particle trajectories, by counting the particles penetrating a field region (mobility analyzers) or by measuring the positions of particles deposited on a surface.

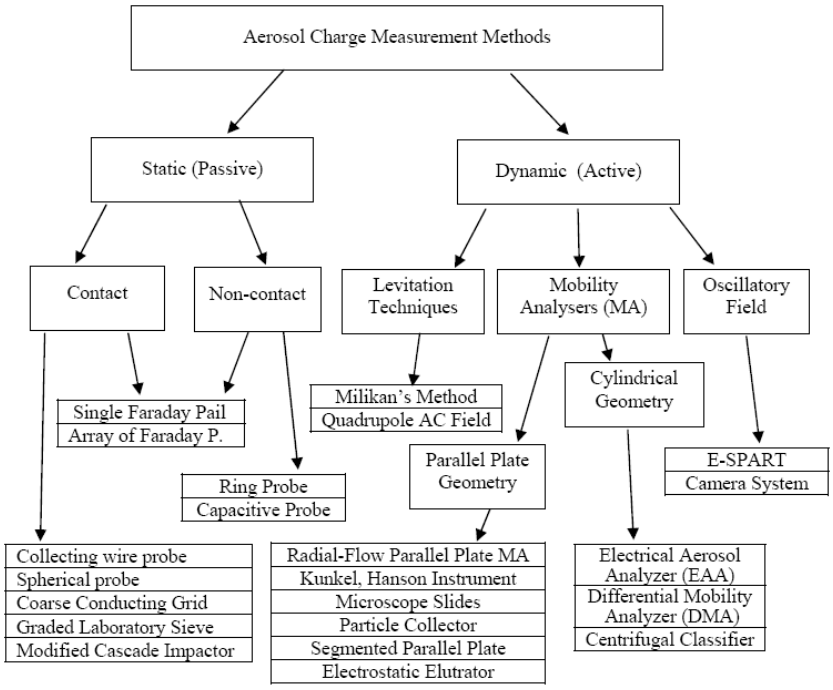

Fig. 2.2. Classification of Aerosol Charge Measurement Techniques (Kulon, 2003).

The electrical mobility obtained in this way is usually combined with independent particle size distribution data to produce charge distribution. Some of the problems associated with these methods like, for instance, very long sampling time and tedious post processing analysis limit their application to relatively stable, spatially homogeneous aerosols continuously supplied over a long period of time. It is necessary therefore to develop an alternative characterization method, which enables measurement of both charge polarities of bipolarly charged aerosols.

In order to measure both charge as well as size of individual particles, Mazumder et al. employed the Laser Doppler Velocimetry (LDV). This was accomplished by subjecting the particles to an oscillatory acoustic field superimposed on a dc electric field and measuring the phase shift between the waveform representing the applied field and the signal indicating the particle response. More recently, the acoustic field and the dc electric field was replaced by an ac field. Although the instrument is elegant, its aerosol sampling mechanism as well as relatively low particle count (below 100 particles per second) becomes an obstacle in characterizing highly charged unstable aerosols. To obtain a representative picture of aerosol electrostatic properties and minimize the loss of expensive pharmaceutical material, it is essential that during the characterization procedure, all released aerosol particles are contained in the measurement system. This constraint as well as other restrictions (health and safety issues) made it very difficult to adopt one of the techniques mentioned above. However, none of those is without practical complications, especially when it comes to the rapidly evolving non-uniform cloud of aerosol particles delivered from a medical dispensing device.

2.2 The cascade impactor & ELPI

Medical aerosols from pressurized metered-dose inhalers (pMDIs), dry powder inhalers (DPIs) and nebulizers are widely prescribed for treating ‘traditional’ diseases of the lung, particularly asthma and chronic obstructive pulmonary disease (COPD). In addition, such devices are of interest for the delivery of medications systemically, using the lung as a gateway. In the case of oral delivery to the lower respiratory tract, it is widely recognized that particle size plays an important part in defining where the aerosol particles will deposit. Reliable techniques that measure the particle size of inhaled aerosols are an essential part of defining both oral and nasal inhaler performance in order to predict respiratory tract

deposition as an indicator of clinical efficacy. In connection with oral delivery of medications to the lungs for either local or systemic effects, it is important to distinguish the proportion of the mass from the inhaler that is contained in so called 'fine' particles that penetrate beyond the oropharynx from the total mass emitted by the inhaler. This component is often referred to as the fine particle or 'respirable' fraction (FPF). The precise limits for FPF are debatable, depending upon the eventual destination of the medication, therapeutic action desired and category of patient (pediatric/adult). The traditional particle size analysis methods for medical inhalers contained in the US (USP) and European (Ph.Eur.) Pharmacopias require that some form of drug assay be undertaken of the collected size fractions, so that there is a direct link between measured particle aerodynamic size and the mass of active pharmaceutical ingredient (API). This is especially important when excipients, such as surfactant particles, are present together with API. Non-invasive techniques that are based on light scattering or the time-of-flight principle that cannot distinguish between API and non-volatile, non-pharmaceutically active substances in the formulation *(e.g.* surfactant) will measure an overall particle size distribution that may not be reflective of the actual API based size distribution (Mitchell & Nagel, 2004). Inertial size-separation by Cascade Impactors has been used as the 'gold standard' to size-analyze inhaler-derived aerosols for many years and is probably the widest used method today. The application of this class of particle size analyzer to the assessment of medical aerosols has recently been extensively reviewed, focusing on the types of impactor that are in current use together with their strengths and limitations for measurements with the different classes of inhalers. In the case of DPI testing, a fixed volume of air is drawn through the inhaler with the valve to the pump downstream of the inertial impactor or impinger operated at critical flow (Figure 3.2), so that the resistance of the inhaler determines the precise flow rate-time profile once the solenoid valve is actuated to begin the process of sampling from the DPI.

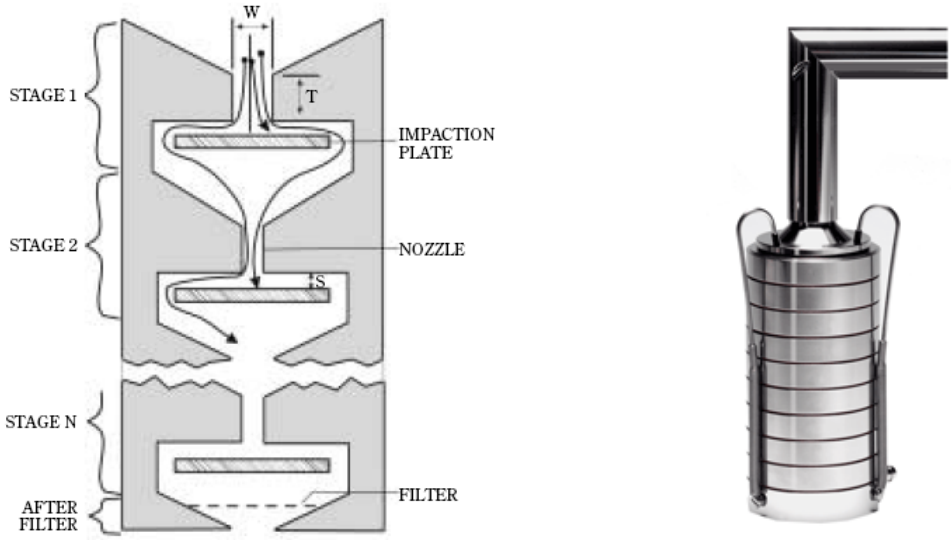

Fig. 2.3. Schematic of a multi-stage Andersen cascade impactor, showing the separation of progressively finer particles as the aerosol passes through successive stages to the after filter.

The final flow rate is achieved rapidly, and is therefore used to define the size-separating performance of the particle size analysis equipment. This process is closer to actual use by a patient, as it simulates the inhalation process, but there is no attempt to replicate actual inhalation flow rate-time profiles. In contrast, the impactor or impinger is always operated at constant flow rate (*i.e.* 28.3 L/min for the Andersen 8-stage CI) for the testing of pMDIs and nebulizers.

A cascade impactor is assembled from several stages with progressively decreasing cut sizes (Figure 2.3), so that an incoming aerosol is size separated into the same number of fractions as there are stages. For inhaler testing, it is desirable to have at least 5 stages with diameter values located within the critical range from 0.5 to 5 μm aerodynamic diameter. There is a link between the cut sizes of individual impactor stages and the likely deposition sites in the respiratory tract of the particles that are size-separated, but it is important to appreciate that diagrams, such as Figure 2.3, which relates to the Andersen 8-stage impactor, are only a guide, since the constant flow rate through a cascade impactor does not simulate the continuously varying flow rate associated with the respiratory cycle. Local climate control may also be appropriate when testing DPIs, either where electrostatic charge associated with the powder particles may have a significant impact on aerosol behavior, or where hygroscopic substances are present.

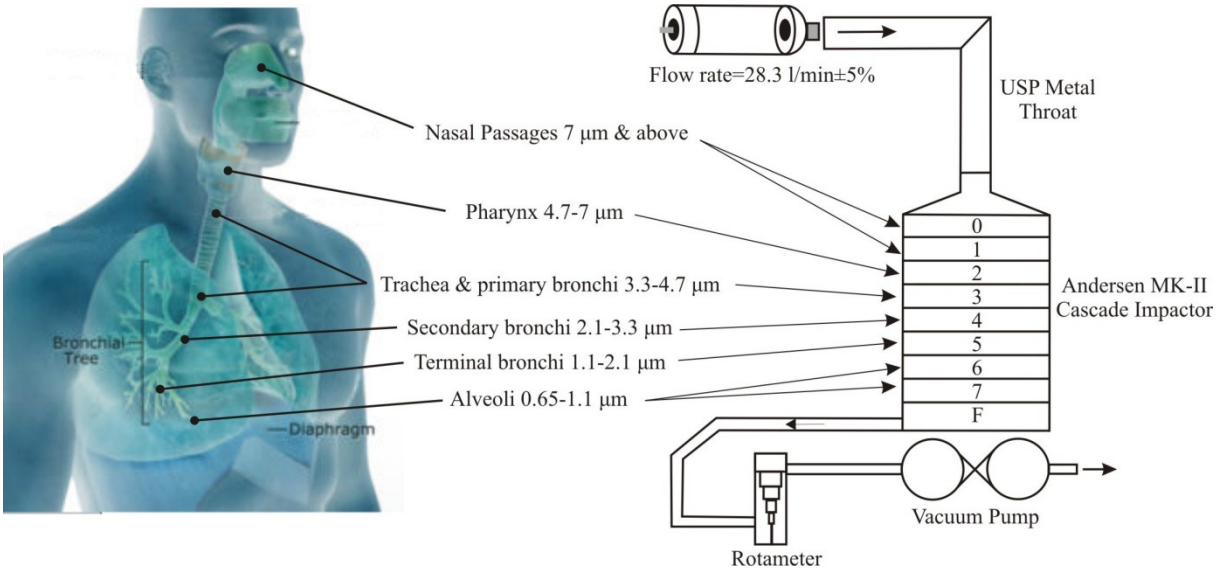

Fig. 2.4. Relationship between Andersen 8-stage cascade impactor cut sizes and likely particle deposition in the respiratory tract (Mitchell & Nagel, 2004).

Aldred et al. (1983) proposed technique to perform simultaneously particle charge and size measurements by means of modified cascade impactor. In order to accommodate charge measurements, the stages of the impactor were made of metal and were separated by insulating spacers; each stage was connected to the separate electrometer, so in each specific size range fractionated by the impactor both the mass and algebraic sum of the particle charge were measured. The technique of modified cascade impactor offers the rare advantage of performing simultaneously particle size and charge analysis. Unfortunately, the bipolar nature of measured aerosol is lost as particles of both polarities deposit on the impaction plates.

Another method for measuring electrostatic charge of pharmaceutical aerosols uses an Electrical Low Pressure Impactor (ELPI) which combines electrical detection with low-pressure cascade impactor (Marjamäki et al., 1999; Virtanen et al., 2001; Glover & Chan, 2004; Hickey et al., 2007). The operation principle of the ELPI involves applying charges to the aerosol particles using a corona, followed by introducing the charged aerosol into the 13-stage impactor (Figure 2.5). Each impactor stage functions as a Faraday well to detect the level of electrostatic charge of the deposited particles. This is achieved by the sensitive electrometers which measure the induced current at femto ampere (fA) level produced by the charged particles. The detected charge level is related to the particle size which allows for a particle size distribution to be constructed between the size limits (0.028–10 µm) of the impactor. By disenabling the corona charging mechanism, the innate electrostatic charge on the aerosol particles caused from the actuation of the aerosol inhaler can potentially be

investigated. An important consideration of using the ELPI for charge measurement is that of image charge produced by a charged particle passing through, but not collected on an impaction stage. For example, as a positive particle enters and exits the stage this will produce a positive current peak followed by a negative one, but the net effect is zero. Therefore charged particles passing to lower stages in the ELPI have no overall effect on the level or polarity of charge measured in the collection stage. Also in addition to diffusion, the space-charge force was a significant loss mechanism in ELPI especially when the high concentrations of aerosols were measured. Again, the bipolar nature of aerosols cannot be revealed with this type of device.

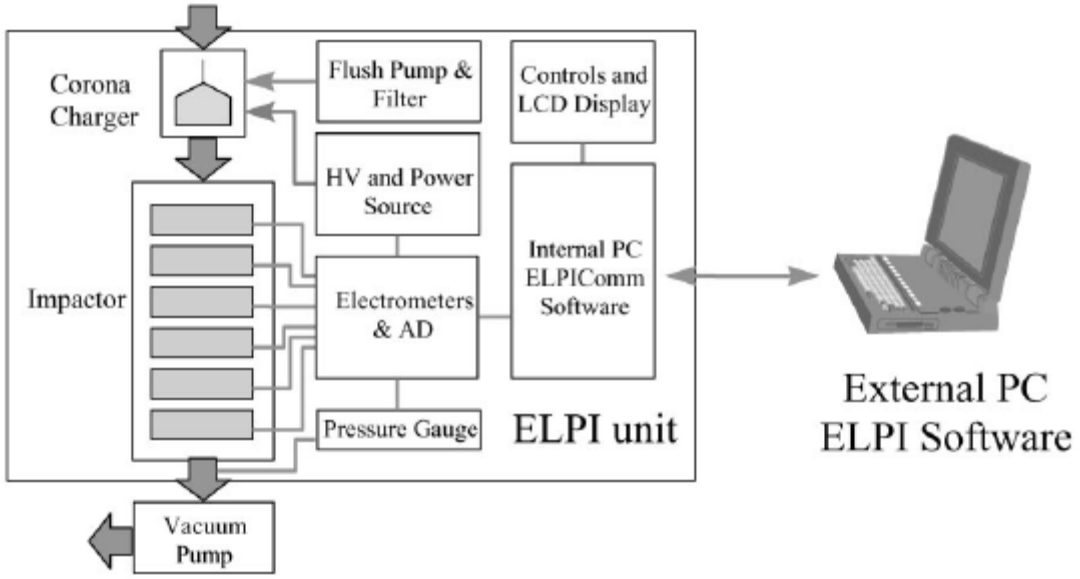

Fig. 2.5. Schematics of electrical low-pressure impactor (Marjamäki et al., 2000).

2.3 E-SPART Analyzer

Mazumder et al. reported the development of an instrument called an Electrical Single Particle Aerodynamic Relaxation Time Analyzer (E-SPART) capable of performing in real-time particle charge and size distribution measurements on aerosols. This was accomplished by subjecting the particles to an oscillatory acoustic field superimposed on DC electric field (DC-E-SPART Analyzer) or more recently to AC electric field only (AC-E-SPART Analyzer) and measuring the phase shift between the waveform of the applied field and the signal indicating the particle response. In DC version of E-SPART Analyzer the aerosol particles are directed through an oscillatory acoustic field and a DC electric field. A phase lag

produced by the particle motion in the acoustic field is measured to obtain the aerodynamic particle size, while the drift velocity in the electric field is proportional to the electronic charge on the particle. In order to determine the phase lag, the analyzer uses a differential laser Doppler velocimeter (LDV) to measure the velocity of individual particles. As shown in Figure 2.6 there are three basic components of the E-SPART analyzer; a dual-beam, frequency-biased laser Doppler velocimeter (LDV), a relaxation cell and an electronic signal and data processing system.

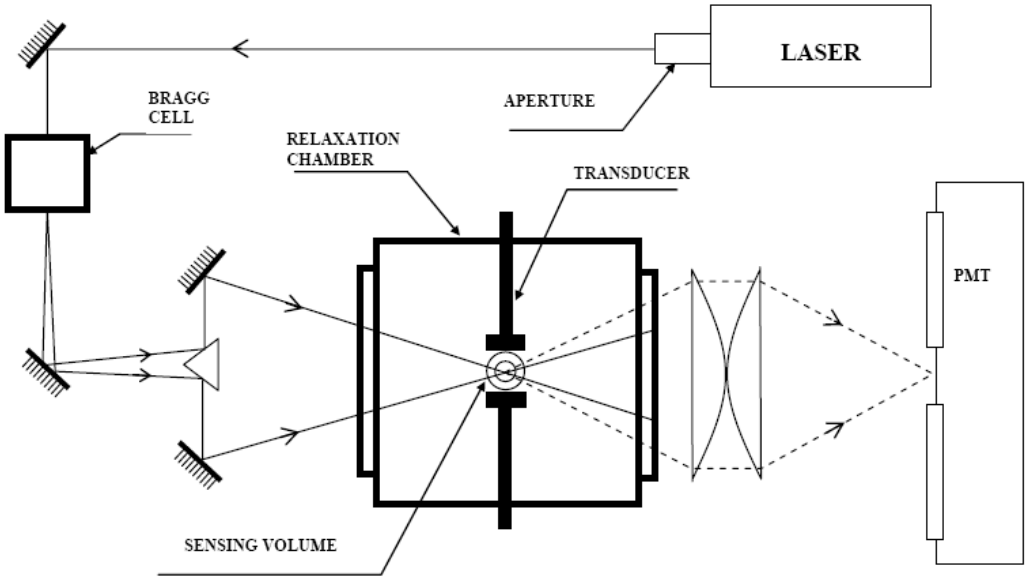

Fig. 2.6. Block diagram of the E-SPART analyzer showing the LDV optics and the relaxation chamber (Mazumder et al., 1991).

In order to obtain particle size, E-SPART analyzer measures particles relaxation time τ_p, from which the aerodynamic diameter of the particle d_p can be calculated:

$$d_p = \sqrt{\frac{18\eta\tau_p}{\rho_p}} \tag{2.1}$$

where: ρ_p the particle density and η is the air viscosity. The relationship between the particle charge and velocity can be determined by solving the equation of spherical particle motion in the presence of a uniform electrical field *E* and can be expressed as:

$$q = \frac{3\pi\eta d_p V_p}{E} \tag{2.2}$$

where V_p is the particle velocity. In the later AC version of E-SPART analyzer, particles are subjected to the oscillating electric field ($E_0 sin\omega t$) only. The relaxation time is obtained from the phase lag in the same manner as for the acoustical E-SPART analyzer. The particle charge in this case, however, is calculated from the following expression:

$$q = \frac{3\pi\eta d_a |V_p|}{E_0}(1+\omega^2\tau_p^2)^{0.5} \qquad (2.3)$$

Both versions of E-SPART are capable of measuring the size and charge distribution of aerosol particles of both polarities. While AC-E-SPART Analyzer is applicable only to charged particles the acoustic version of E-SPART Analyzer can be used for both charged and uncharged species. The E-SPART Analyzer presents very elegant approach and as one of the few instruments offers the capability of measurement simultaneously particle size and charge in real time, however the analyzer also has its own limitations. First only relatively small aerosol volume can be measured with the typical count rate between 100 to 200 particles per second. As already highlighted, this is not a problem with relatively stable atmospheric aerosols. However in case of rapidly evolving, short duration aerosols this sampling rate may not be sufficient to provide representative information of charge distribution in aerosol plum. DC E-SPART Analyzer can be used to measure both uncharged and charged particles with the q/m up to 20μm/g. However, for higher charge levels the particle losses due to the sampling system caused significant error in the charge measurement. Moreover, in the DC field some highly charged particles are precipitated and deflected without reaching the sensing volume. Another measurement problem is due to the acoustically induced flow turbulence. This flow turbulence cased by acoustically generated flow field as well as troublesome multiple reflections inside the operating region (due to short wavelength of acoustic waves) affects the accuracy of the measurement. The AC version of the E-SPART Analyzer solved the problem of the acoustically induced flow turbulence and the sampling losses caused by the DC excitation. However, the main weakness of the AC sinusoidal excitation method in conjunction with the LDV is that the uncharged particles will not respond and the aerodynamic diameter of particles having low charge will be measured with the decreased accuracy.

2.4 ESRG Bipolar Charge Measurement Systems

The main problem in characterization of bipolarly charged aerosols is to separate the particles carrying charges of opposite polarity. The basic idea developed by Hrabar & Balachandran (1998) employs a coaxial electrode arrangement as shown in Figure 2.7. The system incorporates a front-end cylindrical arrangement consisting of two "D" shaped precipitation sections. Each of these sections incorporate wire electrodes maintained at high potential of opposite polarity. The interface between the two "D" sections is a thin wedge, the front-end of which acts as a bifurcation for the incoming aerosol. The test aerosol is drawn through the bifurcation separator using a suction pump, and subject to an appropriate electric field. Depending on the electric field distribution and air flow characteristics particles of opposite polarity to that of the potential applied to the wire electrodes will exit the separator. This separation section is connected to a series of five "D" –shaped Faraday Chambers to collect the unipolarly charged aerosol of different charge to mass ratio.

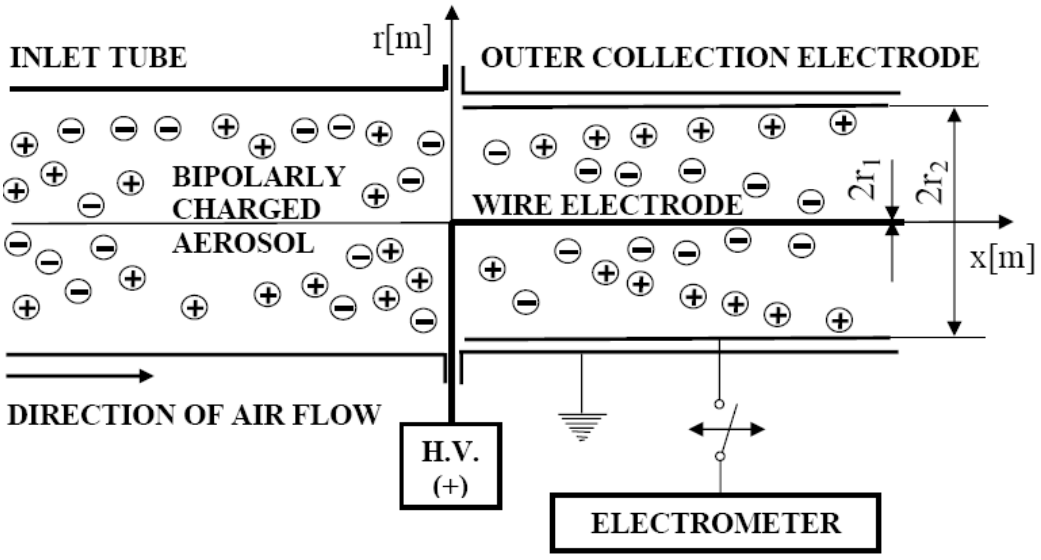

Fig. 2.7. The basic arrangement for the charged particles separator (Hrabar et al., 1998).

The main difference between this arrangement and an ordinary electrostatic precipitator is that the applied high voltage should be lower than the corona onset voltage to avoid intentional charging of the aerosol particles within the device. As shown in Figure 2.7 the particles of the bipolarly charged aerosol are drawn into the inlet tube by a continuous flow of air. It is assumed that the airflow is axisymmetric, laminar, fully developed, and

incompressible. If the electric field fringing effects are neglected, then the electric field within the precipitator will have a radial component with intensity given by:

$$E = \frac{1}{r}\frac{U}{\ln(r_2 / r_1)} \tag{2.4}$$

where: E is the electric field strength, U is the applied voltage, r_2, r_1 are radii of the tube and inner electrode respectively, and r is the radial position. The velocity of the charged particle v_p is given by:

$$\vec{v}_p = \vec{v}_f + \frac{m_p}{6\pi\eta r_p}\vec{g} + \lambda_p \vec{E} \tag{2.5}$$

$$\lambda_p = \frac{q_p}{6\pi\eta r_p} \tag{2.6}$$

where: v_f is the velocity of air, λ_p is the mobility of the charged particle, m_p is the mass of the particle, r_p is the particle radius, q_p is the charge of the particle and η is the viscosity of air. It is initially assumed that the electric field strength is high enough so that the force acting on a charged particle due to gravity is negligible in comparison with the electric force. The experimental results indicate that the constructed instrument can be successfully utilised for charged aerosol characterization by establishing the levels of positively and negatively charge particles present in the aerosol. Since the instrument consists of a series of horizontally positioned measurement chambers it is capable of measuring spatial depositions characteristics of an aerosol and hence provide a means to resolve distribution of particle charge to mass ratio. This is useful especially in the inhalation therapy where it has been shown that particle charge can influence aerosol deposition in human lungs. As presented by Kulon et al. (2001) this basic ideea for separating bipolarly charged aerosols has been developed into a bipolar charge measurement system, as shown in Figure 2.8.

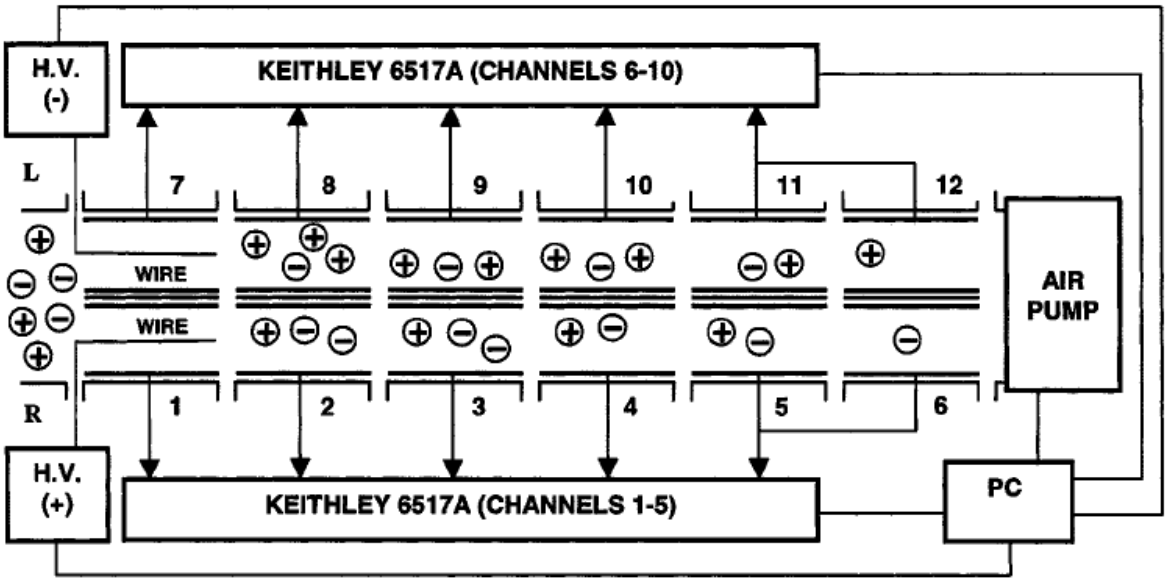

Fig. 2.8. Bock diagram of the bipolar charge measurement system. (Kulon et al., 2001).

The aerosol is delivered into the measurement system using a Copley (Twin Impinger) vacuum pump. The laminar air flow within the precipitator section was ensured by adding another tube section to the inlet with the same diameter. The length of this tube was selected to ensure that the shape of the flow profile at its end was parabolic. Furthermore, it can be shown that the presence of relatively thin wire electrodes (1-mm diameter) inside the tube (39-mm diameter) does not significantly disturb the air flow. The bifurcation-separator device is followed by five sets of "D"-shaped charge measurement Faraday chambers. Once the pump is activated, the aerosol particles are sucked into the system, and two equal fractions enter into the bifurcation sections. The aerosol fractions are subjected to an appropriate electric field. The particles with different range of electrical mobility exiting the precipitator will be gradually deposited in the measurement chambers. The accumulated charge on precipitator and each of the Faraday chambers is measured with a Keithley 6517A electrometer incorporating a ten-channel scanner card. All devices are interfaced to a personal computer via an IEEE-488 interface. The precipitator design was optimized to operate only for particles with the charge to mass ratio (q/m) within a certain range. However, during the operation of this instrument the potential applied to the wire electrodes need to be predetermined such that precipitation efficiency reached the highest level. At the same time, the potential applied to the wire electrodes must be maintained below the corona onset voltage. This voltage was first estimated theoretically from field distribution modelling software. The results obtained for 1-mm-diameter wire indicated that no ion generation should be present for potentials less than 5 kV. This finding was further confirmed by

measuring the ionic current captured by the precipitator tube when positive or negative potentials of magnitudes up to 6 kV was applied to the wire electrodes. The current values detected were less than 10 A, confirming the absence of corona current for potentials below 5 kV. The accuracy as well as the calibration test of an array of electrodes (i.e., open-ended Faraday chambers) attached to the outlet of the precipitator section was carried out experimentally. A DC potential of a known level was applied to each measurement electrode separately and the level of transferred charge as well as the charge acquired by neighbouring electrodes (in both sections) was measured using a Keithley 6517A electrometer. It was concluded that the error due to the shape and geometry of the electrode arrangements was less than 5%.

The working principle of this system relies on an electrostatic precipitator technique in conjunction with aerodynamics. The geometrical features of the precipitator sections were optimized using commercially available software packages, MAFIA and FLUENT, dedicated for solving electric field and fluid dynamics, respectively (Figure 2.9).

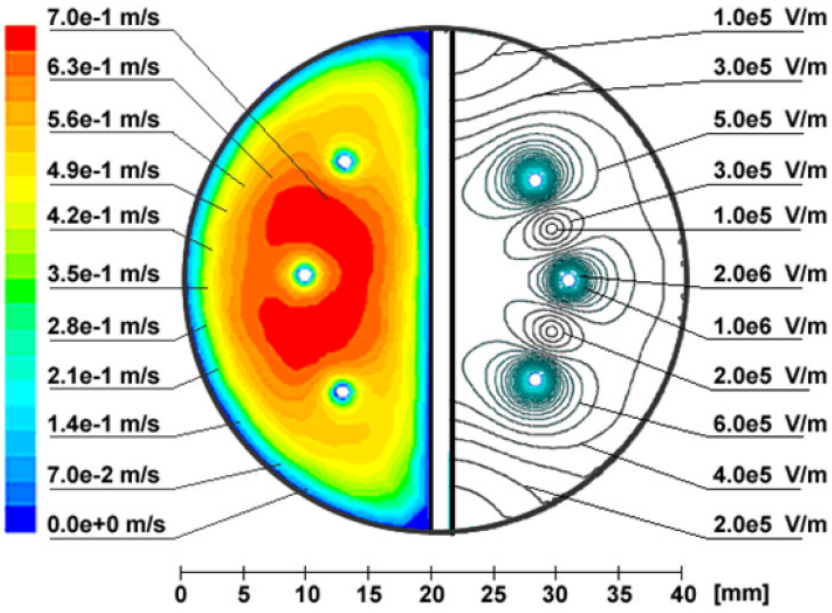

Fig. 2.9. Electric field (right) and velocity contour (left) inside the precipitator. (Kulon & Balachandran., 2001).

The main criteria used for optimization was to generate the required field strength distribution in the whole volume of the precipitators, necessary to achieve desirable particle precipitation without exceeding corona onset. Both the number and location of wire electrodes positioned inside "D"-shaped precipitator tubes, which are required to induce efficient precipitation of particles of opposite charge were established. The combined effect

of an electric field and the aerodynamics eliminated one polarity aerosol in each of the "D"-shaped precipitator tubes. The results of the preliminary experimental study indicate that the constructed instrument can be successfully used for charged aerosol. However, the experimental tests carried out with selected aerosol dispensers showed that the instrument is capable of characterizing bipolarly charged aerosols. Since the instrument consist of a series of horizontally positioned measurement chambers, it is also capable of measuring spatial deposition characteristics of an aerosol and hence provide a means to resolve the distribution of particle charge to mass ratio.

Kulon & Balachandran (2003) developed another noninvasive method of measurement of the charge level on a population of particles employing the Phase Doppler Anemometry (PDA) technique (Figure 2.10). The PDA extends the capabilities of the LDV (used by Mazumder et al., 1991) to simultaneous measurements of velocity and size of the scattering particles with a relatively high data rate of analyzed particles, typically greater than 1000 particles per second. A first step in improving the efficiency of an inhaler device is the correct characterization of the size and charge of aerosols. While there are well established methods of particle size measurement as presented, the charge measurement remains a challenge, especially when we intend to measure them simultaneously. First an analytical study was made in order to solve the equation of particle motion in a viscous medium in the presence of a DC field, followed by an experimental study using Phase Doppler Anemometry technique to measure the charge and size on a population of particles. Also a comparison study was made regarding particle charge and size distribution under different charging conditions: natural charged aerosols and using a positive or negative corona discharge. The experiments were conducted on dioctyl phthalate aerosol droplets produced by nebulising isopropanolic solutions using a Medic-Aid Sidestream nebulizer (Figure 1.7). Various mechanisms intervene during the aerosol droplet formation in such a device and the results showed, as previously stated, that the triboelectrically charged liquid droplet dispersion is often bipolarly charged. Applying a corona discharge proved to be an efficient technique in producing predominantly unipolar charged droplets. In addition to this the negative corona seems to have a better influence in charging the aerosols because particles are charging better when electrons represent the charge carriers.

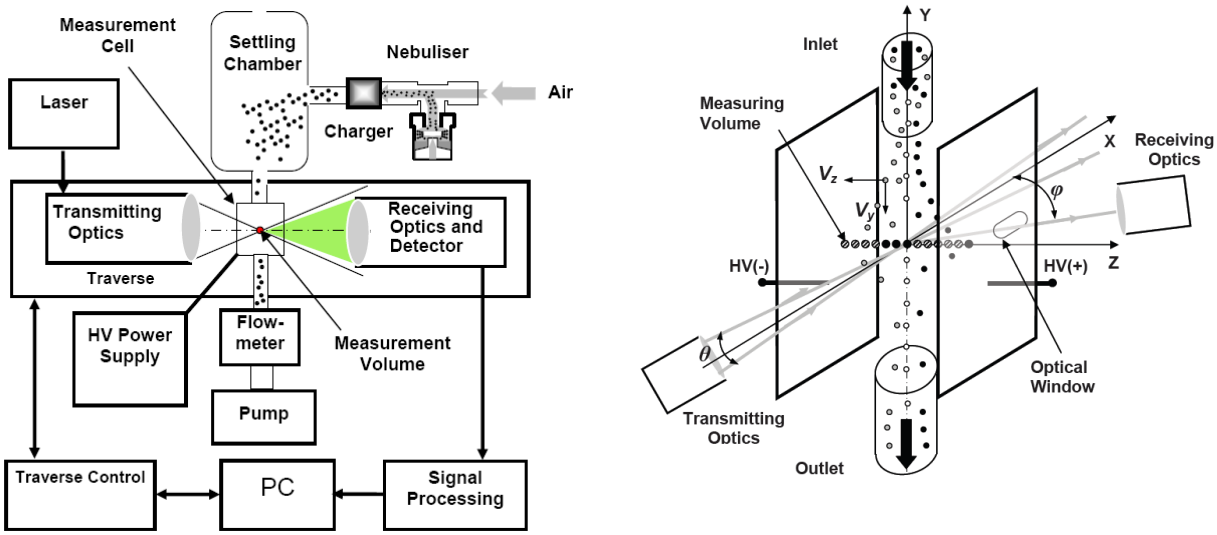

Fig. 2.10. Block diagram of the measurement system (left). The measurement cell with optical window (right). Two laser beams intersect in X-Y plane, φ is the scattering angle, θ is the angle between the incoming laser beams, V_z and V_y are the horizontal and vertical component of particle velocity measured by the PDA (Kulon & Balachandran., 2003).

The data collected from the measurements permitted also other interpretations regarding the particle charge distribution for different size fractions, relative number and average particle charge to mass ratio of aerosols made with a probe in different measuring points inside the plane electrode system.

The system consists of a DANTEC Measurement Technology PDA instrument, measurement cell with optical windows, Medic-Aid Sidestream nebulizer with attached corona charger, settling chamber, vacuum pump, precision flow meter, and the HV power supplies (Figure 2.10). The PDA system comprises the argon ion laser, transmitting and receiving optics, signal processor unit with two velocity channels, PC with an interface board for further processing and storage of data, and a high-precision traversing system. The traverse system is step-motor driven, with the motor directly attached to the high-precision lead screws. Safe positioning of the PDA is achieved with a brake on the vertical axis. Movements of the traverse are controlled either by Dantec Dynamics application software or by an optional manual control unit and PC adapter. The PDA system characteristic parameters are listed in Table 2.1. Channels 1 and 2 correspond to the velocity components measured by the system. The velocity is the drift velocity due to the electric field.

Table 2.1. PDA System characteristics. (Kulon & Balachandran., 2001).

Optical Parameters	*Transmitting Optics*		*Units*
	Channel 1	*Channel 2*	
Laser wavelength	514.5	488	nm
Gaussian Beam diameter	1.35	1.35	mm
Beam separation at focus lens	70	70	mm
Focusing lens focal length	310	310	mm
Fringe spacing	2.29	2.17	μm
Number of fringes	34	34	μm
Measurement volume diameter	77	73	μm
Receiving Optics			
Scattering angle	70		deg
Collection lens focal length	310		mm
Particle refractive index	1.48		

Since the scattered light intensity from the different scattering modes varies at different scattering angles, a linear relationship between measured phase difference and particle diameter exists only if the detector is positioned such that a single light-scattering mode dominates. The first-order refraction as a dominant scattering mode was selected in the experiment. In order to avoid contribution from the reflected light and satisfy the linearity requirement, the optimum scattering angle of 70 (known as: Brewster angle) was chosen in combination with the parallel polarization. Prior to the measurement, an analysis of the linearity of the phase-diameter relationship was performed. This optical arrangement of the anemometer allowed measurement of droplet diameters down to 0.5 μm.

The aerosol being measured is drawn from the settling chamber through a 7-mm-diameter inlet tube to the measurement cell (Figure 2.9). The measurement cell is a cube with optical windows incorporating two parallel-plate electrodes. The separation distance between the electrodes was 20 mm. A dc potential of 5 kV was applied between the electrodes. To ensure the uniformity of the electric field within the cell and control the electric field fringing effect the edges of the electrodes were rounded. As soon as the charged particles enter the cell they are deflected toward the electrodes. Due to the very small relaxation time analyzed particles almost instantaneously attain their terminal velocity. In order to capture a wide range of charged particles, the probe volume was moved between the parallel plates. The successive positions for the measuring volume are shown in Figure 2.10. A low flow rate of 0.06 L/min was maintained throughout the measurement to ensure laminar flow. The Reynolds's number for the flow-in pipe was about 10, indicating that the flow was indeed smooth and laminar. Scattering signals obtained from nonspherical particles were rejected

using a validation method based on comparing phase-shift difference on two pairs of detectors. If the phase shift exceeded 10% the reading was discarded by the signal processing unit. However, more than 95% of the measured droplets satisfied this criterion. The corona charger used in the experiment employed coaxial electrode arrangement. It comprises of a metallic grounded tube with the radius of 8 mm and a coaxial wire electrode with the radius of 0.025 mm maintained at high potential of 4.5 kV. The length of the corona wire and the grounded tube was 10 and 30 mm, respectively. For the given applied voltage and the geometry of the charger and the measured corona current for positive and negative potential was 2.0 and 4.5 μA, respectively.

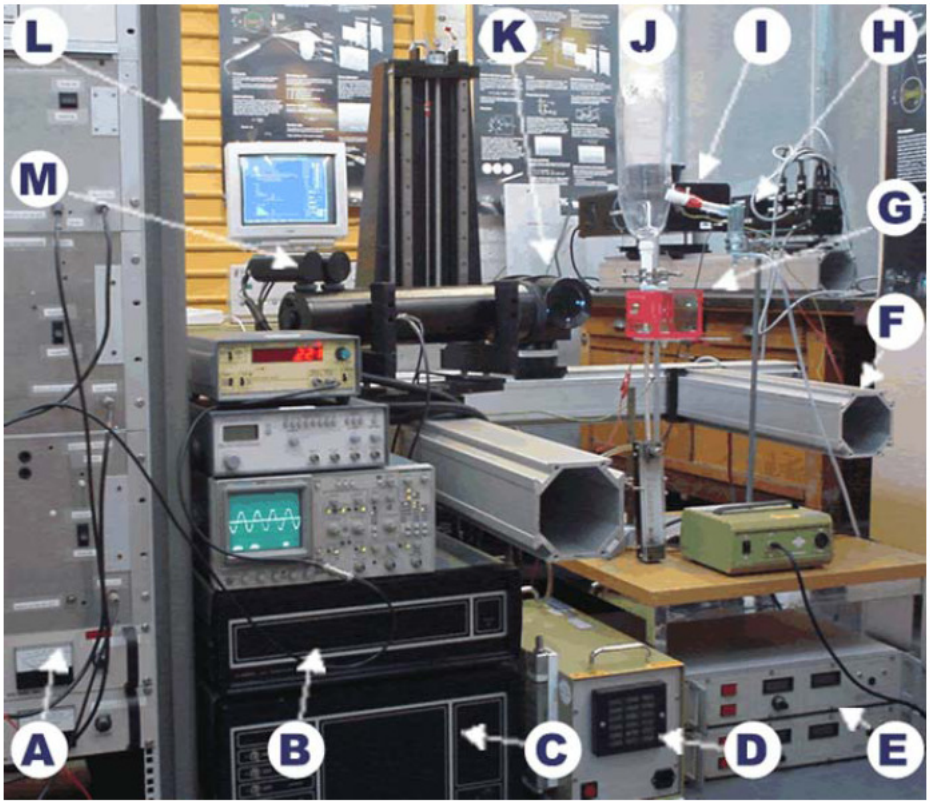

Fig. 2.11. Particle Experimental Arrangement (A – AC High Voltage Power Supply, B – Traverse Control System, C – Signal Processing Unit, D – Pump, E – DC High Voltage Power Supply, F – Traverse, G – Measurement Cell, H – Nebuliser, I – Corona Charger, J - Settling Chamber, K – Transmitting Optics, L – Data processing Computer, M - Receiving Optics) (Kulon & Balachandran, 2003).

The experimental results demonstrate the capability of the technique to determine in real-time particle size and charge distribution. The method does not require calibration, provided that the particle refractive index as well as PDA optical parameters are known accurately. Theoretically the instrument can measure the charge on particles from just a few electrons to almost a saturation level with an accuracy depending on the accuracy of velocity

and particle size measurement, which is usually very high for PDA systems (±0.5%). The number of particles analyzed per second using the PDA system is limited by the coincidence loss and the requirement to maintain laminar-flow within the measurement cell. In the experiments performed the particle count rate varied between 1000 to 2000 particles per second, which is still sufficiently large to provide good statistical representation. However, in the case of highly concentrated unipolarly charged aerosols, the additional error caused by the electric field induced by the space charge has to be taken into account.

3.5 Conclusions

Interparticulate occurring in pharmaceutical powders, dry powder inhalation formulations, and the electrostatics of particles are important surface properties having a significant impact on therapeutic and pharmaceutical performance. Surface charge has also been shown to affect cellular response activity, in vitro. Electrical aerosol measurements date back many decades and have many important applications in medicine and the pharmaceutical sciences. Triboelectrification and triboelectric charging of pharmaceutical powders as a function of surface properties and relative humidity have been investigated. Additionally, electrostatic charging in lactose monohydrate during melt agglomeration and effects of surfactants on charging have been demonstrated. The effect of amorphous content on the triboelectrification of spray-dried lactose monohydrate powder results in increased charge generation with increasing amorphicity and detection of amorphous contents <1% is possible with electrostatic experimental methods.

Techniques for electrostatic measurements and surface potential include Faraday pail method in aerosol charge measurements. Faraday cup measurements of the electrostatics of lactose and glucose powders and air stream Faraday cage measurements of the charge distribution in interactive drug systems have been reported. Bipolar charge measurements on pharmaceutical aerosol powders by using a grid probe, a static Faraday pail/air stream Faraday, and an electrical single particle aerodynamic relaxation time (E-SPART) analyzer to study the charge of aerosols and simultaneous measurement of particle size and particle charge have also been reported. Electrostatic force microscopy has been applied also. E-SPART analyzer has been used in the electrostatic charge and aerodynamic size distributions analysis of poly (D, L-lactide-coglycolide) microspheres (with and without surface coating) in DPIs. Some shortcomings in using Faraday cage methods include an inability to decipher the relationship between the charge and size distributions of the aerosol, and just as importantly, to do so in

real-time. An electrical low-pressure impactor (ELPI) makes it feasible to measure the charge of different particle size fractions in real-time of aerosolization from 10 mm down to 30 nm divided over 13 inertial impactor stages. Each stage is connected to its own individual sensitive electrometer that measures the current at the femto ampere (fA) level of the charged particles following deposition. Furthermore, the mass of deposited aerosol on each stage can be weighed using a high-sensitivity electromicrobalance. ELPI has been successfully used in sizing pMDI particles down to 10 nm for commercially available pMDI products. A predictive lung deposition model, which accounts for the depositional effect of charge on aerosol particles, has been developed with regard to total and regional deposition. Electrostatic properties of aerosols can affect deposition in the lung. It was shown that free ions are deposited very effectively in the upper lung airways whereas charged particles penetrate to the deeper lungs. Measurements of charge are of two types:

- Static methods involve direct charge measurements and rely on charge transfer or induction using a complete or incomplete Faraday cage. The particle charge is usually transferred through a conducting collector to a capacitor or more precisely shared between the particle and the capacitor and subsequently measured by the electrometer. The static methods have been further divided into two categories such as contact and non-contact methods. They tend to be limited to particles of high charge or aerosols that have unipolar charge. Contact methods require the particles to contact the conducting collector and give up their charge, while non-contact methods rely on the measurement of the induced signal as the particle travels in the vicinity of the measuring probe. The relationship between the induced signal and the particle charge is usually established as a function of the geometry of the charge-sensing electrode. However, it should be noted that this classification does not preclude the possibility where the induced signal is also present and measured using contact method or the occurrence of particle-electrode contact in non-contact techniques. The determining factor whether a given method is classified as contact or non-contact depends on how the majority of measurements are performed.
- Dynamic methods usually involve subjecting the aerosol to a high electric field, measuring or inferring the velocity that the particle reaches and relating this to the electrical mobility. The charge on small particles can easily be measured in this way, but the drawback so far as population measurements are concerned is that the

requirement for details of both size and charge necessitates a large number of "bins" and, therefore, a long sampling time.

The Bipolar Charge Measurement Systems (BCMS) developed at Brunel University by Prof. Balachandran research team can provide fast, simultaneous measurement capability of the bipolar charge fractions on pharmaceutical aerosols delivered from the medical dispensers, primarily in the particle size range between 1 to 10μm. The BCMS employs the principle of particle separation by means of the electric field acting perpendicular to the flow-field. The designed integrated flow bifurcator-precipitator is composed of two ("D" shape) sections incorporating three inner wire electrodes, which are energized with the high potential. As the charged particle travels through the BCMS, it is precipitated and deposited on the surface of the collection electrodes where it gives up its charge. The combined effect of the electric field and the aerodynamics effectively eliminates one polarity of the charge in each of the "D"- shaped section of the precipitator. The total aerosol charge of both polarities is measured directly by the sensitive electrometer. The mass of aerosol deposited in each section can be obtained by washing it into a small volume of solvent and quantifying using one of the analytical methods such as high-performance liquid chromatography (HPLC). The BCMS offers several advantages compared to other bipolar charge measurement techniques. First, the BCMS is efficient and robust in detecting the instances of bipolarities in medical aerosols existing in the form of short duration, rapidly evolving aerosol plumes. Secondary, the overall picture of aerosol bipolar fractions is gained almost instantaneously with minimum particle loss in the system. In addition, the fabrication of the BCMS is very simple and straightforward with no exotic materials or production processes required. Finally, the operation of the BCMS is simple, and should require only occasional cleaning and maintenance. As a result, the BCMS should be relatively inexpensive to build and maintain. However, several problems with the BCMS can also be pointed out. The complicated geometry of the precipitation-bifurcation section together with the multiple high-voltage electrodes arrangement results in highly non-uniform electric field and fluid velocity distribution. While this is not inherently problematic in terms of the operation of the BCMS, it does complicate the analysis of the particle precipitation and separation process. The instrument gives only the total bipolar charge of aerosol without details of particle charge distribution within the aerosol plum. In order to address these shortcomings and improve the BCMS performance further research needs to be carried out.

A non-invasive method of measurement of the charge level on a population of particles using the Phase Doppler Anemometry (PDA) technique working in conjunction with a high-resolution computer controlled traversing system was presented. The PDA was used to track the velocity of charged particles of charged particles in the presence of a DC and AC electric field. By solving the equation of particle motion in a viscous medium combined with the simultaneous measurement of its size and velocity, the magnitude as well as the polarity of the particle charge can be obtained. The PDA technique is capable to determine in real-time the particle size and charge distributionon a population of aerosols. The method does not require calibration, provided that the particle refractive index as well as PDA optical parameters are known accurately. The number of particles analyzed per second using the PDA system is limited by the coincidence loss and the requirement to maintain laminar-flow within the measurement cell. In the experiments the particle count rate varied between 1000 to 2000 particles per second, which is still sufficiently large to provide good statistical representation.

Table 2.2 contains a summary of the particle size analysis techniques that are currently in widespread use for the evaluation of medical inhalers, showing the operating principle, size range and inhaler types for which they are most applicable. Most particle sizing methods used for inhaler aerosol assessments are invasive, in that they require either a sample or the entire aerosol produced on actuation to be collected by the measurement equipment. Techniques that are based on either inertial impaction or time-of-flight (TOF) both determine aerodynamic diameter. However only multi-stage CI's or liquid impingers directly provides the mass-weighted data that are more relevant than the corresponding count/number-weighted size distribution results in predicting the mass of API likely to be delivered to different parts of the respiratory tract.

Table 2.2. Summary of particle sizing methods used to characterize medical aerosols from inhalers. (Mitchell & Nagel, 2004).

Technique	Operating principle	Size range (μm)	Assay for API	Direct Measure of Aerodynamic Diameter
Cascade impactor (CI) multi-stage liquid impinger (MSLI)	Inertial size separation in laminar flow	0.1 -15 μm overall range, but varies from one instrument to another. CIs typically have 7-8 stages. The current MSLI has 4 stages_back-up filter.	YES	YES
Single stage impactors/ Twin Impinger (TI)	Inertial size separation in laminar flow	Cut size chosen to separate coarse from fine particles likely to penetrate the lower respiratory tract (*e.g.* 6.4 μm for TI at 60 L/min).	YES	YES

Particle time-of-flight (TOF)	Particle acceleration in ultra- Stokesian flow; transit time between two detectors	Aerosizer® (no longer available): 0.2 - 200 µm, extendable to 700 µm with larger nozzle. TSI 3603 PSD analyzer is successor: 0.2 - 700 µm TSI 3321 APS® with 3306 impactor inlet: 0.5 - 20 µm.	NO	YES
Laser diffractometry (LD)	Low angle laser light scattering	0.5 µm - 3 mm overall range, but varies from one instrument to another.	NO	NO
Phase-Doppler particle size analysis (PDA)	Phase shift observed by several detectors observing particle interaction with interference fringes formed from intersecting laser beams	0.3 - several hundred µm. Precise range depends upon the optical configuration chosen. Particle velocity can also be measured in 1-, 2- or 3-components of direction, depending on sophistication of measurement system.	NO	NO

Chapter 3

Investigations of Electrical Properties of Pharmaceutical Powders

3.1 Introduction

When two solid surfaces make contact, charge transfer can occur at the contact surface. It has been observed that powder and granular material acquire a significant level of charge when transported inside dielectric channels. This is indeed a complex process since there are several "unknowns" and variables in the contact event, i.e. contact pressure, contact area, contact time, material behaviour (fracture, deformation and possible material transfer from one surface to another).

In Dry Powder Inhalers (DPI's) the powder formulation is dispersed primarily using aerodynamic forces created by the patient during inhalation process. While the powder sample is exposed to the high velocity air, the particles gain a significant velocity and start interacting with each other and inhaler walls, including cyclone and or baffles. During the high-speed transportation and interaction, the stream of powder formulation is assumed to be separated into drug and carrier particles. In these processes, powder particles may acquire some additional charge, which is likely to significantly influence the level of their initial (inherent) charge. The level and polarity of charge on the particles will depend on the contact and separation processes that will occur within the device. The consequence of the charge accumulation on the powder particles as well on the surfaces of the channels inside the inhaler may be two-fold. Firstly, the powder may experience an enhanced deposition on the channel surfaces due to electrical attraction created by the image forces as seen in Figure 3.2 Finer particles usually can acquire higher charge levels due to triboelectrification and consequently may contribute towards retention in the hopper. This very much depends on charge propensity of both materials and the local electric field generated within the device due to triboelectrification. Furthermore, Van der Waals and capillary forces will also play a role in powder retention within the hopper and within the cyclone. This phenomenon may in turn contribute to the fluctuation of drug concentration in the emitted dose. Secondly, the aerosol plume emerging from the device may be significantly charged, which in turn may have some effect on drug deposition pattern within the patient's respiratory tract. In order to

control inhaler characteristic with respect to drug dose and it's charge level, it is essential that the origin and nature of these charge related phenomena are well understood and documented.

3.2 Factors Affecting Electrostatic Charge of Powders

- **Contact surface** can be modified by adsorbed impurities or adhered particles. For example a stainless steel surface cleaned in different ways after triboelectrification of lactose, shows considerable difference in charge values for the lactose powder sample. Thus it is important to consider the state of contamination of a contact surface prior to undertaking triboelectrifications experiments. In our experiments all the surfaces that came in contact with the lactose sample were cleaned with alcohol.
- **Surface roughness** comparing various smooth and rough surfaces i.e. steel surfaces, show a greater specific charge value for lactose with the smoother surface due to increase contact area, however these differences are not as marked as those reported for differences in surface contamination.
- **Particle size** fractions of lactose can be prepared by sieving followed by additional air jet sieving to remove fine particles which may be adhered to the courser material in the specific size fraction. Smaller particles sizes will exhibit agglomeration and an increases tendency to adhere at the contact surface, hence the triboeletrification process becomes more complex and the relationship between particle size and specific charge becomes unpredictable.
- **Moisture content** – A survey of the literature (Gotoh, 1997; Booker, 1998; Hinds, 1999; Ermolina et al., 2007; Chow et al. , 2008) reveals a complex and little understood relationship between moisture and electrostatic charging of powders. There is evidence for a decrease in charge properties of powders with an increase in moisture in the powder and atmosphere and vice versa. Recent work has shown that charging can be related to the moisture uptake properties of the powder. α - lactose monohydrate has low moisture uptake less than 1% when equilibrated over a wide range of relative humidities, whereas sodium starch glycollate for example will take up more than 10% moisture at relative humidities > 50%. Thus storage conditions of powder samples prior to use and relative humidity in manufacturing rooms need to be considered in relation to electrostatic charging during pharmaceutical processing and handling of powders.

The above parameters will significantly influence the process of acquiring electrostatic charge on powder particles.

3.3 Water Content calculation (ppm)

Relative humidity is commonly used in many applications, for this case it proves to be of the most interest because of its impact on powder manufacturing control, as low RH causes brittleness and static electricity problems, while high RH can cause swelling and clumping, regardless of temperature (This following information was extracted from the reference and application data published online by Honeywell International Inc., www.honeywell.com).

The gas laws state that the total pressure of a gas mixture is the sum of the partial pressures of the constituent gases, and that the volume ratios of constituent gases are equal to the ratios of their partial pressures. For example atmospheric pressure is the sum of the partial pressures of dry air and water vapour: $p=p_a+p_w$.

When a mixture of air and water vapour is in equilibrium with liquid water, it is considered to be saturated (RH=100%). The saturation pressure over liquid water for the temperature range of 32 to 392º F is given by:

$$L_n(p_{ws}) = \frac{C_1}{T} + C_2 + C_3T + C_4T + C_5T + C_6 \ln(T)$$

With the constants: C_1= -1.044039E+04

C_2= -1.1294650E+01

C_3= -2.7022355E-02

C_4= +1.2890360E-05

C_5= -2.4780681E-09

C_6= +6.5459673;

and p_{ws} – saturation pressure, psia (Pressure measured in psi relative to absolute temperature); T – absolute temperatre, ºR= ºF + 459.67 (Temperature measured relative to absolute zero. Rankine thermodynamic absolute temperature was used because its degrees equal the Fahrenheit degrees). The ratio of the partial vapour pressure to saturation vapour pressure at the dry bulb temperature represents the relative humidity: $RH=p_w/p_{ws}$.

Humidity ratio is the ratio of the mass of water vapour to the mass of dry air. Is is obtained by multiplying the volume ratio of the molecular weights: $W = \frac{M_w}{M_a} = \frac{18.01528 p_w}{28.9645 p_a} = 0.62198 \frac{p_w}{p_a}$

The humidity ratio, is expressed in common use in lb/lb, kg/kg or g/kg, and the ratio is multiplied by one million to obtain ppm (parts per million). Parts per million change with temperature and humidity. The absolute temperature is given by: R°=1.8T+491.67. The absolute temperature value is substituted into L_n equation to give p_{ws}, saturation pressure:

$$p_{ws} = e^{\left[-10440\frac{1}{1.8T+491.67} - 24.5749234 - 0.048636T + 0.00001289(1.8T+491.67)^2 - 0.247810^{-8}(1.8T+491.67)^3 + 6.64\ln(1.8T+491.67)\right]}$$

Combining the equations for relative humidity and humidity ratio we obtain ppm of water:

$$ppmw = 621980\left[\frac{(RH \times p_{ws})}{(14.696 - RH \times p_{ws})}\right].$$

Substituting p_{ws} will give:

$$ppmw = \frac{621980 \times RH \times e^{\left[-10440\frac{1}{1.8T+491.67} - 24.5749234 - 0.048636T + 0.00001289(1.8T+491.67)^2 - 0.247810^{-8}(1.8T+491.67)^3 + 6.64\ln(1.8T+491.67)\right]}}{14.696 - RH \times e^{\left[-10440\frac{1}{1.8T+491.67} - 24.5749234 - 0.048636T + 0.00001289(1.8T+491.67)^2 - 0.247810^{-8}(1.8T+491.67)^3 + 6.64\ln(1.8T+491.67)\right]}}$$

Table 3.1 shows the calculated ppm values of water for the experimental conditions. During the resistivity measurements the temperature was varying between 22 - 23.5 ºC, and the humidity between 30 - 42 %. Values are tabulated in the order in which the experiments were conducted, as these parameters were measured at the beginning of each experiment.

Table 3.1. PPM of water at different temperatures and humidities measured during the experiments.

Temperature (ºC)	Relative humidity (%)	ppm of water $\times 10^3$
22	41.4	6.8
22.5	40	6.8
22.3	34.6	5.8
22.8	35.7	6.1
22.5	38.7	6.5
22.9	30.4	5.2
23.2	30	5.3

3.4 Electrical resistivity

Electrical resistivity (specific electrical resistance) is a measure of how strongly a material opposes the flow of electric current. A low resistivity indicates a material that radily allows the movement of electrical charge (Chow et al., 2008

$\rho = R\frac{A}{l}$ where: ρ is the static resistivity (measured in Ωm);

R is the electrical resistance of a material sample (measured in Ω);

l is the length of the material sample (measured in m);

A is the cross-section area of the material sample (measured in m^2).

The resistivity of powders can be measured in a parallel-plate cell. The measurement is obtained by applying high voltage across a sample of powder packed between the two parallel-plates shown in Figure 3.1.

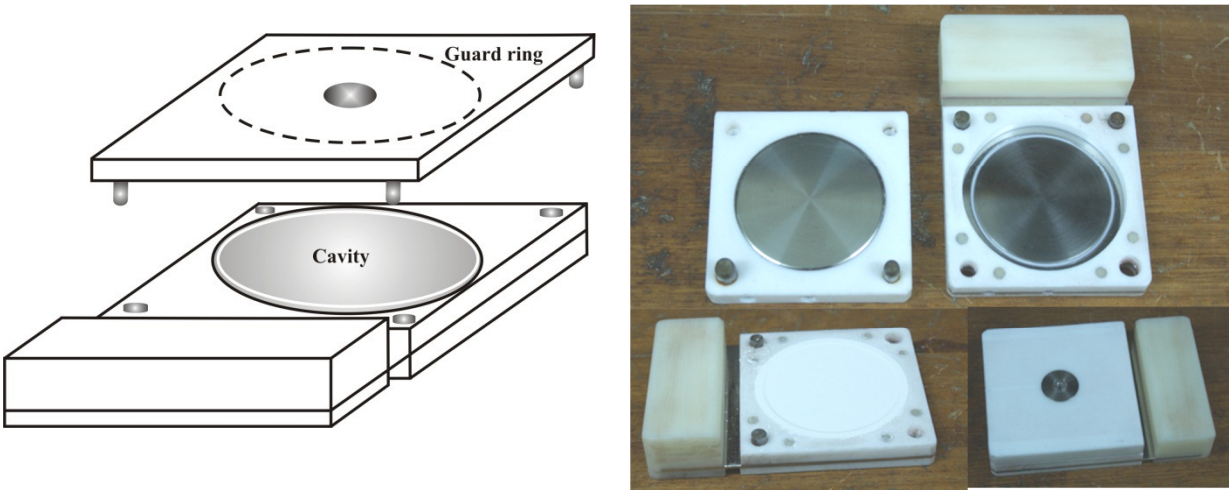

Fig. 3.1. The cell used in resistivity measurement.

The plates (electrodes) are designed to ensure a uniform electric field within the sample, and an earth guard ring is incorporated to eliminate the effect of surface conduction at the sample/cell interface. When the powder is packed firmly between the plates, its bulk resistivity, ρ, is defined as follows: $\rho = \frac{V}{I}\left(\frac{A}{d}\right)$ where: V is the applied voltage, I is the resultant current flow through the sample, A is the effective electrode area and d is the sample thickness. The ratio of the sample area, A, to its thickness, d, is known as cell constant

and in our measurement unit is equals to 0.685 m. The fin powder particles are in a more or less agglomerated state with varying in air quantities and water between the particles.

3.5 Inter-particulate forces

Forces causing primary particles to stick together have been classified as: solid bridging; liquid bridging; attraction between particles; interlocking. The adhesive force between particles plays an important role in powder-handling processes, such as dry dispersion, transportation and classification of particles. The van der Waals force, the electrostatic force and the liquid bridge are the main sources of the adhesive force. Their principle is presented in Figure 3.2.

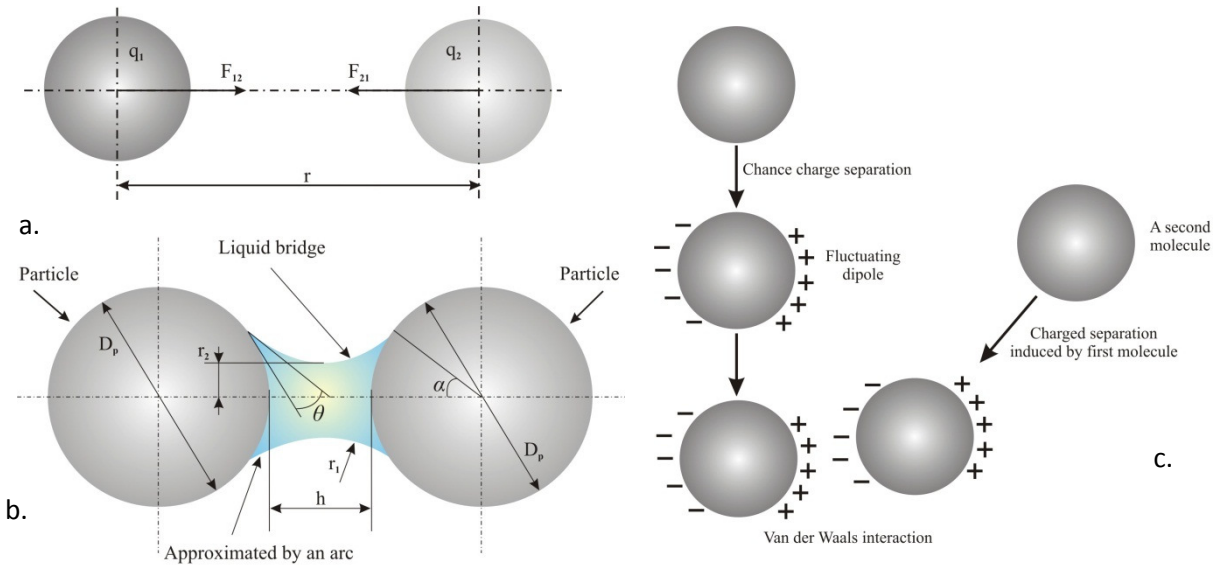

Fig. 3.2. Electrostatic force (a); Liquid bridge force (b); van der Waals interaction (c) (Gotoh et al. 1997).

The van der Waals force is a short-range electromagnetic force interacting between two molecules (or atoms). The potential energy is approximated by: $E_A = -\frac{\beta_{11}}{r^6}$; where r is the distance between centre points of two molecules and β_{11} is a constant which depends on the molecular (or atom) characteristics. In the case studied the London-van der Waals theory can be taken into account as it focuses on the microscopic level of matter, and the so called dispersion force acts between two symmetrical and electrically neutral molecules (or atoms). Therefore the fundamental equation for the calculation of van der Waals potential energy is: $E = -\int_{v1}\int_{v2} \frac{q_1^2 \beta_{11}}{r^6} dv_1 dv_2$; where: q_1 is a number per unit volume in the body and v_1, v_2 are the

volumes of the two bodies (Gotoh et al, 1997). The attraction between the particles is ascribed exclusively to London–van der Waals forces, the repulsion being due to the interaction of electric double layers, so in order to account for the stability of suspensions of comparatively large particles, it is necessary to assume that for long distances the London–van der Waals energy decreases more rapidly than R−6 (the electron energy spectra contain three down-spin energy bands and three up-spin energy bands. When there exists inter-chain coupling, energy levels split off. The energy spectra contain six up-spin energy bands and six down-spin energy bands each with 20 energy levels). As soon as the distance becomes comparable to the wave-length (=λ/2π, λ is the wavelength of light) corresponding to the excitation energies of the interacting atoms; the retardation of the electrostatic interaction between these atoms can no longer be neglected and will presumably lead to a decrease of the attractive force (Jones, 1995). Electrostatic force arises from (1) particle-charge interaction, (2) image charge effect and (3) electrostatic potential difference. Between two charged particles, coulombic force acts, and is expressed as: $F_{el} = \frac{1}{4\pi\varepsilon_0}\frac{q_1 q_2}{r^2}$; where q_1 and q_2 are the charges of the particles, r is the distance between centres of the particles and ε_0 is a dielectric constant of the medium (Horvath et al., 1982; Hinds, 1999).

Liquid bridging can form as a result of sintering, solid diffusion or chemical reaction, all of which are more likely to occur at elevated temperatures. Ex-solutions of soluble matter can form solid bridges at room temperature. In our case liquid bridging results from the presence between the individual particles of bulk liquid (i.e. water). At normal humidity fine powders may contain considerable amounts of water. The forces existing inside an agglomerate, in the presence of liquid, vary between four stages depending on the amount of liquid. The first is that in which insufficient liquid is present to completely fill spaces in the agglomerate and liquid is concentrated in saddles between particles. The second is when the gas is still present, but the liquid forms a continuous network. In the third the space inside the agglomerate is just filled with liquid. In these three stages there is negative capillary pressure in the filled saddles, and, where spaces are only partly filled, surface tension at the liquid-gas interface also contributes to the bonding force between particles. The fourth stage is when liquid coats the agglomerate and surrounds it in a droplet and surface tension forces on the outside of the drop alone keep the particles together. Once a liquid bridge is established any evaporation of liquid reduces the radii of curvature of the liquid-gas interface and thus increases the forces holding the particles together so that they approach each other more

closely. It is also possible for the liquid – particle interface to show appreciable strength. This may occur because of surface irregularities or it may result from some form of bonding between the adsorbed liquid layer and the surface on the particles. Adhesive force caused by the liquid bridge can be obtained as the sum of the capillary force and the force caused by the surface tension of the liquid as follows: $F_L = \pi r^2 P_L + 2\pi\sigma r^2$; where: r_2 is the radius of the liquid bridge, σ is the surface tension of the liquid, and P_L is the capillary pressure inside the liquid bridge (Figure 3.2) (Gotoh et al., 1997. If the cross section of the liquid bridge is approximated by a circular arc, the capillary pressure P_L is expressed by: $P_L = \sigma\left(\frac{1}{r_1} - \frac{1}{r_2}\right)$.

3.6 Charge relaxation

Ohmic charge decay of an electrically polarized powder layer placed on an electrically grounded conductive plate, will loose the polarization charge according to the known exponential relation: $q = q_0 e^{\frac{t-t_0}{\tau}}$ $where: \tau = \varepsilon \cdot \rho$; q – charge remaining after the decay during the time interval t-t_0; t – time when the charge q was measured; q_0 – initial charge at time t_0; τ – relaxation time constant; ε – permittivity of the material; ρ – resistivity of the material (Inculet, 1992; Robinson, 2002; Ermolina et al. 2007). Theoretically the relaxation time constant is independent of the chosen times of measurement t_0 and t. To determine the relaxation time constant it is not necessary to measure for example the entire charge of the powder surface. It is sufficient to measure only a fraction of the electric flux (electric charge) which emerges from the surface of the charged powder and monitor its decay in time. In our case the charge relaxation was calculated with the formula: $\tau = \varepsilon_0 \cdot \varepsilon \cdot \rho$, where ε_0 is the permittivity of the free space and is equal to $8.85*10^{-12}$ F/m, ε is the permittivity of lactose (which is our case was considered as 2), and ρ was calculated from the experimental results. In the second set of experiments a Fraser ionizer probe powered by an AC supply of 5 kV; was used to neutralize the charge of the lactose sample (Figure 3.3). The surface charge evolution was monitored using a John Chubb JCI 140 Static Monitor. The JCI 140 is a compact instrument for easy and direct measurement of the ability of materials to dissipate static electricity and to asses whether significant voltages will arise from practical amounts of charge transferred to the surface. When a unipolar charge is sprayed into the surface of a dielectric material in contact with an electrical ground, the decay no longer follows the exponential law. Some form of space charge is established within the material and under

these conditions the space charge density becomes one of the main factors which governs the decay.

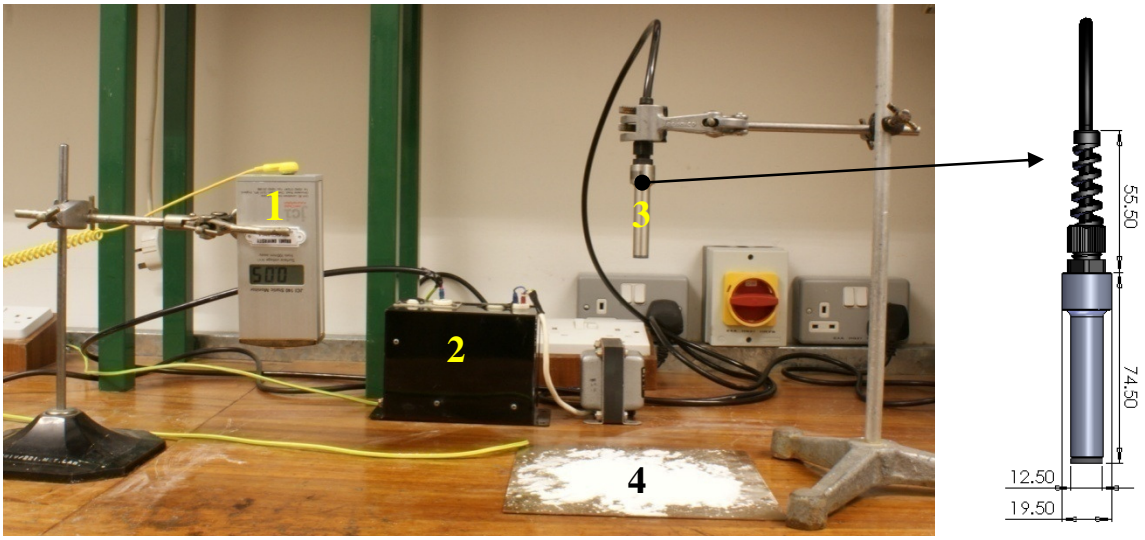

Fig. 3.3. Charge neutralization set-up: 1: JCI 140 Static monitor; 2: AC power Supply; 3: Single point static bar; 4. Lactose sample on grounded plate.

As the charge density decreases, the decay proceeds at a slower rate. If we assume that the measured unipolar charge decay over a time interval is exponential the calculated relaxation time constant under this approximation will be larger and continue to increase as the space charge density decreases. Our case becomes more complicated as the insulating powder is bipolarly charged, and we have variations in particle size - the finer&smaller ones are highly charged and agglomerated.

3.7 Material

The material investigated Lactose (Monohydrate) C12H22O11.H2O (Figure 3.4), is one of the most used excipients in the pharmaceutical industry.

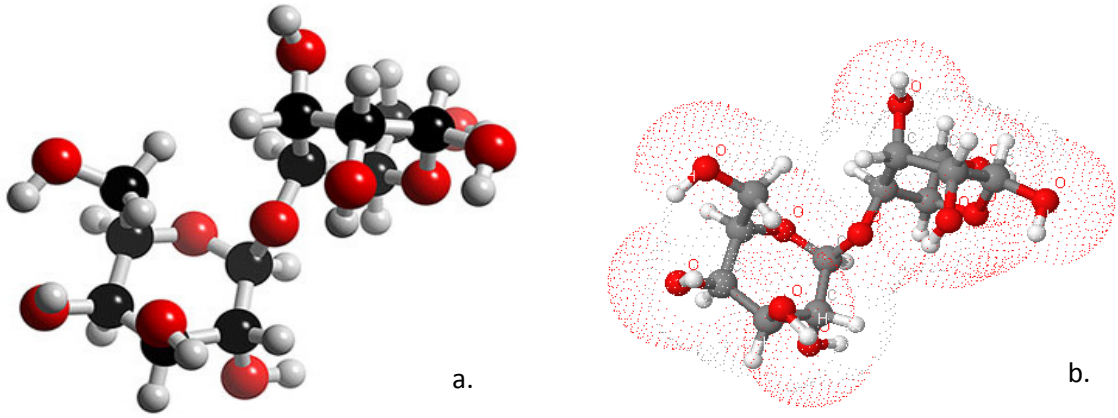

Fig. 3.4. Complex carbohydrates – Lactose: a - 3D molecular structure; b – 3D structure with elements and van der Walls surfaces (red dots). (www.3dchem.com).

Complex Carbohydrates are made up of two or more simple sugars linked together. The following carbohydrates are disaccharides. Disaccharides are compounds that contain a bond between carbon of one sugar and a hydroxyl group at any position on the other sugar. Lactose is a disaccharide that occurs naturally in both human and cow's milk. It is widely used in baking and in commercial infant-milk formulas. Like cellobiose and maltose, lactose is a reducing sugar. It exhibits muta-rotation and is a 1,4'-beta-linked glycoside. Unlike cellobiose and maltose, however, lactose contains two different monosaccharide units. Acidic hydrolysis of lactose yields one equivalent of D-glucose and one equivalent of D-galactose; the two are joined by a beta-glycoside bond between C1 of galactose and C4 of glucose (Veale, 1972; Ermolina et al., 2007).

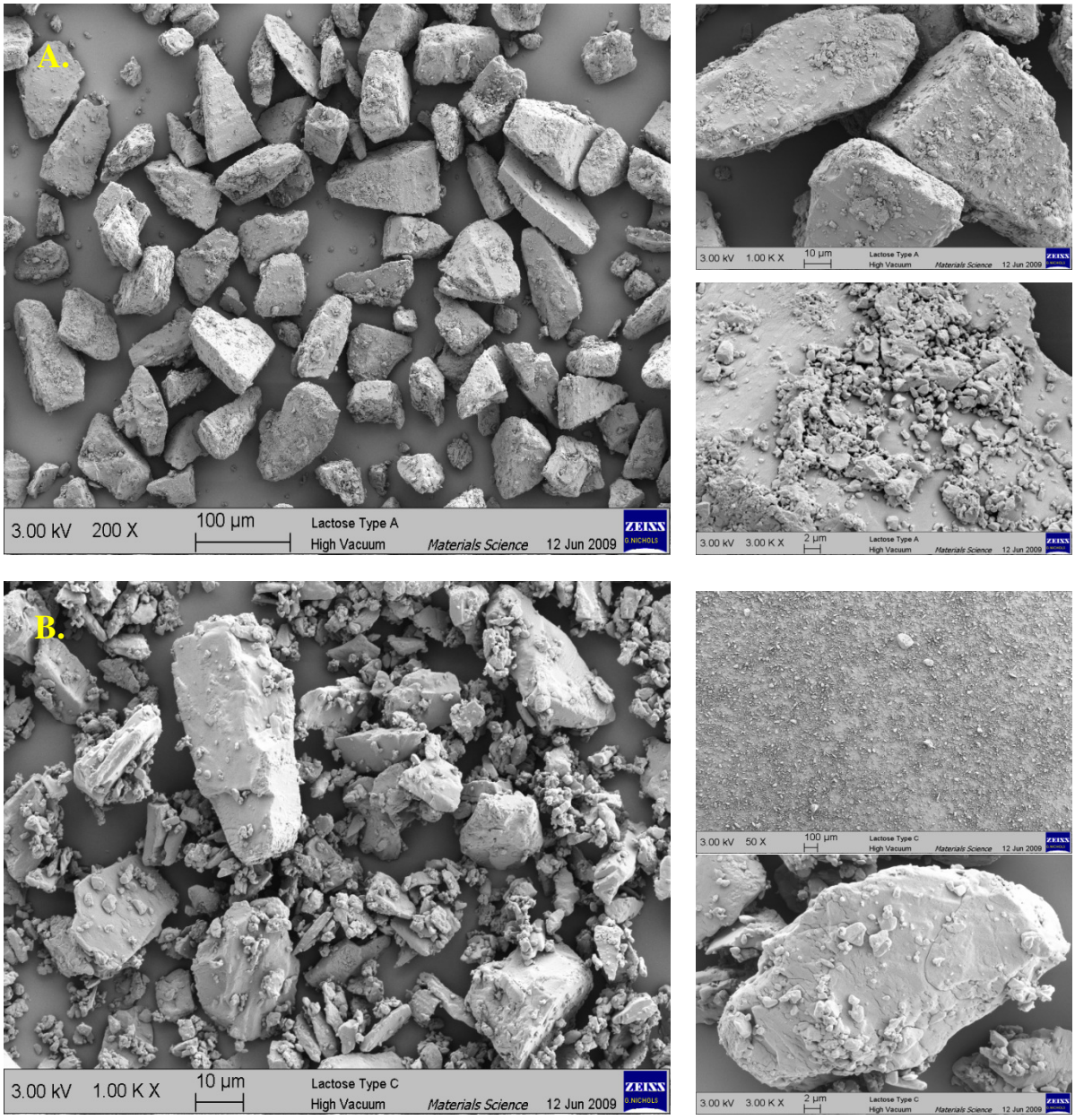

Fig. 3.5. Real-time view of the lactose samples under investigation using Scanning Electron Microscopy. a: Lactose SV003; b: Lactose milled .

There are many reasons for its popularity, such as the fact that lactose is inert (no tendency to react with other ingredients), relatively inexpensive, non-toxic and it has a long history of being applied in thousands of successful formulations world-wide. These successful formulation include Dry Powder Inhalers (DPI), Tablets, Capsules, and Sachets. In the DPI's the powder formulation is dispersed primarily using aerodynamic forces created by the patient during inhalation action. While the powder sample is exposed to the high velocity air, the powder particles gain a significant velocity and start interacting with inhaler's walls and baffles. In these processes powder particles acquire some additional bipolar charge which adds up to their initial (inherent) charge which results mainly from manufacturing processes and powder handling. Resistivity measurements were performed using lactose samples collected from different stages of the manufacturing process: Lactose A &B. The samples were supplied by Pfizer Ltd. Global research & Development, Sandwich Laboratories, United Kingdom. Micrographs of the lactose samples (Figure 3.5) were taken using Scanning Electron Microscopy.

The test materials were kept in room conditions during measurements, at a temperature which varied between 20-25 ºC and a relative humidity varying between 30-40 %.

3.8 Experimental Set-up

The experimental set-up used for resistivity measurements consists of a Spellman high voltage power supply 15kV, reversible polarity, a resistivity measurement unit and a Keithley 610C electrometer as shown in Figure 3.6.

Fig. 3.6. Experimental set-up for resistivity measurements: 1 - High voltage supply; 2 – Resistivity measuring unit; 3 – Electrometer.

Calibration of the Spellman high voltage supply was required (Figure 3.7), in order to validate the accuracy of the experimental values. This was done using a Celine high voltage differential probe which provides a safe mean of measuring circuits with floating potential up to 1000 V from earth to ground and up to 1300 V differential. Accuracy is +/- 3%, input impedance is 8 megaohms, 3.5 pF between inputs.

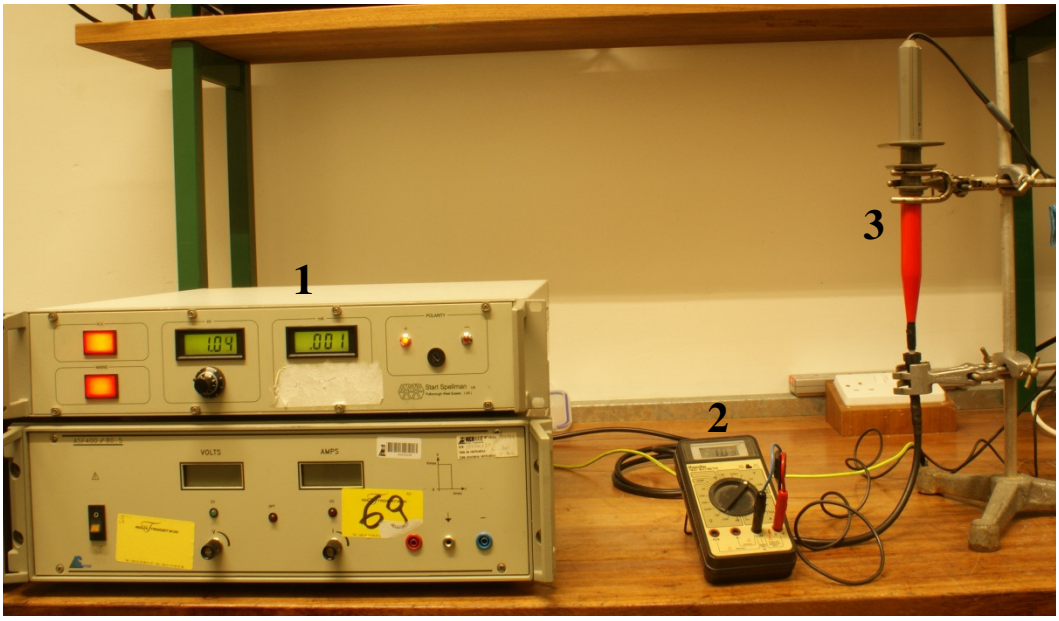

Fig. 3.7. Experimetal set-up for high voltage supply calibration: 1 - High voltage power supply; 2 –Multimeter; 3 – High voltage probe.

3.9 Experimental procedure

Once the experimental set-up is set connectivity and ground connections are checked. Before each measurement the resistivity cell is cleaned with alcohol in order to remove impurities and lactose particles which remain after each previous measurement. A small quantity of powder is taken from the bags using a plastic spoon (13-18 g depending on the sample under test) and poured into the measuring cell. The use of a plastic spoon will add additional electrical charges to the sample throught triboelectrification, however the charge levels will not influence significantly the sample behaviour during experiments. In the second stage of the experiments the powder is neutralized using an AC ionizer, and then gently poured into the measuring cell. Then the powder sample is packed firmly between the plates; the surplus is removed and the cell is introduced into the resistivity measuring unit. The values of temperature and humidity are checked. Voltage is increased slowly in steps of 0.1 kV, at each step the value of the current will be displayed on the electrometer as soon as the zero check function is deactivated. After each current reading the zero check function is reactivated to

avoid erroneous results due to residual currents or static charge. This procedure is repeated until we reach the breakdown point. After this the sample is weighted and replaced by a new sample, not before careful cleaning of the measuring cell with alcohol.

3.9.1 Experimental results for bulk resistivity measurements

The following results were obtained after multiple sets of experiments conducted using the lactose samples. In order to conclude the values of resistivity, the experiments were repeated several times in the same ambient conditions.

Table 3.2. Experimental results for bulk resistivity measurements.

Bulk Resistivity Measurements	
Temperature	22 - 24 °C
Humidity	33 - 42 %
ppm of water	5.44×10^{3} - 7.84×10^{3}
	Resistivity ρ
Lactose ML001	0.5×10^{9} - 2.5×10^{9} Ωm
Lactose SV003	0.4×10^{11} - 1.5×10^{11} Ωm
Lactose Milled	0.2×10^{11} – 3×10^{11} Ωm
	Relaxation time τ
Lactose ML001	0.008 – 0.044 s
Lactose SV003	7.08 – 26.55 s
Lactose Milled	0.035 – 5.31 s

Table 3.3. Experimental results for bulk resistivity of active ingredients.

API type	Resistivity [Ωm]	Relaxation time
A	1.48×10^{15}	7h 28 min
B	2.39×10^{15}	11h 75min
C	1.90×10^{15}	9h 35min
D	1.77×10^{15}	8h 72min
E	1.12×10^{15}	5h 53min
F	0.97×10^{15}	4h 78min
G	0.63×10^{15}	3h 10min

Blends		
0.8%API + Lactose SV003	0.57×10^{11}	1 s
API A + API B	0.7×10^{11}	1.2 s
Lactose		
ML001	0.5×10^{9}	8 ms
SV003	0.4×10^{11}	0.7 s
Milled	0.2×10^{11}	0.3 s

In Table 3.3, Electrical characteristics of API have been investigated. API's have a higher resistivity compared with lactose, thus for highly charged API's time for the charge to dissipate can reach several hours. Also, the charge levels are higher in a blended mixture of API and lactose. The particle sizes have no effect on resistivity measurement, however they play an important role in relaxation time for example: blending 0.8% API with lactose will have no effect on the resistivity level which in this case will be of the predominant material – lactose. In the above scenarios metallic containers seemed to retain higher charge levels on powders compared to plastic bags holders.

3.9.2 Experimental results for Lactose ML001

In the experiment shown below, 17.6 g of lactose sample were compacted in the measuring cell at a temperature of 22.6 °C and a humidity of 33.4%.

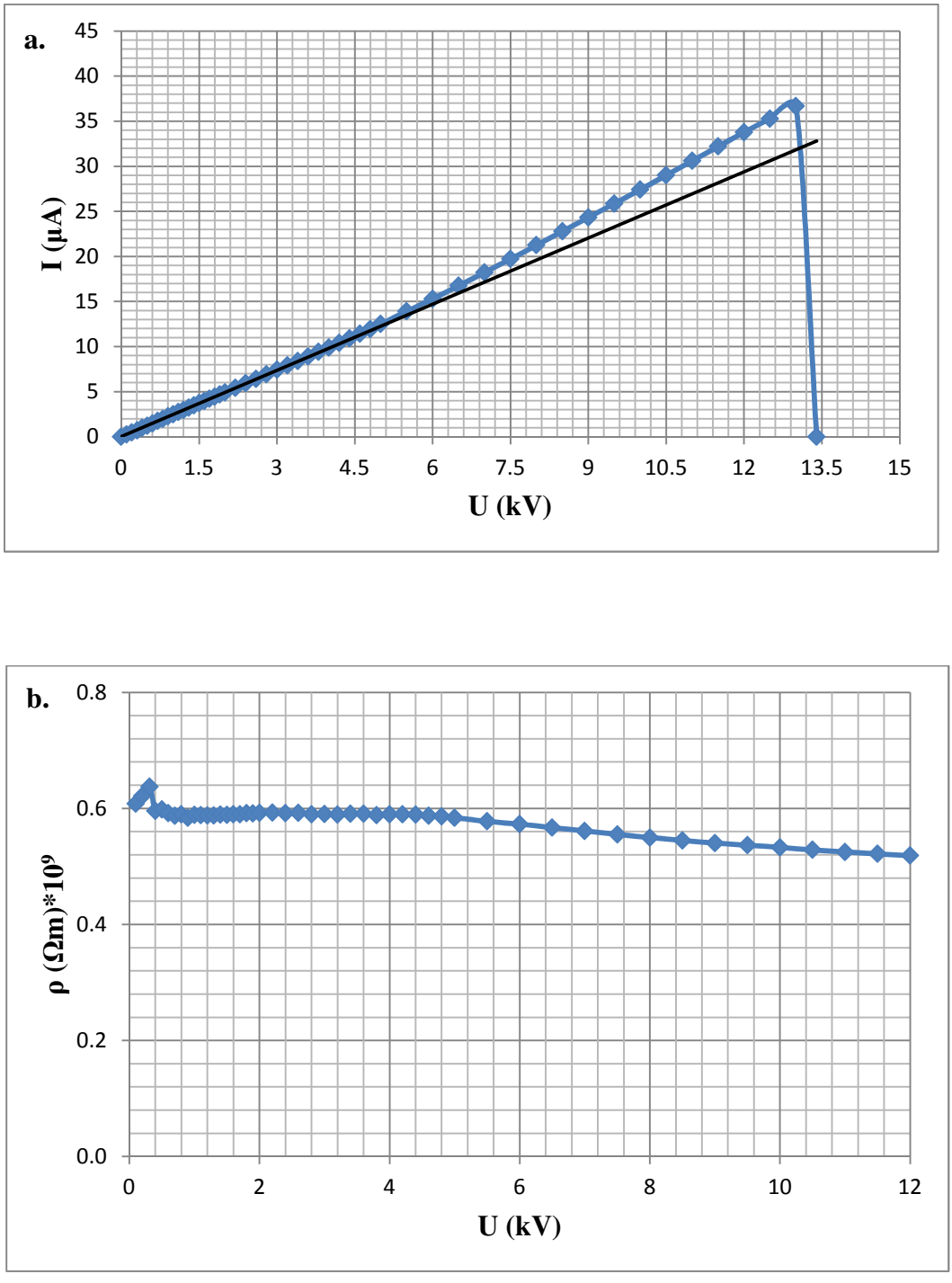

Fig. 3.9. Current-Voltage characteristic (a) and Resistivity vs Voltage (b) for lactose ML001.

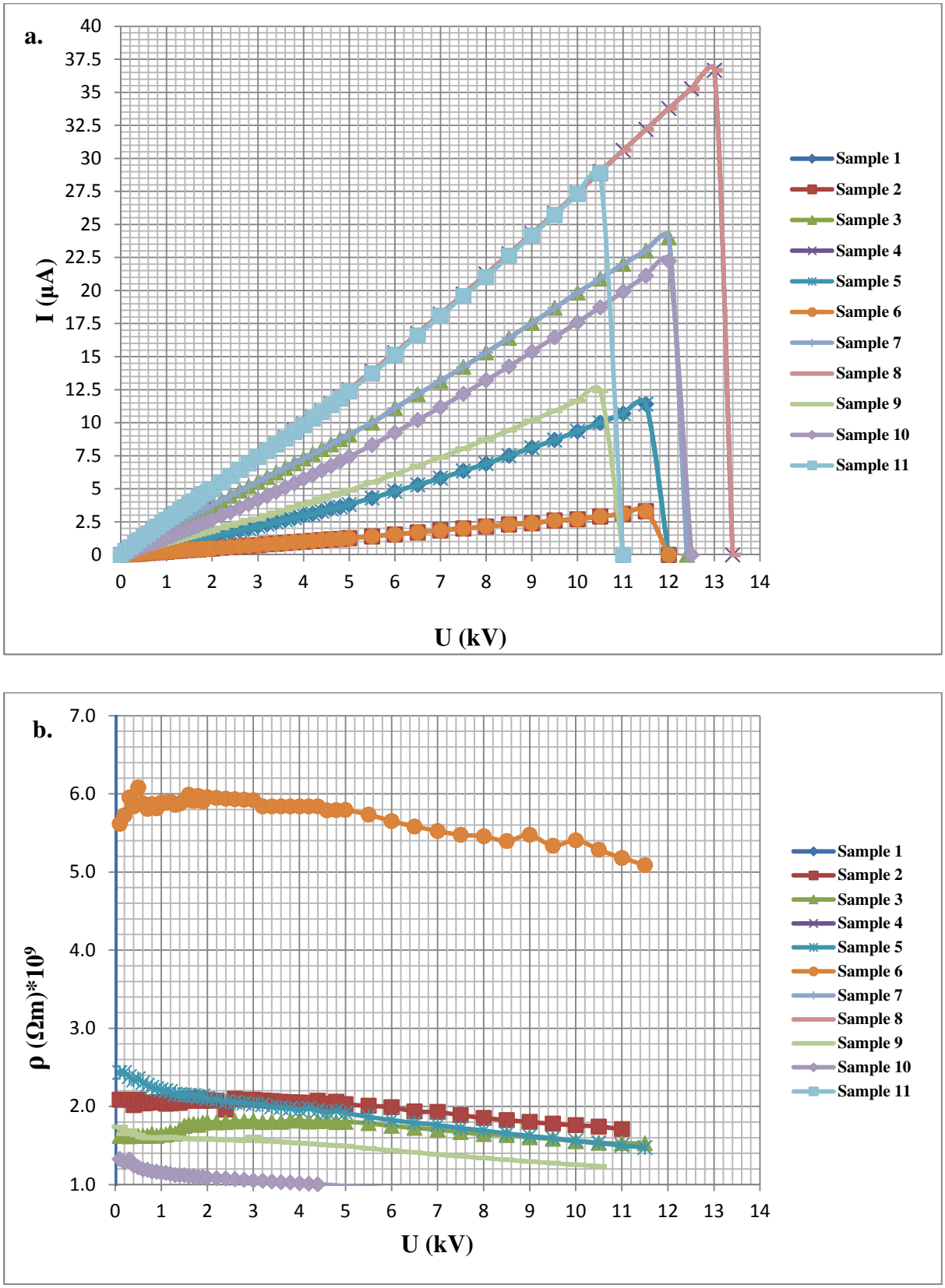

Fig. 3.10. Current-Voltage and Resistivity (a) vs Voltage characteristics (b) for 10 samples of lactose ML001.

The current-voltage graph has an ohmic behaviour as expected and as the voltage passes 6 kV the current increases slightly until the breakdown is reached at 13.5 kV (Fig. 3.9.a). For this measurement the bulk resistivity can be approximated at the $0.6*10^{9}$ Ωm value calculated at the 2kV reading (Fig. 3.9.b). These tests were repeated several times in order to obtain a repeatability of the results (Fig. 3.10.a&b). Variations between results are due mainly to the electrostatic charge contained by each sample tested, particles properties, the charge obtained during handling of the sample, the packing (more or less dense) and also by the slight variations of ambient conditions during the experiments. Due to these variations each sample used (lactose, active ingredient or blend) in the experimental plan has been tested until the breakdown voltage, Powder packing between the electrodes is a crucial element in obtaining fesible resistivity results which then lead to a better understanding of the powder electrical properties (e.g charge decay).

3.9.3 Experimental results for Lactose SV003

In this experiment 15g of lactose were compacted in the measuring cell at a temperature of 22.8° C, and a humidity of 35.7%. The resistivity considered at 2 kV reading is $7.5*10^{11}$ Ωm. For this dry lactose type the bulk resistivity was very challenging to measure and so to obtain a repeatability of the results was difficult as it contained a significant amount of bipolar charge which varied due to the handling process correlated with the ambient conditions.

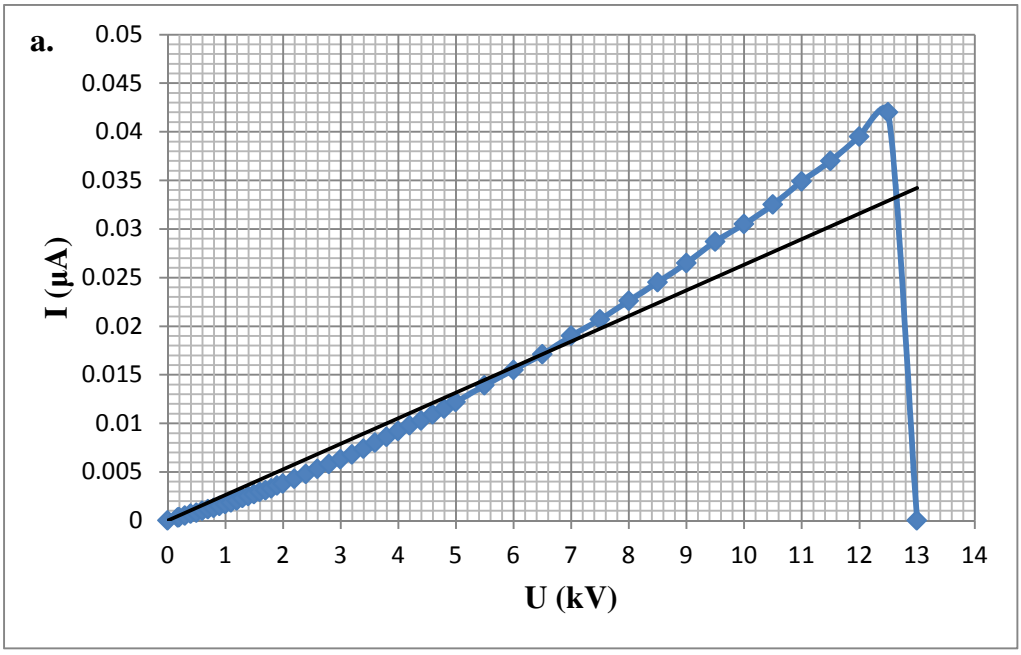

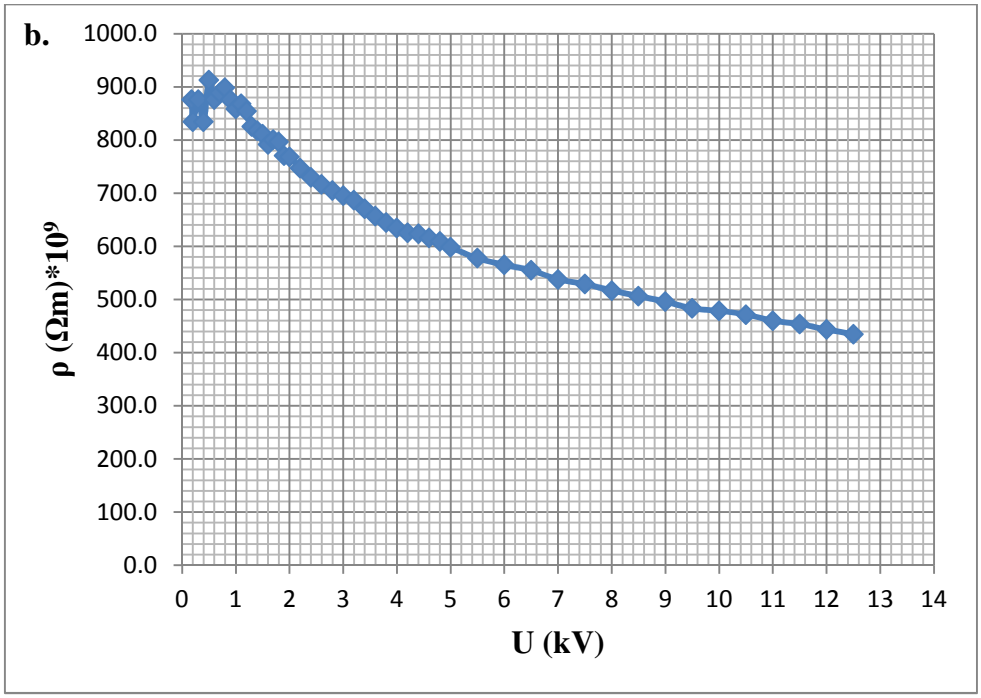

Fig. 3.11. Current-Voltage characteristic (a) and Resistivity vs Voltage (b) for lactose SV003.

3.9.4 Experimental results for Lactose Milled

This type of lactose highly hygroscopic had also variations in values of currents and calculated resistivity during the experimental procedure, the causes again remained the same as for the previous powder samples described above. A sample measurement presented below (Fig 3.12) was done compacting 14 g of powder at a temperature of 22.2 °C, and a 40.1% humidity. The value calculated of the bulk resistivity at a 2 kV reading was $1.4*10^{11}$ Ωm.

Lactose Milled allowed good repeatability of the initial test as presented in Fig 3.13 a&b. Variations between results are due mainly to the electrostatic charge contained by each sample tested and mainly due to packing (more or less dense). Due to these variations each sample has been tested until the breakdown voltage which gave a good indication on how well the powder was packed between the electrodes. As described in previous resistivity measurements powder sample condition and packing are crucial element in obtaining fesible resistivity results which then lead to a better understanding of the powder electrical properties (e.g charge decay).

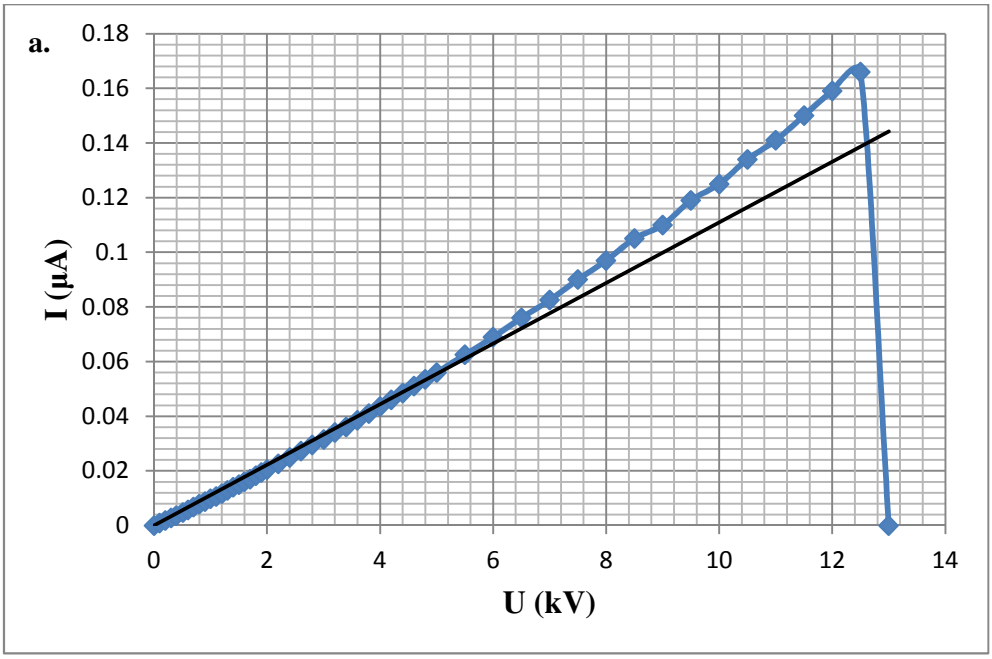

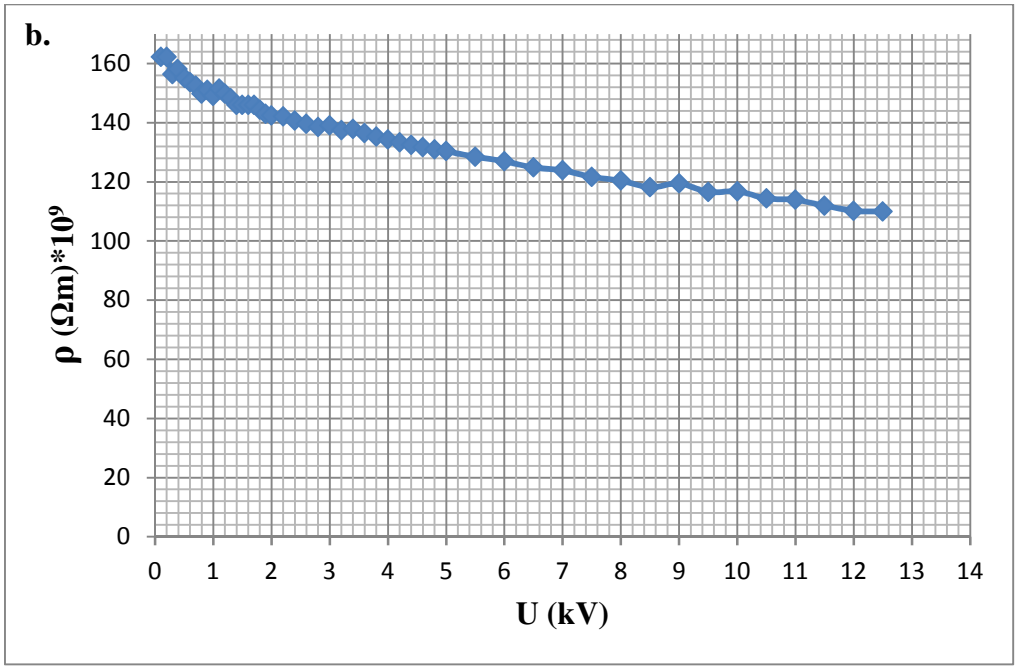

Fig. 3.12. Current-Voltage characteristic (a) and Resistivity vs Voltage (b) for lactose Milled.

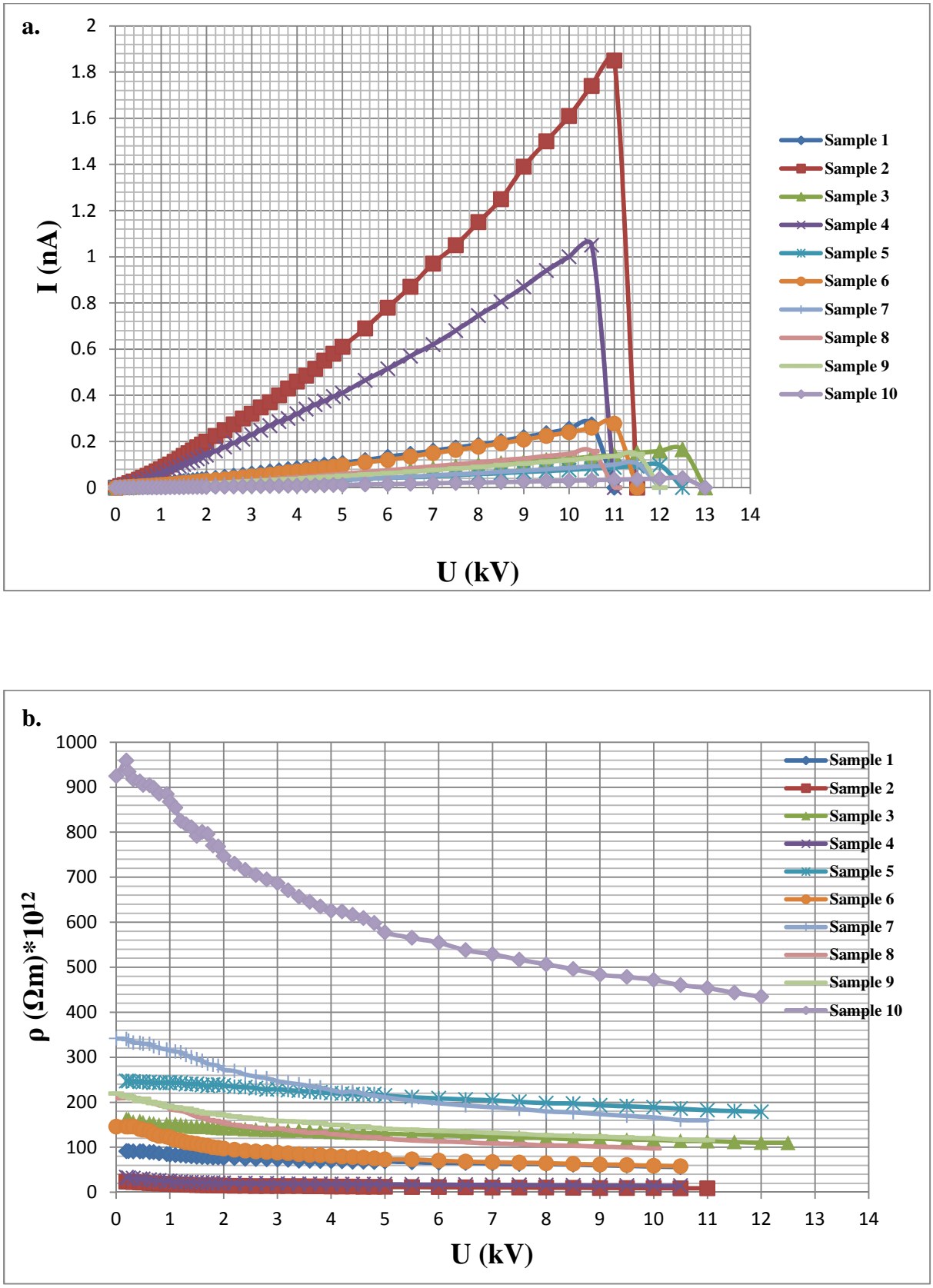

Fig. 3.13. Current-Voltage and Resistivity (a) vs Voltage characteristics (b) for 10 samples of lactose Milled.

3.10 Discussion

The characteristics of each lactose monohydrate sample were different from the point of view of particle characteristics (shape, size, surface), hygroscopicity, electrostatic charge (small particles are usually more charged) and inter-particulate forces as these samples came from different industrial manufacturing processes: blending, milling, sieving. Those characteristics made these samples difficult to handle and as a result many of the experiments failed to reach a point of calculating the bulk resistivity. The ambient conditions during the experiments remained constant. To assure repeatability of the results the same handling technique had to be maintained. The values of resistivity varied with two orders in magnitude due to powder characteristics: SV003 (dry) with a resistivity reaching an order of 10^{11} Ωm, lactose Milled with an order of 10^{11} Ωm has shown hygroscopic properties, ML001 as observed under microscope to be a mixture of the previous two types with an order of 10^{9} Ωm. Surface charge of the each sample was monitored using the John Chubb static monitor instrument. The differences in the values of the surface charge values are due to size variation of particles, water content, handling, storage and initial charge acquired during manufacturing. Attempts to neutralize the bipolar charge of the lactose sample were made using a single point static bar connected to an AC high voltage power supply. The time this ionising probe is kept active is crucial as if it is too short there will be little effect on neutralizing the bipolar charge and if it was too long the powder would easily acquire charge and being a very good insulator will retain it for a long time. It is very difficult to spread the powder as a monolayer especially the samples which shown agglomeration due to water absorption and particle size, and so between the layers of powder the charge is retained. Some improvements have been observed, but this technique requires further investigation and improvements, as it will be ideally to measure resistivity of a neutral powder sample. However due to the particle properties of each type of lactose this neutralization method proved to be little effective. In order to achieve a proper neutralization a wider grounded surface is to be used in order to spread the required quantity of powder as a monolayer with a special set-up (e.g. using a speaker) coupled with the use of a pulsed AC static neutralization bar with controlled ion current control (ICC) such as Keyence SJ-G series. One electrode probe applies high positive and negative voltage alternately and generates ions of both polarities. Compared to a conventional AC method used (Figure 3.7), the amount of ions generated is higher and the oscillating frequency can be changed. With the pulse AC method,

each electrode alternates between generating positive (+) and negative (-) ions. This method helps prevent a bias from forming in the local ion balance and preserves uniformity while if a normal DC method is used, each electrode generates only positive or only negative ions, which creates a bias in the ion balance along the bar length. By sensing the ion current generated by the potential difference between the electrode probe and the amount of charge of our powder sample, this method performs calculations and controls the supplied ions based on the amount of charge to achieve rapid static elimination. The I.C.C. method provides high-precision ion balance control for rapid and effective static elimination. The advantages of this product and method compared to the standard simple AC method used in our measurements.

3.11 Net Charge Measurement using a Faraday Pail

The Faraday Pail (or cup) in conjunction with an Electrometer is the most fundamental net electrostatic charge measurement system. In general, a quantity of the material being tested, such as an aerosol, is delivered into a Faraday Pail and some particles deposit on the surface of the inner vessel and give up their charge whereas other particles are suspended in air inside the chamber, inducing equal charge in the vessel. The charge measured by the electrometer is due to the combined effect of the induced charge at the inner vessel as well as the charge transferred directly to an input capacitor. By dividing the measured charge by the number of particles sampled, the average particle charge can be obtained. Although, there are several modifications of the Faraday Pail technique to accommodate individual experimental requirements, all operate on the same basic principle.

Understanding the mechanisms associated with the transport and deposition of charged powders is of interest for the prediction of aerodisperse system behaviour, in a whole range of natural and technological processes. The generation of bipolar charges has been known to occur in powders used in various industrial applications, which require pneumatic conveying or fluidization. This bipolar charging appears to be found in powders having similar or dissimilar chemical compositions with the common characteristic being that they consist of differing sizes. From the point of view of practical industrial applications, the presence of opposite charges implies the possibility of the generation of localized electric fields. This can affect both powder handling and introduce possible electrostatic hazards.

The Faraday Pail technique can only indicate the net level and polarity of the aerosol charge, and gives accurate results only for unipolarly charged aerosols. For bipolarly charged aerosols such method gives meaningless results and, in the extreme case, i.e., for equal

amount of positive and negative charge present in a sample, it may indicate that the aerosol does not carry any charge (neutral). In the case of the aerosol plum released from an inhaler device there is a need for a real time, non invasive measuring method in order to characterize the aerosols and reveal their bipolar nature.

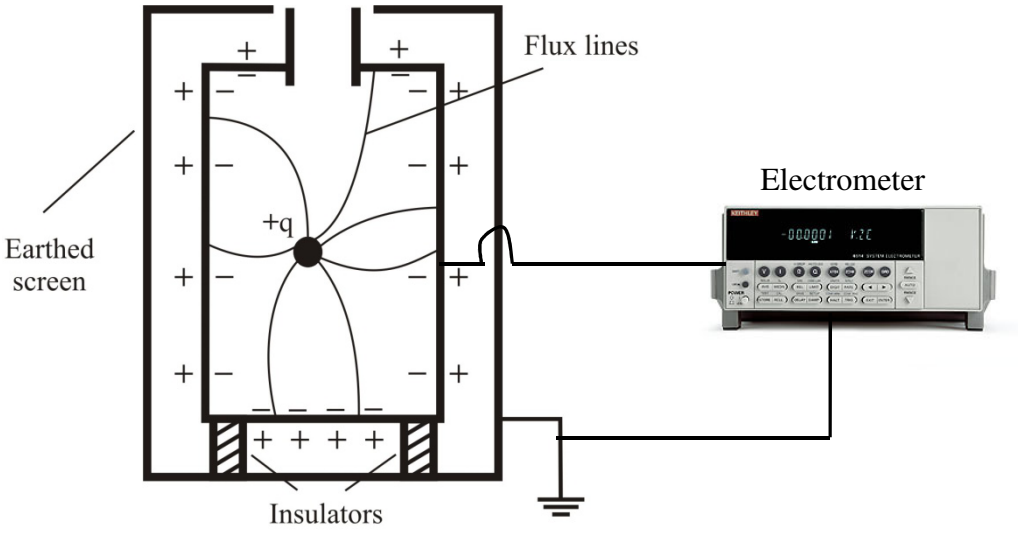

Fig. 3.14. Cross-section through a cylindrical Faraday Pail.

A cross-sectional view of a typical Faraday Pail is given in Figure 3.14. It consists of a closed conducting chamber with a small entrance through which particles can enter. The pail is isolated from ground and has an earthed screening vessel surrounding it to prevent external charges from being measured and to reduce noise from extraneous electrical sources. If a particle with charge $+q$ enters the Faraday Pail, it induces a charge –q distributed over the inner surface of the isolated chamber. To retain the electrical neutrality of this isolated chamber, a positive charge +q is distributed over its outer surface, setting up an electric field, and, therefore, a potential difference between it and the earthed outer screen.

3.11.1 Experimental Set-up

The experimental set-up consists of standard Faraday Pail connected to a Keithley 617 Programmable Electrometer to monitor the net charge levels of a DPI hopper content as showed in the figure below.

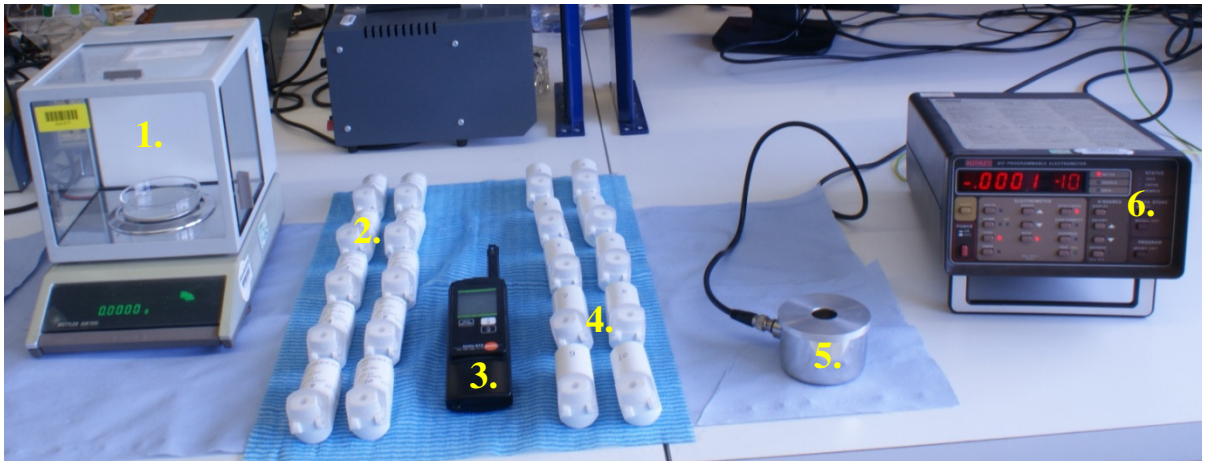

Fig. 3.15 Experimetal set-up for Net Charge Measurement of Hopper Content of DPI's: 1. High precision scales for mass measurement; 2. DPI's with active ingredient; 3. Humidity and Temperature monitoring Probe; 4. Placebo DPI's; 5. Faraday Pail; 6. Keithley 617 Electrometer.

3.11.2 Experimental procedure

For this set of experiments 10 DPI's with placebo and 10 DPI's with blend were used. The DPI devices were carefully disassembled, taking care not to make direct contact with the content and not to introduce additional triboelectric effect. The content of the hopper was then poured into the Faraday Pail and the electrostatic net charge level was monitored using the Keithley Electrometer. The mass of the sample was measured using a highly accurate weighing scale. All measurements were performed in ambient air. This procedure has been repeated for all 10 different devices. Temperature and humidity was monitored during each measurement. After each measurement, the Faraday Pail was cleaned and dried before the next sample was introduced. The charge to mass ratio for both scenarios is show in Table 3.4. The humidity level was at 24.3% and temperature at 22.8 ºC. The placebo content of the hopper of all listed devices displayed an inherent positive polarity and the values obtained for net charge were within the range (0.3 - 0.7) $\times 10^{-8}$ C. The blend from all the devices displayed net positive charge within the range (0.3 - 0.7) $\times 10^{-8}$ C except the content of the device 6 which displayed net negative polarity, and the value was -0.07 $\times 10^{-8}$ C. However, during the experiments a significant quantity of the hopper content (with blend) remained within the hopper as seen in Figure 3.16. This is believed to be primarily due to electrostatic charge effects. The particles and the surface of the hopper may have acquired opposite polarity due to triboelectrification and as a consequence the particles adhered to the surface of the hopper. In addition Van def Waals and capillary forces also may have played a part in retaining some of the contents within the hopper.

Fig. 3.16 Triboelectric effect inside the DPI hopper with blend, once the content has been poured into the Faraday Pail.

The charge/mass ratio of placebo and blend hopper contents were calculated and the values obtained are as follows: The Placebo hopper samples were in the range 0.36-0.8 x 10^{-8} C/g, while the blend hopper samples varied from - 0.11 x 10^{-8} to + 2.39 x 10^{-8} C/g. The measurement results are displayed in Figures 3.17 and 3.18. The average net charge level recorded for the tested powder samples of placebo and blend is 0.6 x 10^{-8} C/g. From these results is difficult to conclude which charging mechanism is dominant i.e. particle-particle/ particle-wall.

Table 3.4. DPI hopper net charge levels for Placebo and Blend.

DPI's with Placebo				DPI's with Blend			
Device	Net Charge Q [C]	Mass [g]	Q/M [C/g]	Device	Net Charge Q [C]	Mass [g]	Q/M [C/g]
1	0.3 x 10^{-8}	0.82	0.36 x 10^{-8}	1	0.7 x 10^{-8}	0.642	1.09 x 10^{-8}
2	0.4 x 10^{-8}	0.78	0.51 x 10^{-8}	2	0.08 x 10^{-8}	0.603	0.13 x 10^{-8}
3	0.5 x 10^{-8}	0.837	0.59 x 10^{-8}	3	0.14 x 10^{-8}	0.633	0.22 x 10^{-8}
4	0.5 x 10^{-8}	0.803	0.62 x 10^{-8}	4	0.032 x 10^{-8}	0.615	0.05 x 10^{-8}
5	0.5 x 10^{-8}	0.76	0.65 x 10^{-8}	5	0.15 x 10^{-8}	0.705	0.21 x 10^{-8}
6	0.6 x 10^{-8}	0.87	0.69 x 10^{-8}	6	-0.07 x 10^{-8}	0.63	-0.11 x 10^{-8}
7	0.6 x 10^{-8}	0.803	0.74 x 10^{-8}	7	1.17 x 10^{-8}	0.66	1.77 x 10^{-8}
8	0.5 x 10^{-8}	0.81	0.61 x 10^{-8}	8	0.2 x 10^{-8}	0.673	0.29 x 10^{-8}
9	0.7 x 10^{-8}	0.87	0.8 x 10^{-8}	9	0.2 x 10^{-8}	0.681	0.29 x 10^{-8}
10	0.5 x 10^{-8}	0.85	0.58 x 10^{-8}	10	1.7 x 10^{-8}	0.71	2.39 x 10^{-8}

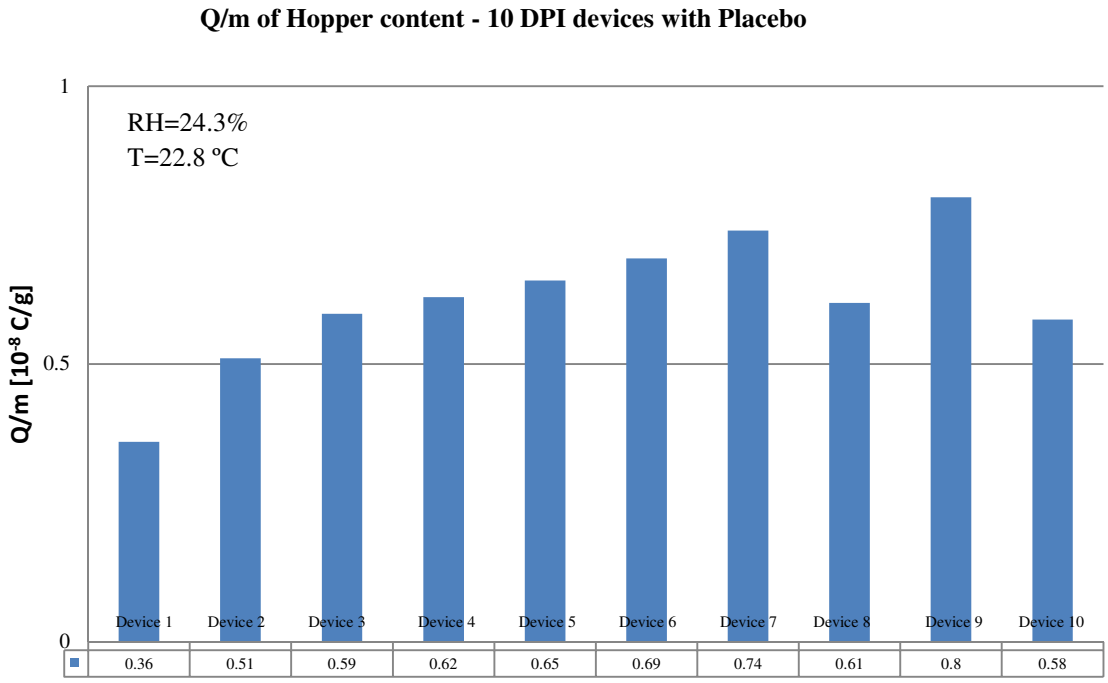

Fig. 3.17 Q/m levels of Hopper content of DPI with Placebo.

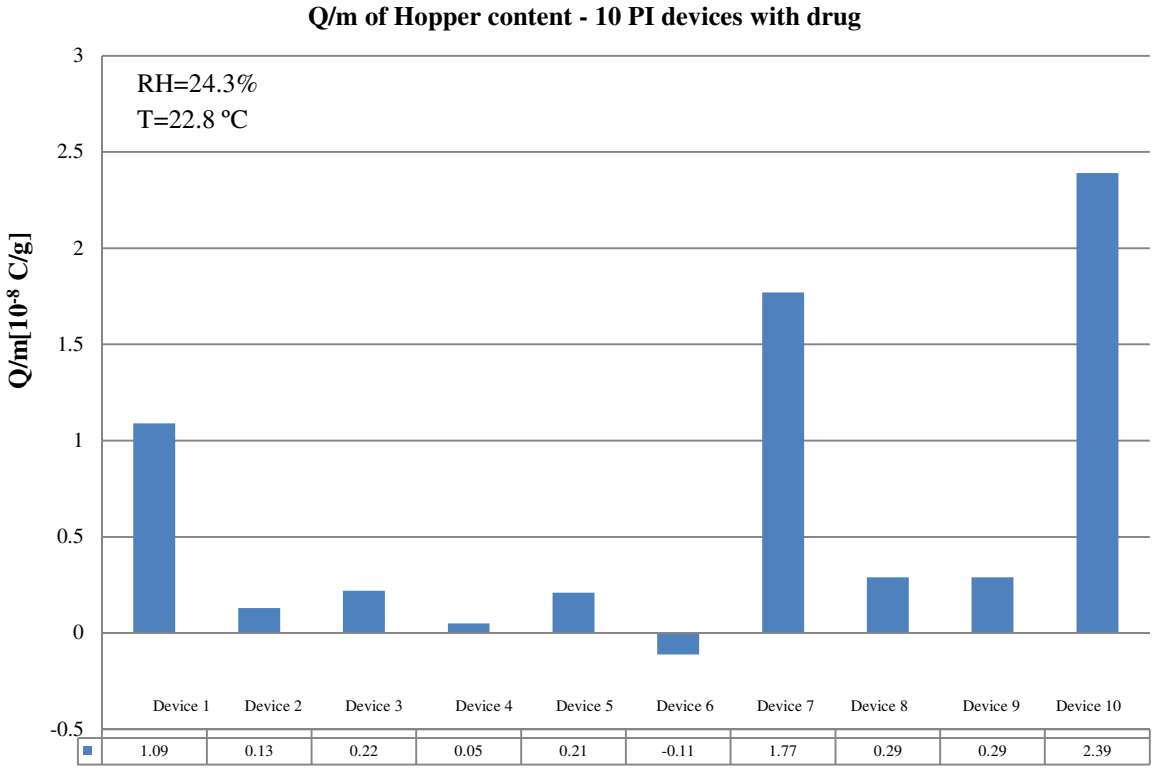

Fig. 3.18 Q/m levels of Hopper content of Spiromax DPI with blend.

It was observed that the values of Charge/mass (Q/m) ratio for the hopper content of placebo & blend are not consistent.

3.12 Net Charge Measurement of Aerosol Delivered by DPI's with blend/placebo using a Flow-through Faraday Cylinder

The experimental set-up consists of modified Dosage Unit Sampling Apparatus (DUSA tube) to mimic a Faraday Pail. The modified DUSA tube is connected to a Keithley 617 Programmable Electrometer to monitor the net charge levels of the DPI actuated aerosol plumes. The DPI devices were actuated using a Copley Scientific HCP5 High Capacity Pump (Fig. 3.19).

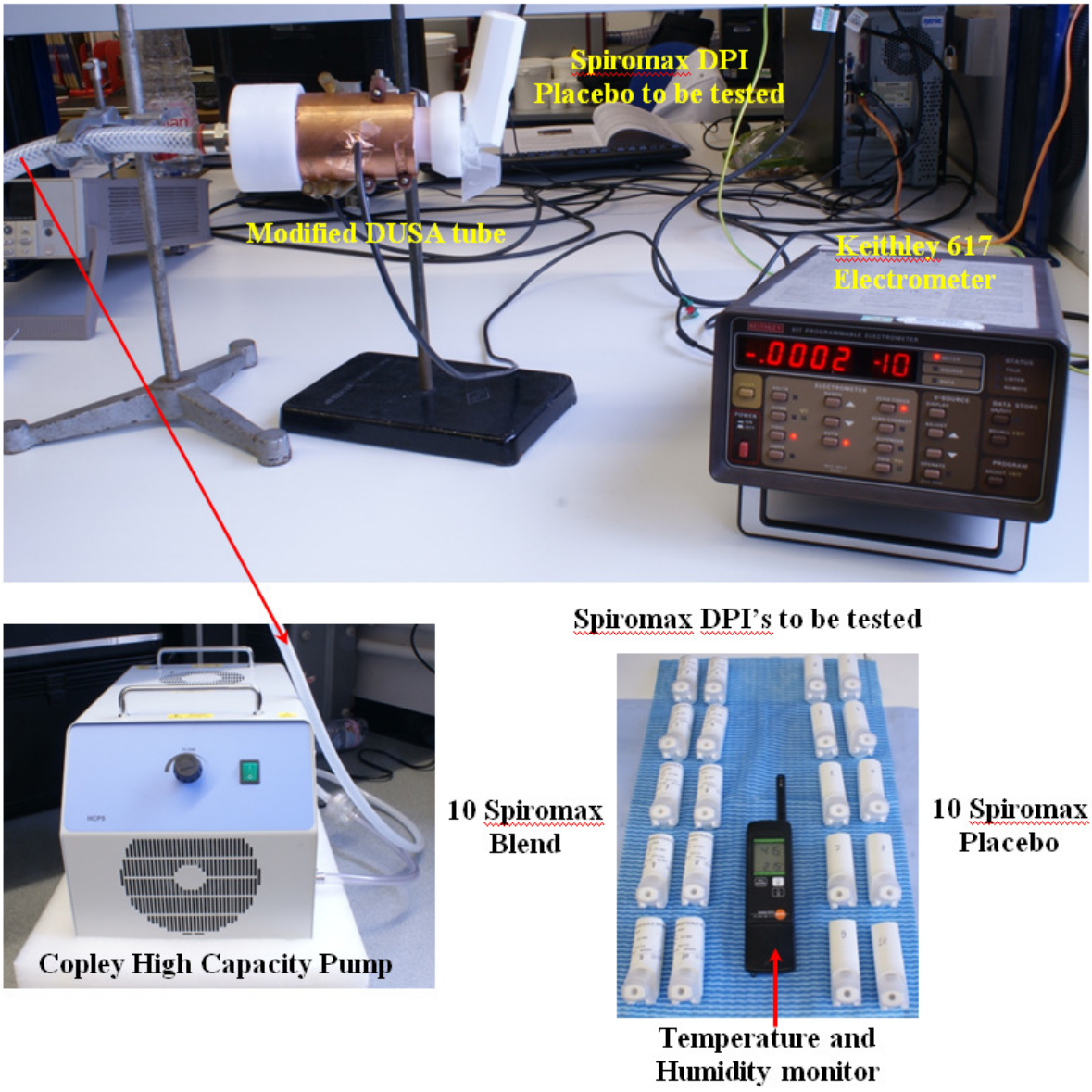

Fig. 3.19 Experimetal set-up for Net Charge Measurement of Aerosol Delivered by DPI with placebo/blend using a Flow-through Faraday Cylinder.

3.12.1 Experimental procedure

This measurement was carried out to understand the charging behaviour of placebo/blend during deaglommeration in the DPI cyclone. In order to actuate the device, an open system has to be used that can mimic the inhaling procedure. This was achieved using a DUSA tube and Copley High capacity Pump. Net charge measurement of the aerosol plume was monitored by modifying the DUSA tube to mimic Faraday Pail. In order to make the inner surface of the DUSA tube conducting, the inner surface was lined with copper tape and connected to the Keithley Electrometer. The outer surface of the DUSA tube was also covered with copper tape and this was connected to ground potential to avoid any external electrical interference (Fig. 3.20). This arrangement mimics the function of a Faraday Pail. In order to maximize the net charge measurement levels of the actuated DPI aerosols plumes, we used a wire wool mesh at the outlet of the DUSE tube as seen below.

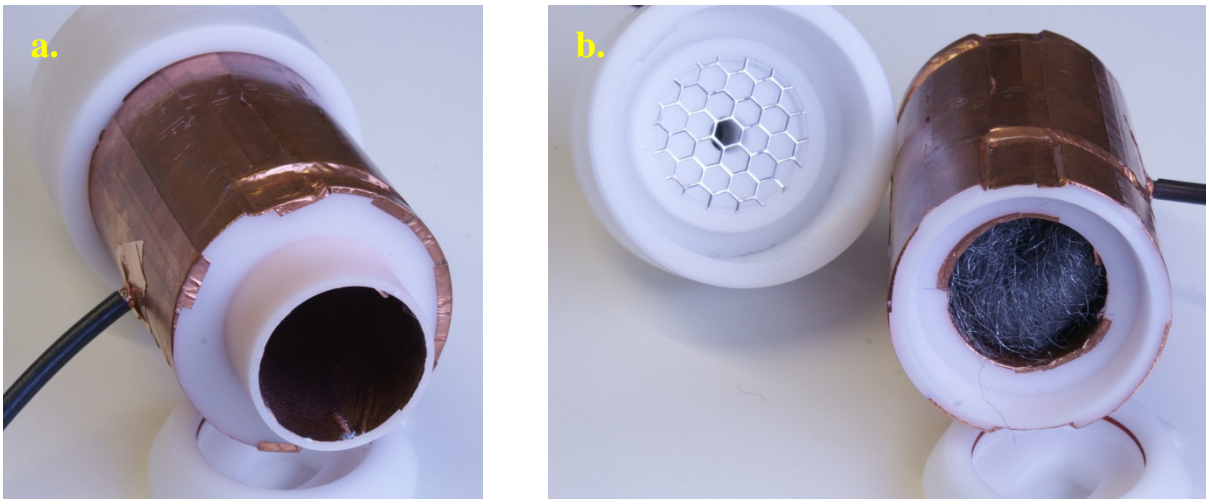

Fig. 3.20 Modified DUSA tube to mimic a Faraday Pail: a) Front detail – both inner/outer surfaces have been lined with copper tape; b) Back detail – wire wool meshing.

10 DPI's with placebo and 10 DPI's with blend were used for each set of experiments in order to be able to compare the electrostatic behaviour of blends against the placebo. The humidity and temperature was monitored during each measurement. After each set of experiments using one DPI device, the modified DUSA tube was cleaned using ethanol and dried.

3.12.2 Experimental results

Initial tests have been performed to check the capability of the measurement set-up to provide relevant data. The DPI devices were numbered 1-10 for blend & 1-10 for placebo so that for each set of experiments the same device identity could be maintained. Three devices of each type (blend/ placebo) were used and actuated ten times. Net charge levels were monitored with the Keithley Electrometer and plotted in Figure 3.21.

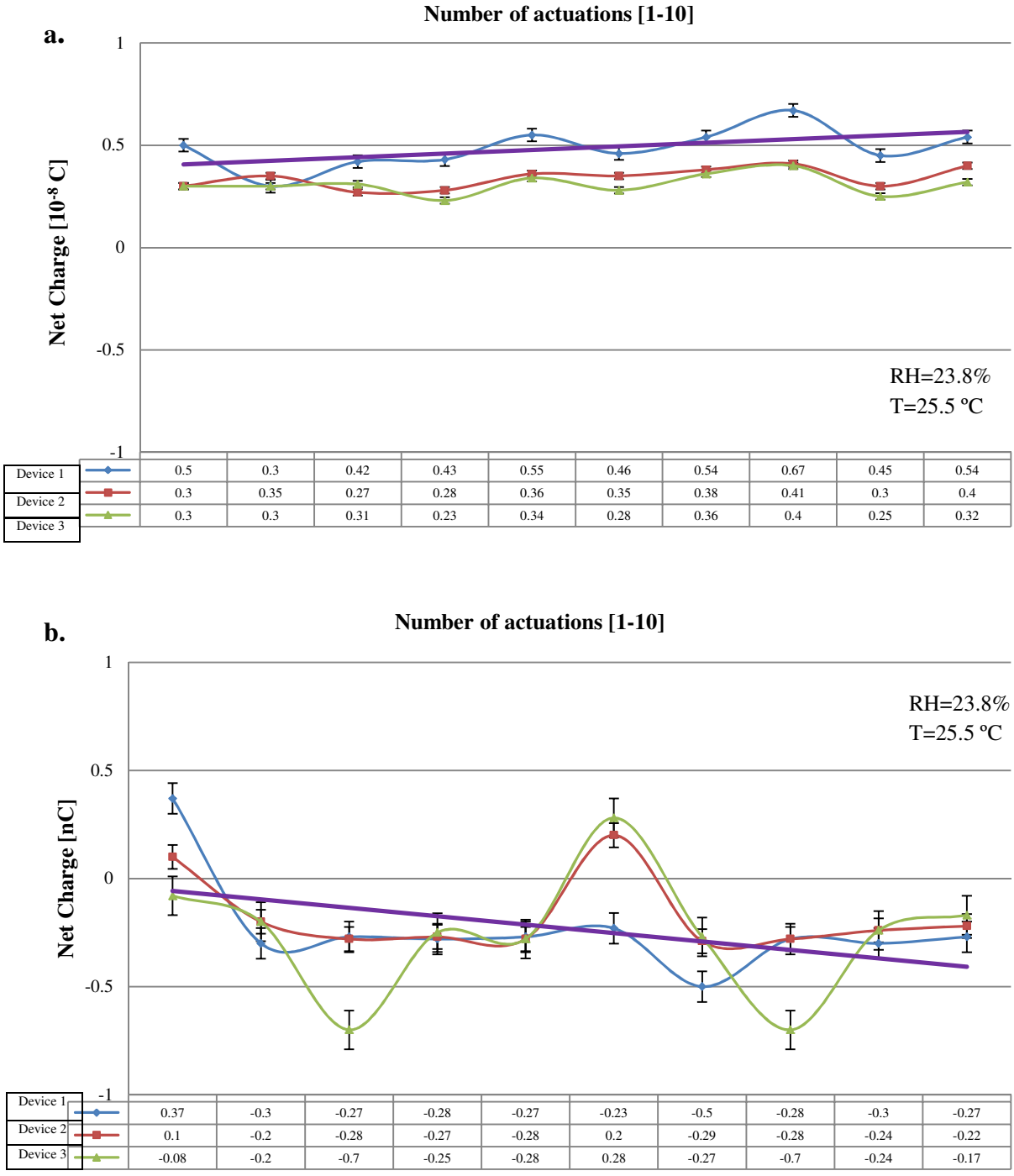

Device 1	0.5	0.3	0.42	0.43	0.55	0.46	0.54	0.67	0.45	0.54
Device 2	0.3	0.35	0.27	0.28	0.36	0.35	0.38	0.41	0.3	0.4
Device 3	0.3	0.3	0.31	0.23	0.34	0.28	0.36	0.4	0.25	0.32

Device 1	0.37	-0.3	-0.27	-0.28	-0.27	-0.23	-0.5	-0.28	-0.3	-0.27
Device 2	0.1	-0.2	-0.28	-0.27	-0.28	0.2	-0.29	-0.28	-0.24	-0.22
Device 3	-0.08	-0.2	-0.7	-0.25	-0.28	0.28	-0.27	-0.7	-0.24	-0.17

Fig. 3.21 Net charge levels of DPI's: a) Placebo; b) Blend.

In the experiments shown above the humidity was at 25.5 % and ambient temperature was at 23.8 ºC while the average for 3.21.a was 0.38 with a standard deviation of 0.028; as for 3.21.b the average was -0.22 and a standard deviation of 0.054. DPI deaglommeration of placebo provided net positive charge of average value equal to 0.4×10^{-8} Coulombs, while the blend fluctuated between positive and negative net charge levels and then values were one order of magnitude less than placebo (10^{-9} C). This variation in net charge levels from positive to negative charge is due mainly to the influence of drug. In order to conclude the values of charge for both scenarios, the experiments were repeated several times in the same ambient conditions. In Figure 3.22, all 10 DPI devices with blend were used in normal operating conditions and actuated 10 times. Charge levels remained in the same order of magnitude (10^{-9} C) while the polarity varied from positive to negative. A general trend could be observed as after several actuations of the device the net charge levels tended to move towards the positive polarity.

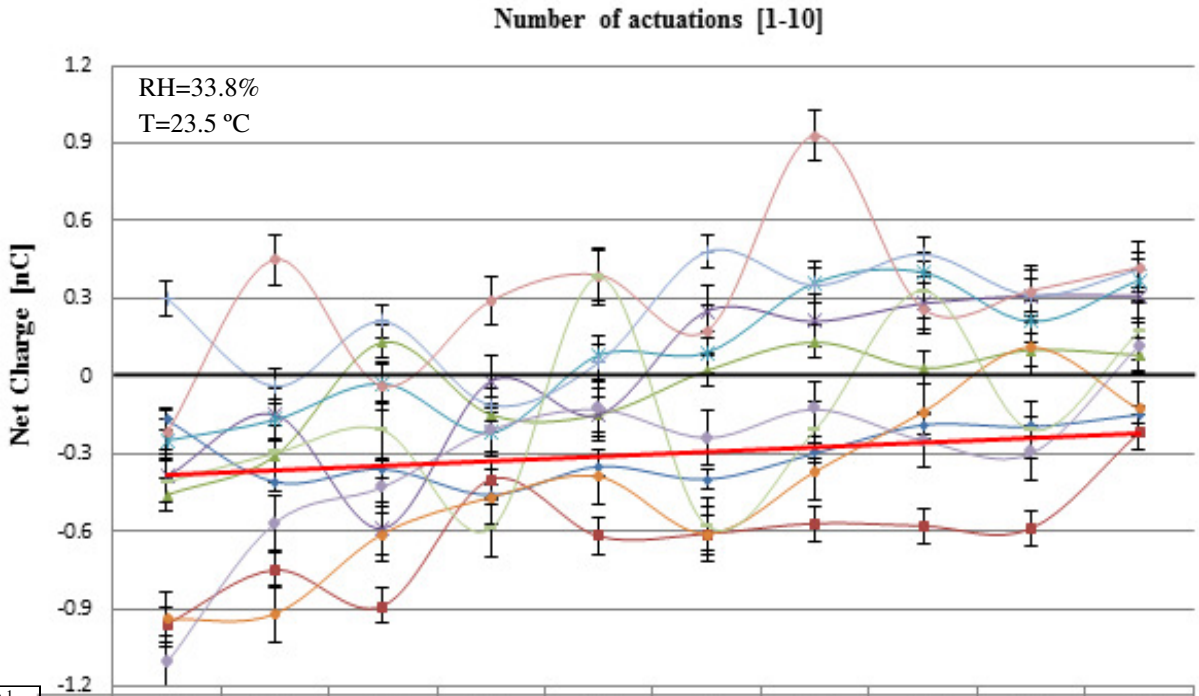

Device 1	-0.17	-0.41	-0.36	-0.46	-0.35	-0.4	-0.3	-0.19	-0.197	-0.15
Device 2	-0.96	-0.75	-0.89	-0.4	-0.62	-0.61	-0.57	-0.58	-0.59	-0.22
Device 3	-0.46	-0.31	0.13	-0.15	-0.15	0.02	0.13	0.03	0.1	0.08
Device 4	-0.39	-0.15	-0.59	-0.02	-0.15	0.25	0.21	0.28	0.31	0.31
Device 5	-0.25	-0.17	-0.03	-0.22	0.08	0.09	0.36	0.4	0.21	0.37
Device 6	-0.94	-0.92	-0.61	-0.47	-0.39	-0.61	-0.37	-0.14	0.11	-0.13
Device 7	0.3	-0.04	0.21	-0.113	0.052	0.48	0.35	0.47	0.31	0.41
Device 8	-0.22	0.45	-0.04	0.29	0.39	0.175	0.93	0.26	0.33	0.42
Device 9	-0.41	-0.3	-0.21	-0.59	0.38	-0.58	-0.21	0.33	-0.21	0.17
Device 10	-1.11	-0.57	-0.43	-0.21	-0.13	-0.24	-0.13	-0.25	-0.3	0.117

Fig. 3.22. Net charge levels of 10 DPI's with Blend - direct use.

In order to test this hypothesis another set of experiments were performed with the DPI's with blend. In this scenario, before each actuation, the DPI was shaken to induce triboelectrification in the hopper. Again for this scenario 10 devices were actuated 10 times and the charge levels obtained are shown in Figure 3.23. The relative humidity was at 33.8 % and temperature was at 23.1° C. Compared with the initial tests in Figure 3.21, the humidity went up almost 10%. This change in humidity may have played a role in the blend net charge levels measured.

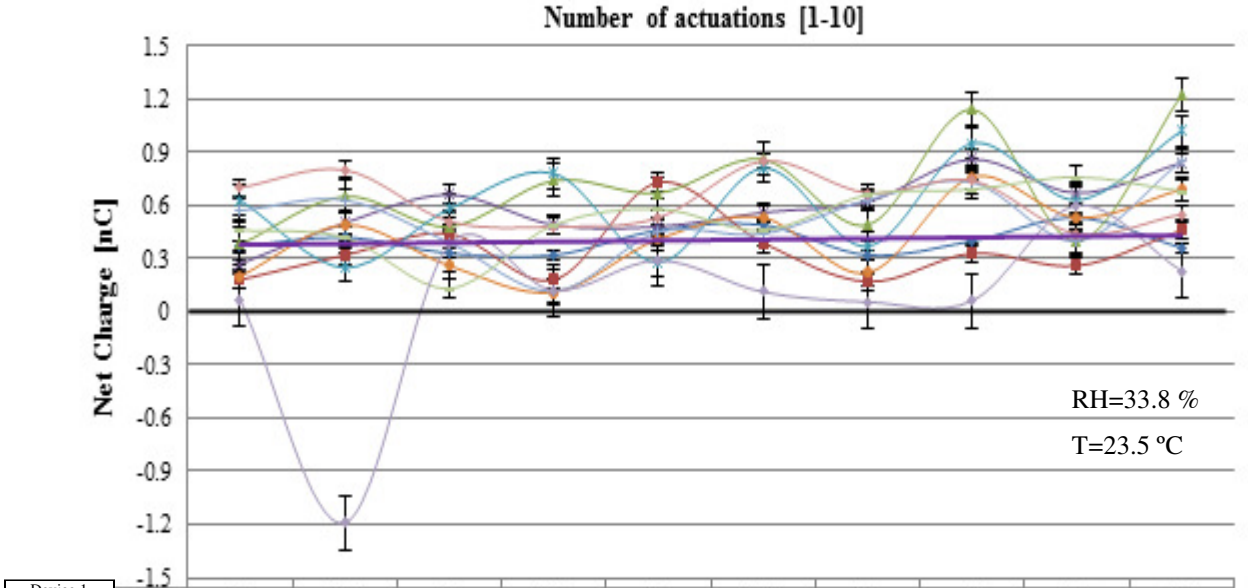

Device 1	0.37	0.42	0.33	0.32	0.46	0.49	0.32	0.4	0.53	0.36
Device 2	0.18	0.32	0.44	0.18	0.73	0.39	0.17	0.33	0.26	0.46
Device 3	0.38	0.65	0.48	0.74	0.67	0.86	0.49	1.14	0.4	1.22
Device 4	0.27	0.5	0.66	0.49	0.48	0.56	0.62	0.86	0.67	0.84
Device 5	0.63	0.25	0.58	0.78	0.28	0.81	0.37	0.95	0.63	1.02
Device 6	0.2	0.49	0.26	0.11	0.41	0.53	0.22	0.76	0.53	0.69
Device 7	0.57	0.63	0.39	0.115	0.45	0.44	0.63	0.73	0.4	0.85
Device 8	0.7	0.8	0.51	0.48	0.53	0.85	0.67	0.74	0.44	0.55
Device 9	0.46	0.42	0.132	0.49	0.58	0.46	0.66	0.69	0.76	0.68
Device 10	0.07	-1.19	0.38	0.12	0.29	0.112	0.056	0.062	0.6	0.23

Fig. 3.23. Net charge levels of 10 Shaken DPI's with Blend.

This experimental observation confirms that the average value of net charge of all devices is about 0.6×10^{-9} C, and the polarity is positive. One negative value was obtained, probably due to an artefact of the monitoring instrument. Same sets of experiments were carried out employing 10 DPI's with Placebo (Fig. 3.24). The relative humidity was at 35% and temperature was at 22.6 ºC. The average net charge value is about 0.3×10^{-8} C and of positive polarity. The experiment confirms and validates the previous experiments (Fig. 3.23.). For comparison, a set of experiments were carried out by shaking the DPI with

placebo before actuation but the net charge levels remained in the same range and same polarity as the results shown in Figure 3.25 for one DPI device with placebo.

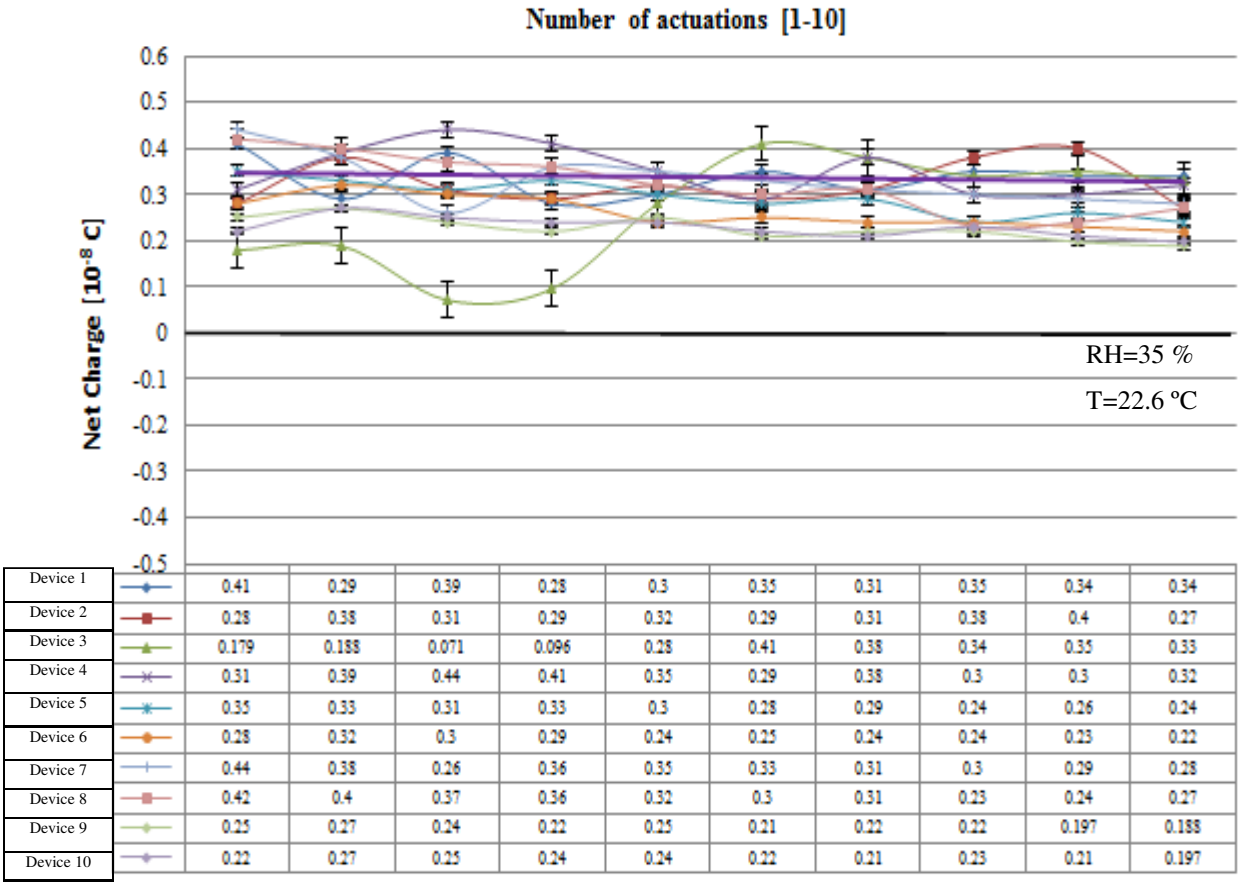

Device 1	0.41	0.29	0.39	0.28	0.3	0.35	0.31	0.35	0.34	0.34
Device 2	0.28	0.38	0.31	0.29	0.32	0.29	0.31	0.38	0.4	0.27
Device 3	0.179	0.188	0.071	0.096	0.28	0.41	0.38	0.34	0.35	0.33
Device 4	0.31	0.39	0.44	0.41	0.35	0.29	0.38	0.3	0.3	0.32
Device 5	0.35	0.33	0.31	0.33	0.3	0.28	0.29	0.24	0.26	0.24
Device 6	0.28	0.32	0.3	0.29	0.24	0.25	0.24	0.24	0.23	0.22
Device 7	0.44	0.38	0.26	0.36	0.35	0.33	0.31	0.3	0.29	0.28
Device 8	0.42	0.4	0.37	0.36	0.32	0.3	0.31	0.23	0.24	0.27
Device 9	0.25	0.27	0.24	0.22	0.25	0.21	0.22	0.22	0.197	0.188
Device 10	0.22	0.27	0.25	0.24	0.24	0.22	0.21	0.23	0.21	0.197

Fig. 3.24 Net charge levels of 10 DPI's with Placebo Direct Use.

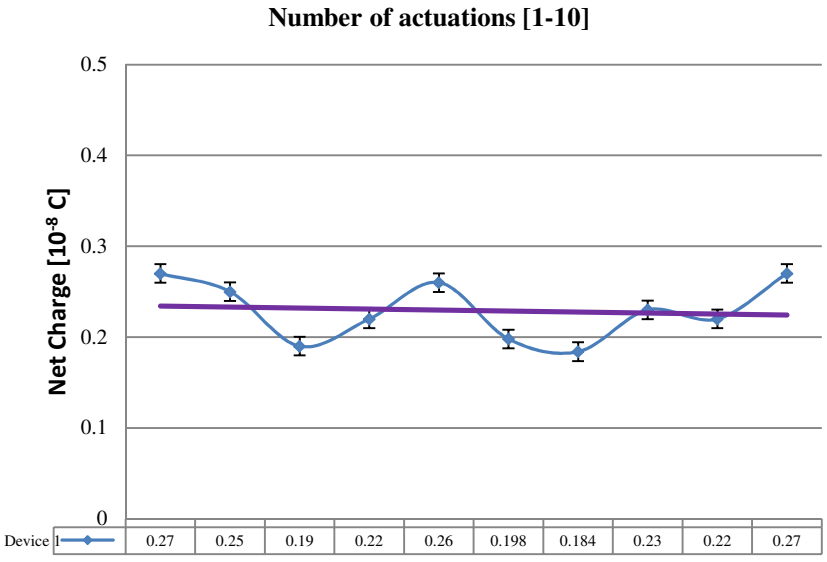

Device 1	0.27	0.25	0.19	0.22	0.26	0.198	0.184	0.23	0.22	0.27

Fig. 3.25 Net charge levels of one Shaken DPI with Placebo with an average of 0.22 and a standard deviation of 0.032.

To investigate further the dispersed aerosol charging characteristics a new set of experiments were performed. The DPI numbered 1 with blend and The DPI numbered 1 with placebo were actuated, each 100 times and net charge levels monitored with the Keithley Electrometer. For placebo we have an average of 1.95 and a standard deviation of 0.44 while for blend an average of 0.88 with a standard deviation of 0.33.

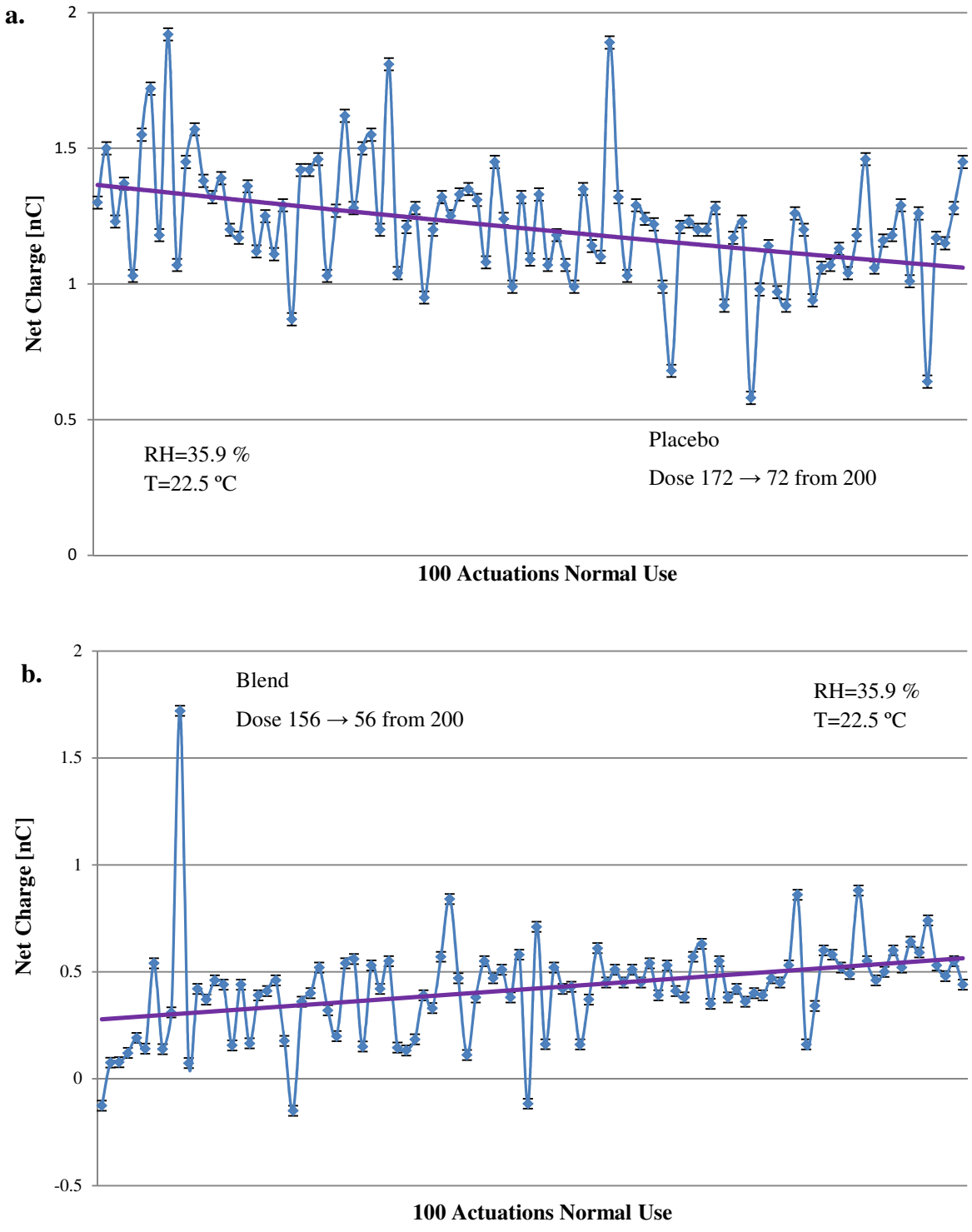

Fig. 3.26. Net charge levels of one DPI's: a) Placebo; b) Blend.

Figure 3.26.a, shows 100 continuous actuations of DPI with Placebo. It has obviously a higher charge level than the blend with a straight positive net charge trend. From the graph we can distinguish some patterns of charge dissipation and accumulation after several actuations which provided a straight decaying trend and finally settling to a constant value. This trend could be attributed to particles surface and dispenser surfaces coming into contact, achieving a steady state electric work function values. The DPI with blend Fig. 3.26, b., shows a mirror image effect. The general trend is similar, with respect to fluctuations in absolute values of charge. Figure 3.27 shows the comparison of net charge level evolution for both samples. For placebo we have an average of 0.42 with a standard deviation of 0.23 while for blend we have an average of 1.22 and a standard deviation of 0.22.

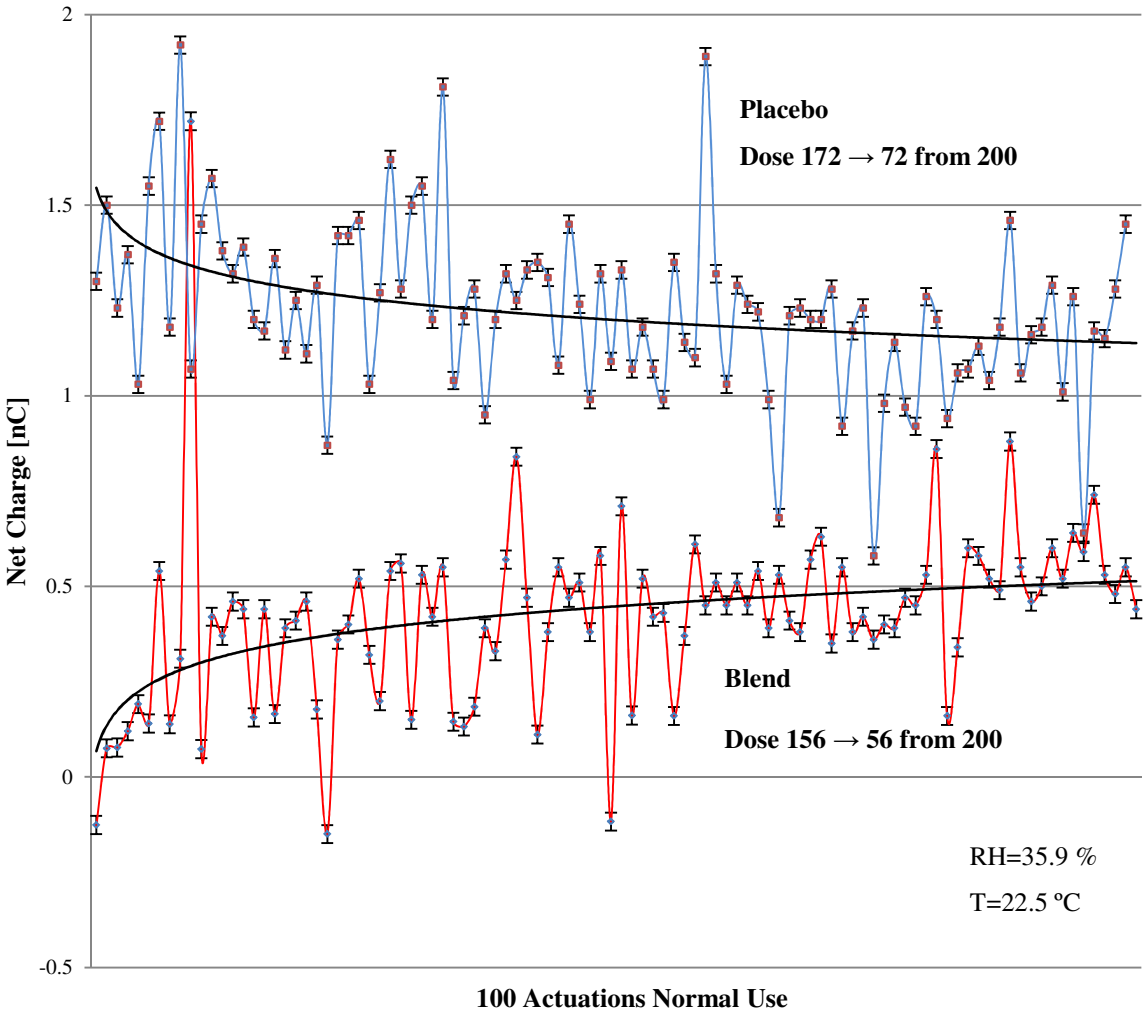

Fig. 3.27. Trend Comparison of the net charge levels of DPI numbered 1 and actuated 100 times.

For comparison a new set of 100 actuations was performed using the DPI numbered 9 for both blend and placebo. The charge fluctuation trend is shown in Figure 3.28. For placebo we

have an average of 1.98 and a standard deviation of 0.41 while for blend we have an average of 0.88 with a standard deviation of 0.34.

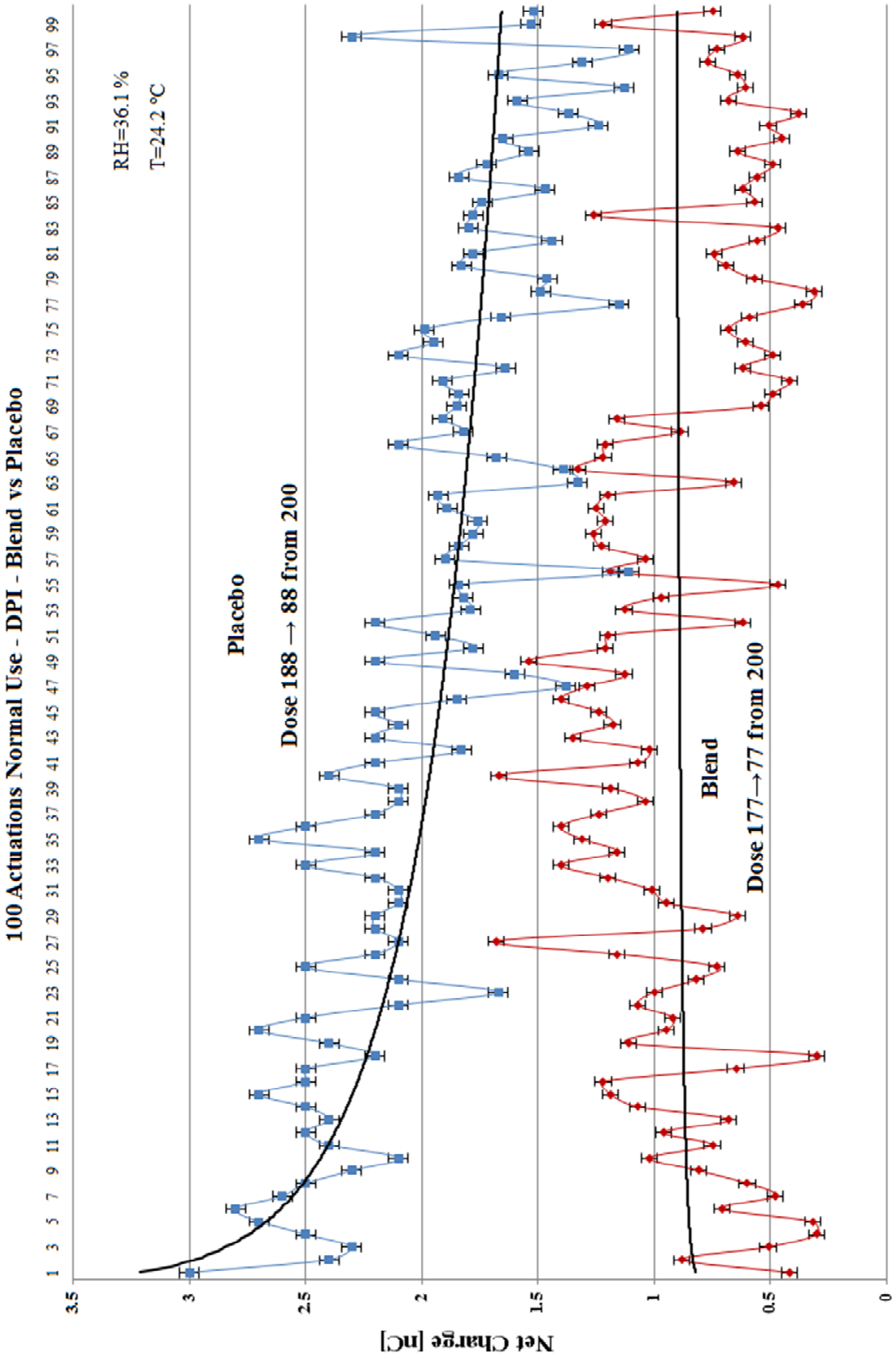

Fig. 3.28. Trend Comparison of the net charge levels of DPI numbered 9 - 100 times.

3.13 Conclusions

To summarise we can say that the properties of particles, contact surface and the contact event have to be considered when resistivity is measured. On separation, the two surfaces may have opposite charges and this charge can be distributed over the solid surface by electrostatic forces. The main cause of such a phenomenon is triboelectrification process, i.e. exchange of charge carriers between the powder particles and the surface. The magnitude and polarity of the charge generated during such a process depends on the electronic structure (value of work function) of the material with which the particles come into contact, as well as surface morphology. Work function is defined as the minimum energy required to extract the weakest bound electron from the particle/solid surface to the next energy level. Perfect insulators do not exhibit contact charging, but this is misleading since the presence of defects and impurities can serve as active sites for electron transfer. This indicates that the charging process with pharmaceutical powders and polymers will be complex and unpredictable.

Based on the experimental results of the DPI testing the following conclusions can be derived:

- For hoppers containing placebos, variations in charge to mass ratio (Q/m) values between each device is within the experimental errors. The average value is about 0.6 x 10^{-8} C/g and the net charge polarity appears to be positive. In the case of blends, the order of magnitude of the net charge level remained the same but variation in (Q/m) values could be up to about 300%. Such a variation in the case of hopper content of blends is thought to be due to additional tribocharging effect of the blend (carrier-drug interactions) and blend and hopper surface interactions. In the latter case, significant amount of the material remained in the hopper. However, to make firm conclusion, experiments need to be carried out in a wide range of humidity.
- The net charge measurement results obtained using the modified DUSA tube reveal that with placebo the average net charge of the aerosol delivered by the device is about 0.3 x 10^{-8} C and remained positively charged. The blend aerosol net charge values recorded were an order of magnitude less and fluctuated between (-0.9 to + 0.6) x10^{-9}. The polarity of all the devices started negative and the general trend moved towards positive at the 10^{th} actuation. However, some devices output remained negatively charged. Tit is believed that the order of magnitude change in net charge

values is primarily due the drug particles present in the blend. Further experiments are needed at varying humidity levels to confirm the observed trend.

- Another experiment was carried out to determine the influence of triboelectrification due to shaking of the device before delivery. The average net charge values observed were 0.6 x 10^{-9} C and 0.3 x 10^{-8} C with the blend and the placebo respectively. The net charge polarity in both cases remained positive. This would indicate that if the contents of the hopper are initially charged to a known value, it may be possible to achieve a constant value of net charge of the aerosol exiting the device after passing through the cyclone. If the humidity remained constant, it may be possible to control the tribocharging characteristics within the device by shaking the device. For this to take place, the work function of the material should remain reasonably constant. Further work needs to be done to confirm this hypothesis.

Through life test (100 actuations) was carried out to determine the variability between actuations. Test results with placebo content of one device reveals that the net charge remained positive but the level fluctuated on average about 100% and showed a tendency to decay slightly. The trend observed with the blend is almost the mirror image of that of placebo. In this case the net charge increased slightly and reached a steady state after 100 actuations. This test was repeated with another set of devices. The trend with placebo contents remained the same but with higher levels of net charge. The trend observed for the blend appears to be different, in that the pattern displayed is almost of sinusoidal shape. However, in both cases the net charge polarity remained positive. It is difficult to make firm conclusions based on the limited results. However, the effect of tribocharging, the influence of the mouth piece deposition and device variability are evident from these limited experimental study. It would be useful to compare dose output at each actuation with the observed trend of net charge results. It is recommended that further study should be carried out at different humidity values (25% - 60% RH) to make firm conclusions with respect to the electrostatic properties of the device.

Chapter 4

Investigation of Electrostatic Properties of Pharmaceutical Powders using Phase Doppler Anemometry

4.1 Introduction

Characterization of pharmaceutical powders in terms of their electrical properties has become a subject of considerable research in the development of drug manufacturing and product performance. Electrostatic charge of dry powder for inhalation plays an important role in respiratory therapy. Inhalation of dry powders used to treat a variety of respiratory diseases has become a standard procedure especially for asthma and COPD (chronic obstructive pulmonary disease) affecting more than 300 million people worldwide (Haughney et al., 2008). Both theoretical and experimental studies have demonstrated that aerosols generated by inhalers acquire bipolar charge during the dispersion process (Kulon & Balachandran, 2001; Saini et al., 2007; Rawley G., 2001). The electrostatic charge distribution of the particles affects the efficiency of drug delivery by influencing both the transport and deposition of inhaled particles in the human lung due to space and image charge forces (Balachandran et al., 1997).

Powder mixing / blending, coating, drying, transport are generating electrostatic charges which are attributed mainly to the process of triboelectrification (Saleem et al., 2008; Engers et al., 2006; Pingali et al., 2010). The charge levels on particles could be affected by several factors related to the particle morphology such as size distribution, shape, surface roughness, purity / surface contaminants, contact area, as well as the inherent electrical and physical properties (Chacrabarty et al, 2007; Adi et al., Jones et al., Valverde et el., 2008). The atmospheric conditions such as: relative humidity, temperature, atmospheric pressure are known to affect charge generation and dissipation (Grosvenor & Staniforth, 1996).

Accurate devices for measurement of the levels of charge resident on the pharmaceutical powders have to be developed with a measurement capability in the bipolar domain. Various techniques used for charge and size measurement of powder particles have been presented (Brown R.C., 1997). The most common method used for charge measurements is Faraday pail. When a charged particle, of any form or conductivity, reaches the Faraday pail interior, an equal and opposite charge is induced on the inner wall and displayed on an electrometer. By dividing the measured total charge of the powder sample by the number of particles, the

average particle charge can be obtained. However this technique can indicate only the net level and polarity of the charged powder sample and cannot be used for a polydispersed powder.

Methods for powder charge measurement have been developed, based on optical techniques or electrostatic precipitation. Mazumder et al. invented the Electrical-Single Particle Aerodynamic Relaxation Time (E-SPART) analyzer based on Laser Doppler Velocimetry (LDV), which measures both the size and charge of individual particles, at low particle flux rates. This proved to be an obstacle when characterizing highly charged, rapidly evolving, non-uniform aerosol clouds from inhalers.

The solution concept for equations of aerosol particle motion in an electric field was presented by Wells and Gerke which measured the size of ultramicroscopic particles by their oscillation amplitudes in an electric field reversed by a rotating commutator. The supplied voltage had a rectangular waveform while in Mirgel experiments saw tooth waveform was used.

Balachandran et al. promoted and developed new methods of bipolar charge measurement and particle characterization based on electrostatic precipitation techniques and Phase Doppler Anemometry (PDA) respectively. Bipolar Charge Aerosol Classifier in conjunction with aerodynamics was successfully used to obtain bipolar charge fractions and mobility classification of charged aerosols while it is also capable of measuring spatial deposition characteristics of an aerosol plume. The Multi Stage Precipitator developed by O'Leary et al. compliments the commercially available Electrical Low Pressure Impactor (ELPI). The net charge data obtained with ELPI is incomplete when calculating the charge of a bipolarly charged aerosol. Kulon et al. developed PDA based bipolar charge measurement of liquid aerosols. PDA extends the capabilities of LDV, allows a real time simultaneous determination of particle size and charge distributions.

Phase-Doppler anemometry is a well-established measuring technique for simultaneous measurements of particle velocity, size, flux and concentration and its usefulness has been demonstrated in a wide range of applications to multiphase flows. Since its introduction in 1975 (Durst & Zaré, 1975), it took until 1980 to re-discover the measuring technique for particle sizing. Moreover, the increased understanding of the influence of the Gaussian intensity distribution in the probe volume of a Phase-Doppler anemometer (PDA) revealed an important feature of PDA in a planar configuration, namely the temporal separation of the contributions of two scattering mechanisms, reflection and refraction, to the light received by the photodetectors (Tropea et al., 1996; Damaschke et al., 1998; Qiu et al.,

2000; Webb & Jones, 2004). This implies the possibility of suppressing measurement errors caused by the mixing of the two modes of scattered light and even makes it possible to perform refractive-index measurements by comparison of the reflective and the refractive phases (Kerker, 1969; Haken, 1981;1985; Waldman, 1983). In the most recent development of the so-called dual-mode PDA, the planar set-up is one essential part of the system which ensures accurate measurement of the particle size and, therefore, the particulate volume flux is obtained (Tropea et al., 1996; Webb & Jones, 2004).

Subsequent contributions to the development of phase-Doppler anemometry (Durst et al., 1981; Naqwi & Ziema, 1992) were essential to the development of the technique and the recognition of its capabilities and have essentially assisted the development of commercial instruments. For many significant applications, such instruments provide reliable measurements of spherical particles of known refractive index and diameters exceeding about 5 μm. Early measurements revealed certain contradictory information when large particles of known size were employed in the investigation of the performance of a phase-Doppler anemometer (PDA). Improvements to the phase-Doppler anemometer were therefore necessary to increase the accuracy of particle-size determinations under these conditions, for applications with particles of unknown refractive index or in multiphase flows and for the accurate determination of the particle-volume flux. The PDA configuration which had the most significant impact on these developments is without any doubt the planar PDA system. Its phase-shift–particle-size characteristics for fine particle sizes are similar to those of a standard PDA with a large beam-intersection angle. It is therefore suitable for size measurements in the micrometre and sub-micrometre range, in particular in an extended version. This feature of the planar PDA for accurate size measurements has only recently been recognized. Since it offers the possibility of separating refracted and reflected scattered light, even refractive-index measurements of the particles can be carried out with this system. Finally, it has become the essential component of the recently introduced dual-mode PDA, which is capable of providing accurate volume-flux measurements of the particulate phase in two phase flows. Balachandran & Kulon (2003) have proposed a novel application of the Phase Doppler Anemometry to simultaneous analysis of particle size and bipolar charge of pharmaceutical aerosols. The non-invasive nature as well as the ability to perform accurate measurements have made this technique attractive for use in a number of different fields including sprays and liquid atomization processes, combustion measurements, design of ink-jet printers, powder production, bubble dynamics (Dantec Dynamics, 2008).

4.2 Principles of Phase Doppler Anemometry

Phase Doppler system comprises a light source (which is always a laser), optical arrangements to transit and collect light, a photocathode and a signal processing arrangement (Durst et al., 1981). The principle of velocity measurement can be explained with so called Fringe model. The Phase Doppler technique is a single-point measurement method. Therefore, the characterization of an entire spray requires traversing of the system, transmitting and receiving optics.

In PDA the laser is a source of coherent light of appropriate intensity. Its beam may be split into two parts which cross to provide an interference pattern in the local region of the flow where velocity measurements are required. The beams cross at the focal point of the probes front lens. Thus, the measurement volume formed by the laser beams is an ellipsoid. The beams crossing each other form interference fringes, and so there are high intensity planes of light and between them low intensity planes which are perpendicular to the laser beam plane. The spacing between the planes is determined purely by optical parameters of the set-up, namely the laser wavelength, and the angle between the beams. Part of the volume of interference is observed by a light collecting system which is looking to the same focal point at a certain angle. This angle is very critical since the scattered light intensity and polarization depend strongly on the viewing angle and the refractive indexes of the continuous and dispersed phase. The size measurement is based on the phase difference between the signals received by the two detectors. The photo-detector converts the optical signal into an electric signal which is processed by an appropriate signal-processing set-up. The flow is seeded with small particles, which can flow the turbulent motion of the fluid. When these particles pass by the measurement volume they scatter light according to the Mie-theory (Mie, 1908; Booker et al., 1998; Cox et al., 2002; which is used to determine the angular distribution of scattered light for particles larger than 0.05 μm), so the scattered light intensity in different scattering modes changes at different scattering angles, thus a linear relationship between the measured phase difference and the particle diameter only exists, if the detector is positioned such that one light scattering mode dominates (Figure 4.1). The intensity fluctuation of the scattered light depends also on the velocity of the particle. Time can easily be measured and then it is very simple to calculate the velocity of the particle by dividing the traveled distance by the spent time (Kulon et al., 2003; Dantec Dynamics, 2008)

The signal to noise ratio of the PDA signal depends directly on laser power, angle of the receiving optics and particle diameter, among other parameters. These three parameters can be adjusted by the user. The scattering intensity of particles depends strongly on the viewing angle. The sampling frequency depends on the arrival frequency of the particles to the measurement volume. The signal is therefore time series with random (Poisson distributed) time intervals between the samples and at the same time biased towards high velocity particles. Random interval makes the use of common time series analysis non-applicable to the PDA data. The bias can be removed from the data by using residence time (time spent in measurement volume by the particle) weighting to the data. This allows common statistical data analysis to the velocity information.

In Figure 4.1 as it is described by (Durst et al., 1981; 1997; Tropea et al., 1996; Qiu et al., 2000; Webb & Jones, 2004) the most common optical Phase Doppler configurations are illustrated. The standard system, Figure 4.12. a) has the receivers located at the same off-axis angle Φ_r, but at different elevation angles (ψ_2=-ψ_1; ψ_3< ψ_1). The receiver pair U_1/U_3 with the smallest elevation angle difference have the largest phase conversion factor and determine the particle diameter range, which is limited by the 2π ambiguity of the phase difference. The receiver pair U_1/U_2 with the smallest phase conversion factor have the highest phase difference sensitivity to particle diameter changes and is used for the diameter measurement. The 2π ambiguity of this receiver pair over the whole size range of the instrument can be solved by using the less accurate measurement from the pair U_1/U_3. Furthermore, the two independent particle diameter measurements from the two receiver pairs can be used as a validation criterion. The size range and resolution of the system can be varied by using different aperture masks in front of the receiving optics or different focal lengths of the transmitting or receiving optics which influence the intersection angle Θ and the elevation angles ψ_r.

The second system illustrated in Figure 4.1. b), is the planar phase Doppler configuration, with two receivers in the plane of the incident beams (off-axis angle Φ_r=0) at different elevation angles $\psi_{1,2}=\psi_r \pm \Delta\psi_r$. With such a system we can measure besides spherical particles, the diameter of cylinders which are oriented along the *y*-axis, because the cross section of the cylinder is identical to that of a spherical particle. For a very large elevation angle difference $\psi_{1,2}$=±30, the planar system can also measure particles in the nm region but with a limited size range to several μm.

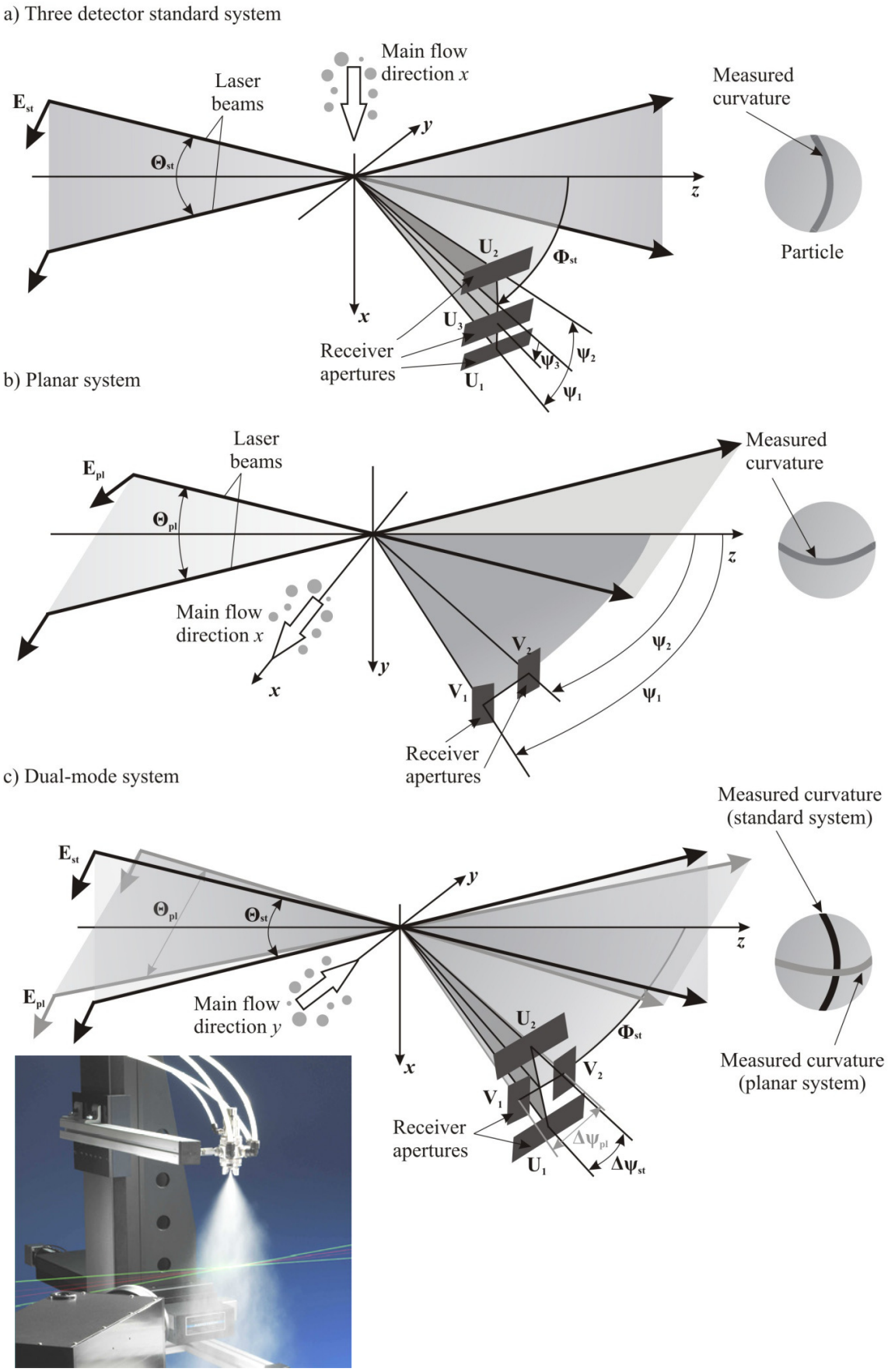

Fig. 4.1. Optical configurations of Phase Doppler Systems (Webb & Jones, 2004).

The dual-mode system illustrated in Figure 4.1. c) is a combination of a standard and a planar system. The planar system with a large phase conversion factor is used to resolve the 2π ambiguity of the standard system with higher diameter sensitivity. As indicated by the measured curvatures on the particle, the dual-mode system measures two orthogonal surface curvatures of the particle, therefore this system is much more sensitive to non-spherical particles. Only when the both systems (planar and standard) measure the same diameter, the particle is validated as being spherical. The system can detect sphericity or non-sphericity but cannot measure the volume or volume-equivalent diameter of non-spherical particles.

For calculating fluxes and concentrations of the disperse phase, the size of the detection volume and the projected area of the detection volume in the direction of the particle motion have to be known. Both depend on the particle size, because smaller particles scatter less light, and therefore, the spatial region from which the signals are detected is reduced. Moreover, the projected detection area also depends on the direction of the particle trajectory through the measurement volume. For a more precise estimation of the detection volume size and derived measurement quantities a pinhole or slit is used as a spatial filter in the receiving optics.

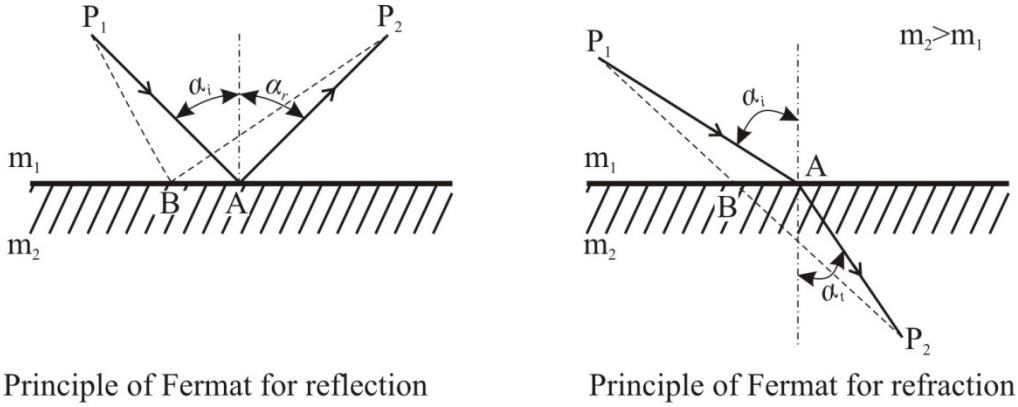

Fig. 4.2. Laws of reflection: $\alpha_i=\alpha_r$, refraction: $m_1\sin\alpha_i=m_2\sin\alpha_t$, and deduced from Principle of Fermat (Durst et al, 1981; Waldman, 1983).

If a light beam passes the interface of two media of different refractive indices, the light is partly reflected and partly transmitted (Figure 4.2). The normal to the interface, the incident beam, the reflected and transmitted beams form one plane. For the reflected beam the angle between the incident beam and the normal to the interface is the same as the angle between the outgoing beams and the normal $\alpha_i=\alpha_r$ and in the case of refraction the angle

between the incident and transmitted beam is $m_1 \sin\alpha_i = m_2 \sin\alpha_t$, $\sin\alpha_t \leq 1$. It is very important in this stage to have a proper correction of the refraction of the beams for the imaging system, otherwise several images will be produced (Durst et al, 1981; Mishchenko et al., 2006).

The properties of a plane linearly polarized light wave (Figure 4.3) can be described by the scalar quantity E_1. $\{E\}_i = \{E_1, 0, 0\}$.

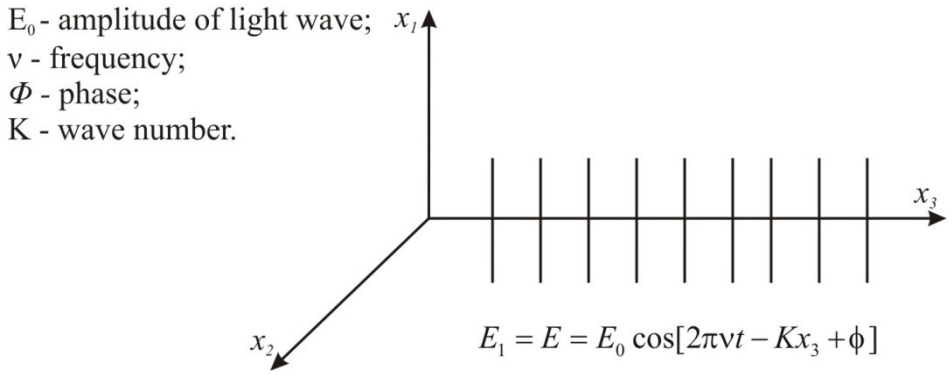

Fig. 4.3. Properties of a plane linearly polarized light wave (Kerker, 1969; Durst et al, 1981).

The refractive index of light can be expressed as the square root of the product of the magnetic permeability μ, and the dielectric constant ε, $m = \sqrt{\mu\varepsilon}$. The propagation velocity of the light waves can be expressed as follows: $c = \frac{c_0}{\sqrt{\mu\varepsilon}}$.

The PDA technique is based on the assumption that only one scattering order dominates. Two effects could lead to dominance of a scattering order differing from the expected one. One is the Gaussian beam effect (Figure 4.4), which can appear for particle sizes near or larger than the size of the incident shaped beam. If a large particle penetrates the probe volume, the Gaussian intensity profile of the incident beams causes a non-uniform illumination of the particle and induces reflected and refracted rays which have roughly equal intensities on the detectors. When the incident point of the dominant scattering order is more weakly illuminated than the incident point of the unwanted scattering order, due to the inhomogeneous intensity profile of the incident beam, the intensity of the unwanted scattering order dominates the signal and the phase difference is falsified. This effect can be prevented by using larger beam diameters or by choosing an appropriate receiver mask.

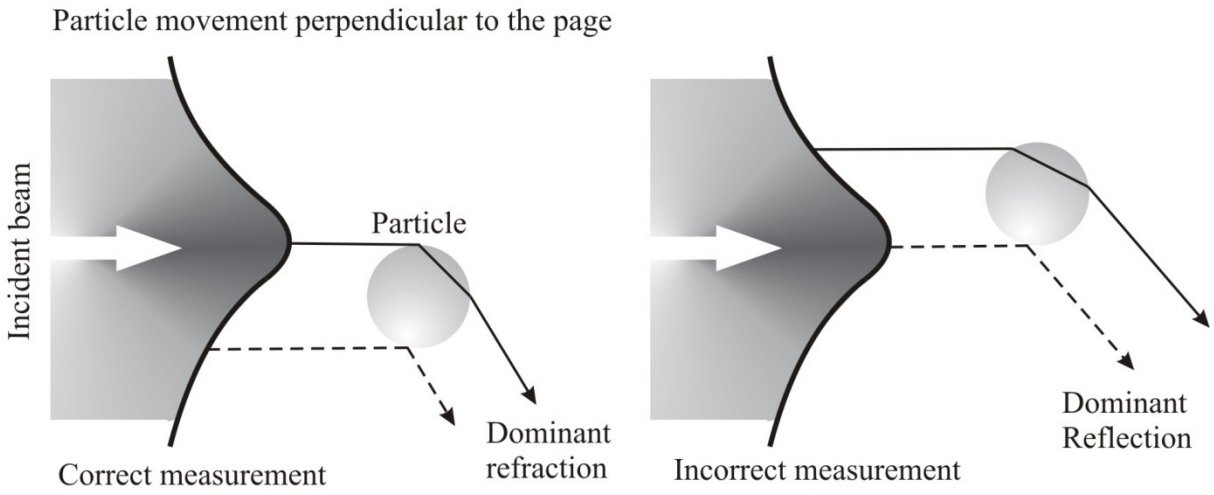

Fig. 4.4. Gaussian beam effect resulting in the dominance of the unwanted scattering order (Tropea et al, 1996).

When spatial filters are used in the receiving optics for reducing the detection volume size, the slit effect can also lead to the dominance of an unwanted scattering order (Figure 4.5). Because the receiving optics is focused on the detection volume, the light of the dominant scattering order for larger particles and trajectories near the edge of the slit could be blocked. The light of the unwanted scattering order leaves the particle at a glare point, which is located just inside the slit and, therefore, generates a signal with an incorrect phase difference. Appropriate receiver masks can suppress the slit effect.

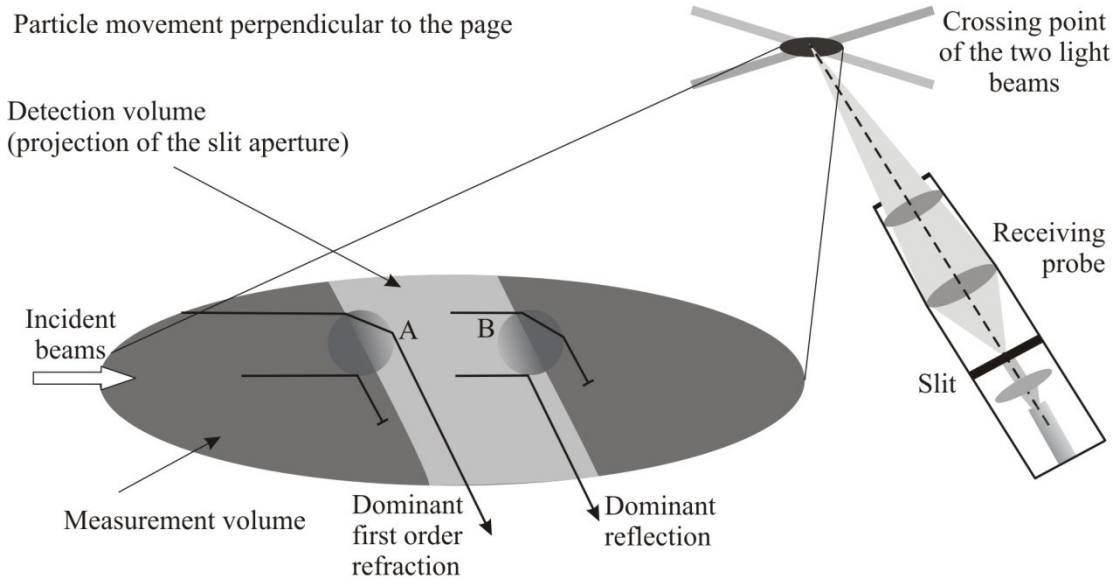

Fig. 4.5. Slit effect resulting in the dominance of the unwanted scattering order (Webb & Jones, 2004).

Small particles suspended in a flowing fluid scatter the oncoming laser radiation, thus, we can consider these particles as moving receivers and transmitters of light source. The frequencies received by the detectors are functions of the particle velocity and can, therefore, in principle be employed to measure the particle velocity. Practical use for measurements of particle velocity is prevented by the low response time of the available detectors. These do not permit the frequency of light waves to be measured, and so it became a general practice to superimpose two light waves scattered in different directions in order to obtain a signal with a frequency corresponding to the frequency difference of the two scattered light waves. The signal frequency depends on the wave length of light, the geometry of the optical system and the particle velocity. The optical system taken in consideration for this discussion is a single light beam to scatter light from a single particle and light waves collected in two different directions have been superimposed to obtain a beat signal the frequency of which contained the required velocity information (Durst et al., 1981; Mishchenko et al., 2006).

When light is reflected from a moving object, the frequency of the scattered light is shifted by an amount proportional to the speed of the object. So we could estimate the speed by observing the frequency shift. A flow is seeded with small, neutrally buoyant particles that scatter light emitted with a known frequency from a laser. The scatter light is detected by a photo-detector, an instrument that generates a current in proportion to absorbed photon energy and then amplifies that current. The difference between the incident and scattered light frequencies is called the Doppler shift.

The Doppler shift f_D depends on the speed v, and direction of the particle motion, the wavelength of the light λ, and the orientation of the observer. The orientation of the observer is defined by the angle α, between the incident light wave and the photo detector. The direction of particle motion is defined by β, the angle between the velocity vector and the bisector of angle ABC (Figure 4.6). Then:

$$f_D = \frac{2v}{\lambda}\cos\beta\sin\frac{\alpha}{2} \tag{4.1}$$

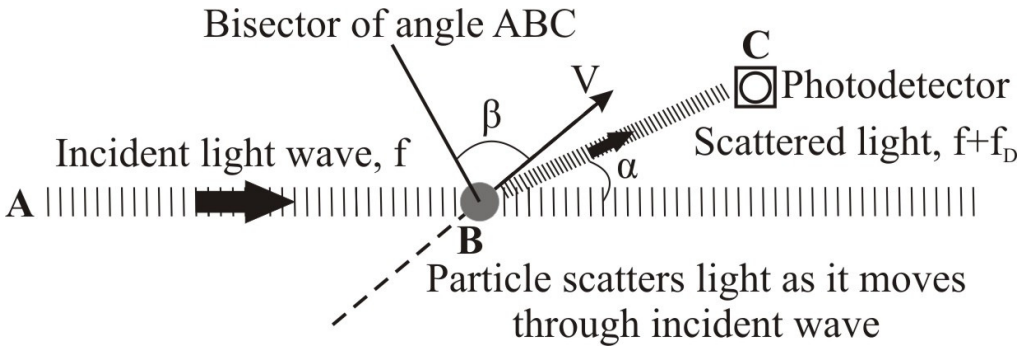

Fig. 4.6. A particle moves through an incident light wave of frequency f and scatters light in all directions. The scattered light picked up by the photo detector will be shifted by f_D (Durst et al., 1981).

A direct way to estimate f_D, is to measure the incident frequency f, and the observed frequency f_0, and find the difference. However, the Doppler shift is a very small fraction of the incident frequency, so this results in estimating a small value from the difference of two large values, a process with a high degree of uncertainty. To improve the estimate of f_D, a method using two incident beams has been developed. In this configuration the incident beam is split into two beams of equal intensity. The beams are directed to intersect, and the point of intersection is the measurement volume. Particles pass through the measurement volume scattering light from both beams. The frequency shift of the light scattered from each beam will be different because the orientation of the two beams relative to the photo detector and relative to the particle's velocity vector are different (Figure 4.7). The angles α and β defined in Figure 4.18 are different for the two beams. The Doppler shift for the two scattered beams is in this case f_{D1} and f_{D2}, and the scattered beam will have frequencies $f+f_{D1}$ and $f+f_{D2}$, both f_{D1} and f_{D2} are much smaller than f and so the scatter light waves will have nearly equal frequencies. When waves of equal amplitude and nearly equal frequency are superimposed, the amplitude of the resulting signal periodically rises and falls – this modulation is called a beat. The beat frequency is one half the difference between the two signals frequencies. Thus, when the two bursts of scattered light are superimposed within the photo detector the resulting signal has a beat with the frequency $\left|f_{D1} - f_{D2}\right|/2$.

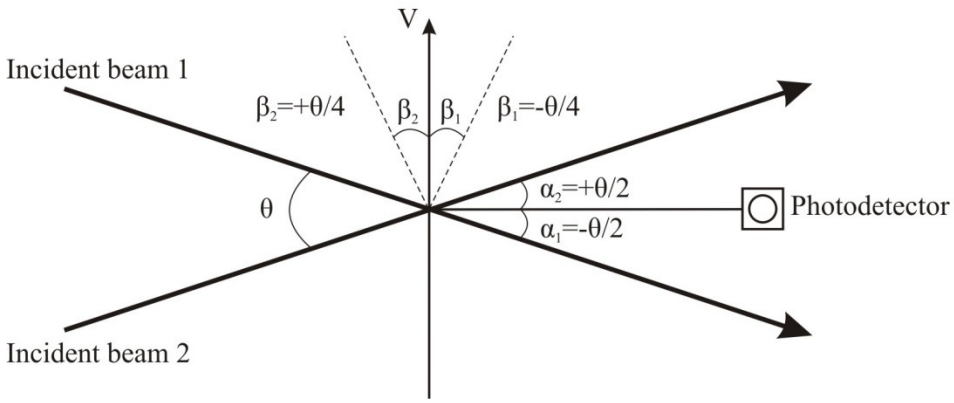

Fig. 4.7. Beam and photo detector configuration for forward scatter, differential PDA (Durst et al, 1981).

If we take for example the geometry in Figure 4.7, using equation (4.1), the frequencies shifts for beam 1 and 2 will be:

$$f_{D1}=\left(\frac{2v}{\lambda}\right)\cos\left(-\frac{\theta}{4}\right)\sin\left(-\frac{\theta}{4}\right) \quad ; \quad f_{D2}=\left(\frac{2v}{\lambda}\right)\cos\left(+\frac{\theta}{4}\right)\sin\left(+\frac{\theta}{4}\right) \tag{4.2}$$

Because sin(-a)=-sin(a) and cos(-a)=cos(a) we obtain $f_{D1}= - f_{D2}$, which is consistent with the symmetry of Figure 4.7, and so the beat frequency is:

$$\frac{\left|f_{D1}-f_{D2}\right|}{2}=\frac{2v}{\lambda}\cos\left(\frac{\theta}{4}\right)\sin\left(\frac{\theta}{4}\right)=\frac{2v}{\lambda}\sin\left(\frac{\theta}{2}\right) \tag{4.3}$$

which is the absolute value of the Doppler shift.

Another way to interpret the signal recorded by the photo detector is in terms of the interference fringe pattern generated at the beam crossing. The fringe pattern shown in Figure 4.8, consists of alternating zones of brightness and darkness. The fringe spacing, d_f, is the distance between sequential bright (or dark) zones.

$$d_f=\frac{\lambda}{2\sin(\theta/2)}. \tag{4.4}$$

As a particle crosses the fringe pattern, the intensity of the scattered light varies with the intensity of the fringes. Thus, the amplitude of the signal burst varies with time-scale d_f/v, where v is the velocity component perpendicular to the fringe pattern – perpendicular to the bisector of the two incoming beams. The frequency of the amplitude modulation is:

$$\frac{v}{d_f} = \frac{2v}{\lambda}\sin\left(\frac{\theta}{2}\right) \tag{4.5}$$

which is the Doppler frequency f_D. With the two beam system the Doppler frequency is not dependent on the position of the photo detector as we do not consider the angles α and β.

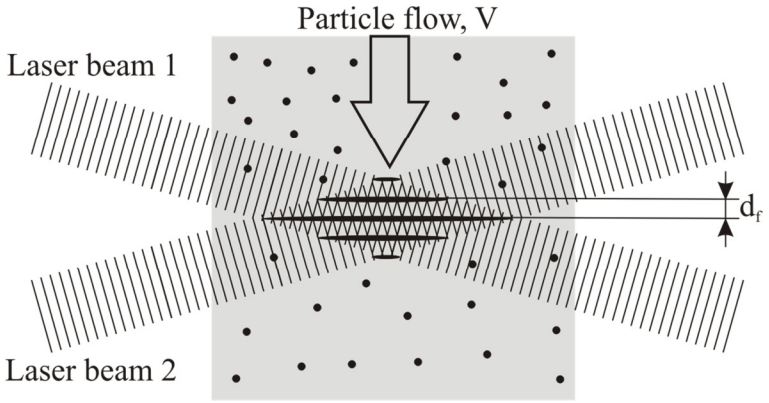

Fig. 4.8. The fringe pattern created at the intersection of the two incident beams, with a fringe spacing d_f. The frequency of the modulation is the Doppler frequency f_D, and v is the velocity component perpendicular to the fringes.

The Doppler frequency depends only on the magnitude of v, not the direction, positive or negative values of v will produce the same Doppler frequency. To correct for this directional ambiguity, the frequency of one of the incoming beams is shifted by a known value, f_s. This causes the fringe pattern to move at speed $v_s = f_s \cdot d_f$ toward the incoming unshifted beam. The frequency recorded by the photo detector is now:

$$f_d = \left| f_s + \frac{2v}{\lambda}\sin\left(\frac{\theta}{2}\right) \right| \tag{4.6}$$

and the sign of v is reflected in f_D. That is a particle moving through the fringes at speed v shifts the detected frequency, f_D, up (positive v) or down (negative v) from f_s. To avoid directional ambiguity, $f_s > \left|(2v/\lambda)\sin(\theta/2)\right|$, as shown in Figure 4.9. Thus, to optimize the system, a different frequency shift will be required for different flow conditions. An acoustic-optical device called a Bragg cell generates the required frequency shift.

A Bragg cell (acusto-optic modulator) in the measurement system allows the measurement of direction and absolute zero-speed of the object. In this device laser diode is mostly used as

the source of coherent light with punctually stabilized wavelength. The Bragg cell splits light from a laser into two beams and introduces a frequency shift (typically 40MHz) to one of the beams.

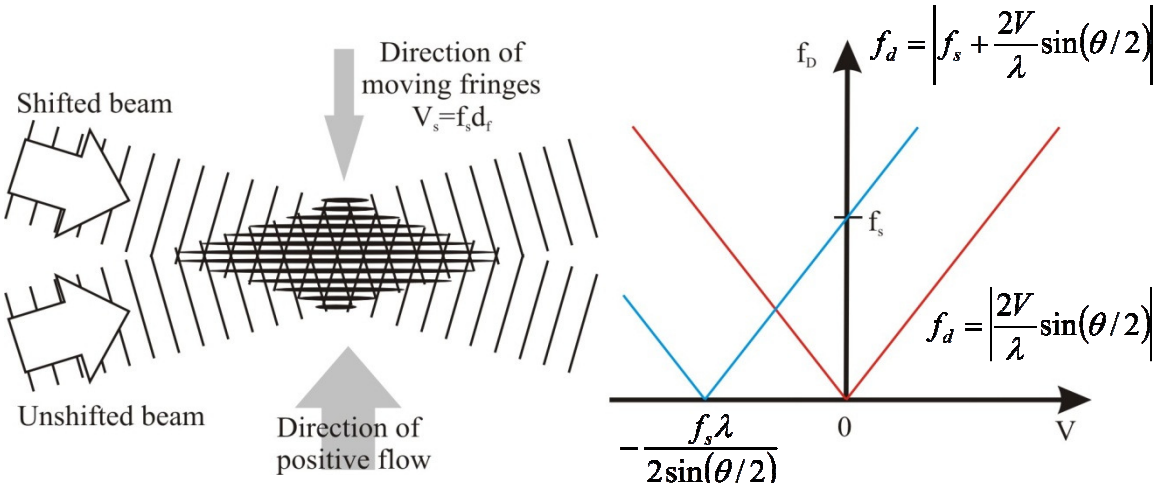

Fig. 4.9. Removing directional ambiguity with frequency shifting.

With stationary fringes the detected frequency, f_D, is the same for $+v$ and $-v$ (red curve) – we cannot distinguish direction. To remove this ambiguity we add a frequency shift, f_s. Then as shown by the blue curve, $+v$ and $-v$ produce unique values of f_D. The frequency shift is introduced optically by shifting one of the incident light beams by f_s. This causes the fringes in the interference pattern to move at $v_s = f_s \cdot d_f$, and shifts the frequency of the scattered light by f_s. Directional ambiguity is then removed for $v > f_s\lambda/(2\sin(\theta/2))$.

As described above, a single pair of incident beams measures a single velocity component, perpendicular to the bisector of the two beams. Additional components can be measured by adding additional pairs of beams that cross at the same measurement point. Each pair must have a unique wavelength so that the burst signals can be distinguished by filtering. Commonly the blue, green and violet lines of an argon-ion laser are used for multi-component measurements, the measurement volume, defined by the volume of intersection for all beams is elliptical. The best scattering signals are obtained when the particle diameter is several times the wavelength. However the particles must be small enough to follow the flow. The particles will scatter light in all directions but the highest intensity of scattered light will be on the forward side of the particle in the direction away from the incident light. Much less light is scattered in other directions. However, positioning the photo detector for forward

scatter requires that the photo detector should be opposite to the light source. It is more convenient to use the back scattered light, because this allows integration of transmitting and receiving optics in a single head. This is simpler for maintaining alignment among multiple velocity components.

Fringe spacing can be calculated for the case where two plane waves interfere forming an angle θ between the norms to the wave planes as presented in the example below.

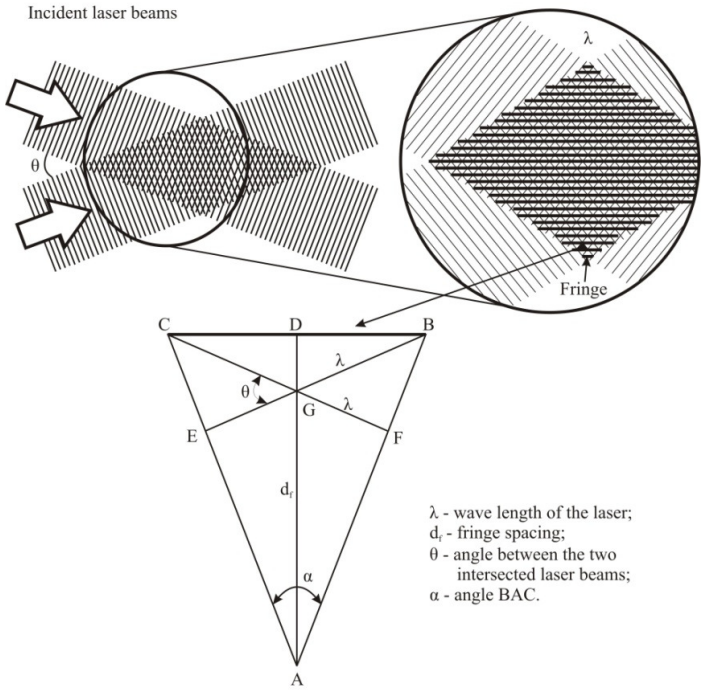

Fig. 4.10. Typical laser Doppler anemometer using two equal-intensity laser beams (split from a single beam) that intersect across the target area at a known angle θ.

Consider an isosceles triangle bounded by a fringe and two wave fronts as illustrated in Figure 4.10. The following three triangles (and sub-triangles) are geometrically similar:

$$\Delta ADB \sim \Delta BEC \sim \Delta CFB \tag{4.7}$$

If we take in consideration the angle BAC=α we have the following relationships between three of the triangle's angles:

$$\begin{cases} \angle ABC = \angle ACB = \dfrac{1}{2}(\pi - \alpha) \\ \angle ABE = \angle ACF = \dfrac{\pi}{2} - \theta \\ \angle CBE = \angle BCF = \angle BAD = \dfrac{\alpha}{2} \end{cases} \tag{4.8}$$

Simplifying the above equations we obtain:

$$\angle ABC = \angle ABE + \angle CBE \Rightarrow \frac{\pi}{2} - \frac{\alpha}{2} = \frac{\pi}{2} - \theta + \frac{\alpha}{2}. \tag{4.9}$$

In order to link d_f to λ and θ, the base of the triangle ABC is used in the following equations:

$$BC = BE\sec\left(\frac{\theta}{2}\right) = \lambda\frac{1}{\cos\left(\frac{\theta}{2}\right)} = 2BD = 2AD\tan\left(\frac{\theta}{2}\right) = 2d_f\frac{\sin(\theta/2)}{\cos(\theta/2)} \quad . \tag{4.10}$$

The fringe spacing d_f can now be expressed in terms of the laser properties:

$$d_f = \frac{\lambda}{2\sin\left(\frac{\theta}{2}\right)}. \tag{4.11}$$

The fringe distance is only dependent on the wave length of the light waves and the half angle between the wave fronts.

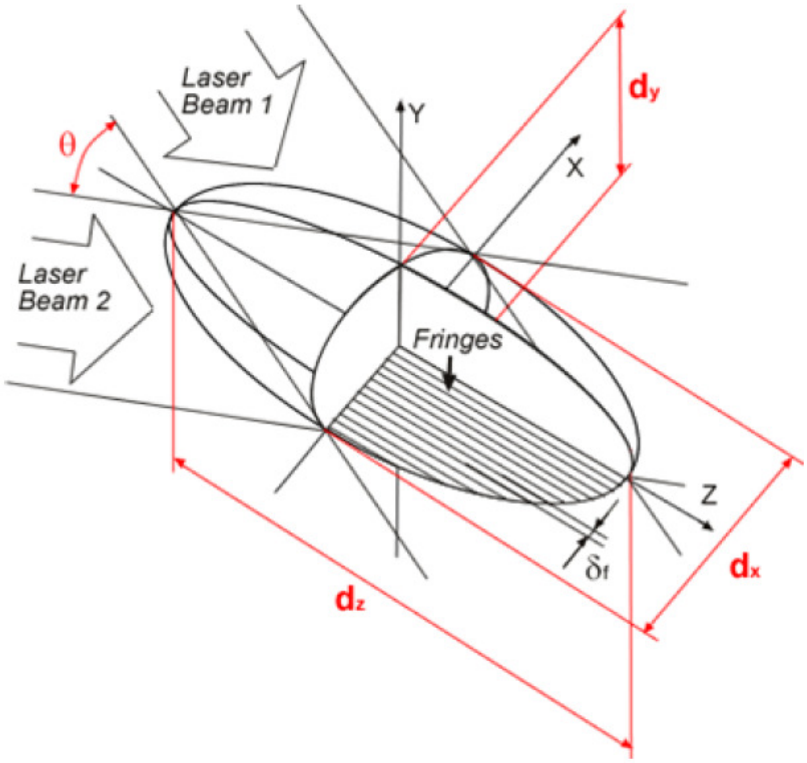

Fig. 4.11. The measurement volume dimensions (Kulon et al., 2003).

4.3 Charged Powder Particle Motion in the Presence of DC Electric Field

Charged particles, in the presence of an electric field, experience a force exerted on them. The relative motion of a particle in a viscous medium leads to a drag force. When the drag force and the externally applied force are equal, then the particle is in mechanical equilibrium and a steady-state velocity of the particle relative to the medium results. The drag force F_{drag} for spherical particles moving through air is given by:

$$F_{drag} = \frac{-C_d \pi \rho_{air} d^2 V^2}{8} \tag{4.12}$$

where C_d is the drag coefficient, V is the relative velocity between the gas and the particle, ρ_{air} is the air density, and d is the particle diameter by equating drag resistance force and the electrical force $F_e = qE$, the charge q on an individual particle can be calculated as follows:

$$\frac{-3\pi\eta V d}{C_c} = qE, \tag{4.13}$$

therefore,

$$q = \frac{-3\pi\eta V d}{C_c E} \tag{4.14}$$

where E is the electric field strength in the direction of particle drift velocity, η is the dynamic viscosity of air and C_c is the Cunningham slip correction factor.

4.3.1 Experimental set-up

The PDA technique measures the speed and size of particles without disturbing the electric field or the particle motion. The principle of the PDA is based on light scattering from two-plane light beams incident on the particle. The light from a laser is split into two parallel beams which are focused by the lenses to the measuring point. Each pair of beams is coherent and polarized so that when they intersect an interference pattern of light and dark fringes is formed. The phase shift between the signals from different detectors is proportional to the size of the spherical particle. According to Lorenz–Mie theory the scattered light intensity in different scattering modes changes at different scattering angles, thus a linear relationship between the measured phase difference and the particle diameter only exists, if the detector is

positioned such that one light scattering mode dominates. The phase shift between the two detectors depends on the scattering mode and is given by the following expression:

For *reflection*

$$\Phi = \frac{2\pi d_p}{\lambda} \frac{\sin\theta \sin\psi}{\sqrt{2(1-\cos\theta\cos\psi\cos\varphi)}} \tag{4.15}$$

and for *first-order refraction*

$$\Phi = \frac{-2\pi d_p}{\lambda} \frac{n_{rel} \sin\theta \sin\psi}{\sqrt{2(1+\cos\theta\, cos\,\psi \cos\phi)(1+n_{rel}^2 - n_{rel}\sqrt{2(1+\cos\theta\cos\psi\cos\phi)}}} \tag{4.16}$$

where λ is the wavelength of the laser light, θ is the angle between the incoming laser beams, φ is the scattering angle, ψ is the elevation angle, and n_{rel} is a particle relative refractive index. There is no calibration constant in these equations, therefore, no calibration is required providing that the particle refractive index as well as PDA optical parameters are known accurately. The velocity measurement is based on the Doppler effect and can be visualized using the fringe model. As a powder particle passes through the measurement region it scatters light at a frequency based on its velocity normal to the fringes and the spacing between the fringes.

A receiving device measures the frequency of this scattering signal, and the spacing of the fringes is known based on the wavelength of the laser light and the angle between the beams. The relationship between the Doppler frequency (f_D) and particle velocity (V) is expressed as:

$$f_d = f_s + \frac{V}{d_f} = f_s + \frac{V \cdot 2\sin\frac{\theta}{2}}{\lambda} \tag{4.17}$$

where d_f is the distance between the fringes and f_s is the frequency shift introduced to one of the beams to resolve the velocity directional ambiguity. PDPA comes as an extension of the LDV technique, the photograph of the experimental arrangement and the schematic diagram of the measurement system are shown in Fig. 4.12 while the PDPA system characteristics are listed in Table 4.1.

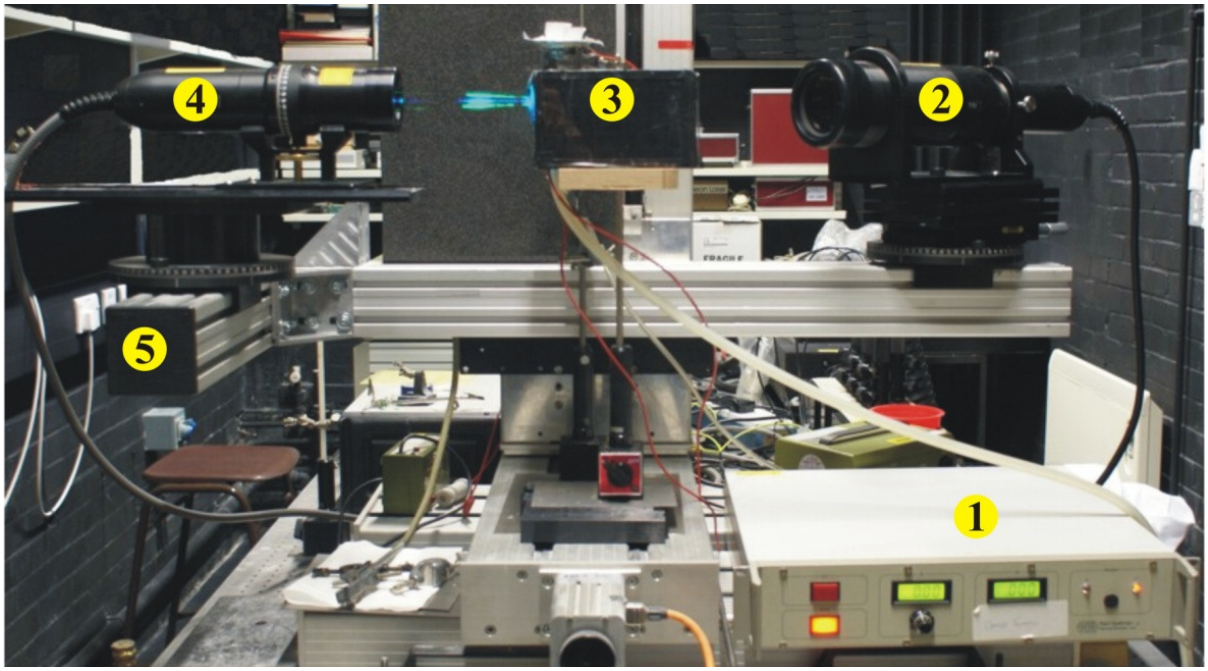

Fig. 4.12 Experimental set-up: 1 – dc high-voltage power supply; 2 – receiving optics; 3 – measurement cell with particle feeder; 4 – transmitting optics; 5 – traverse system.

TABLE 4.1 PDPA SYSTEM CHARACTERISTICS

Optical Parameters	Transmitting Optics		Units
	Channel 1 [V_z]	Channel 2 [V_y]	
Laser wavelength	514.5	488	nm
Gaussian Beam diameter	2.65	2.65	mm
Beam separation at focus lens	50	50	mm
Focusing lens focal length	363	363	mm
Fringe spacing	3.74	3.55	μm
Number of fringes	34	34	μm
Measurement volume diameter	128.18	121.58	μm
	Receiving optics		
Scattering angle	30		deg
Collection lens focal length	363		mm
Particle refractive index	1.533		-

The PDPA system comprises of an air cooled Argon-ion laser, a fibrelight multicolor beam generator with two fiber optic couplers, transmitting and receiving optics, signal processing unit with multiple velocity channels, a high-precision traversing system and a PC with interface board for data processing and storage. The experimental system of measurement consists of a TSI - PDPA system, a measurement cell with optical windows and a particle

feeder, vacuum pump and the high voltage power supplies. The performance of a PDPA system is mainly determined by the properties of the beam configuration system (laser wavelength (λ), power (P), beam waist radius (ω), and beam crossing angle (θ)), the optical detection system (off axis angles (φ), elevation angles (ψ), detector field of view (Ω)), and the particle (size, shape and refractive index (n)).

Each pair of beams is coherent and polarized so that at their intersection point, a fringe pattern is formed. A particle which travels across the intersection volume of the incident laser beams of the PDPA system scatters light non-uniformly in all directions depending on the particle properties and refractive index. The light incident on a particle is partially reflected from the surface and partially transmitted and refracted in both forward and backward directions after one internal reflection (Fig. 4.13).

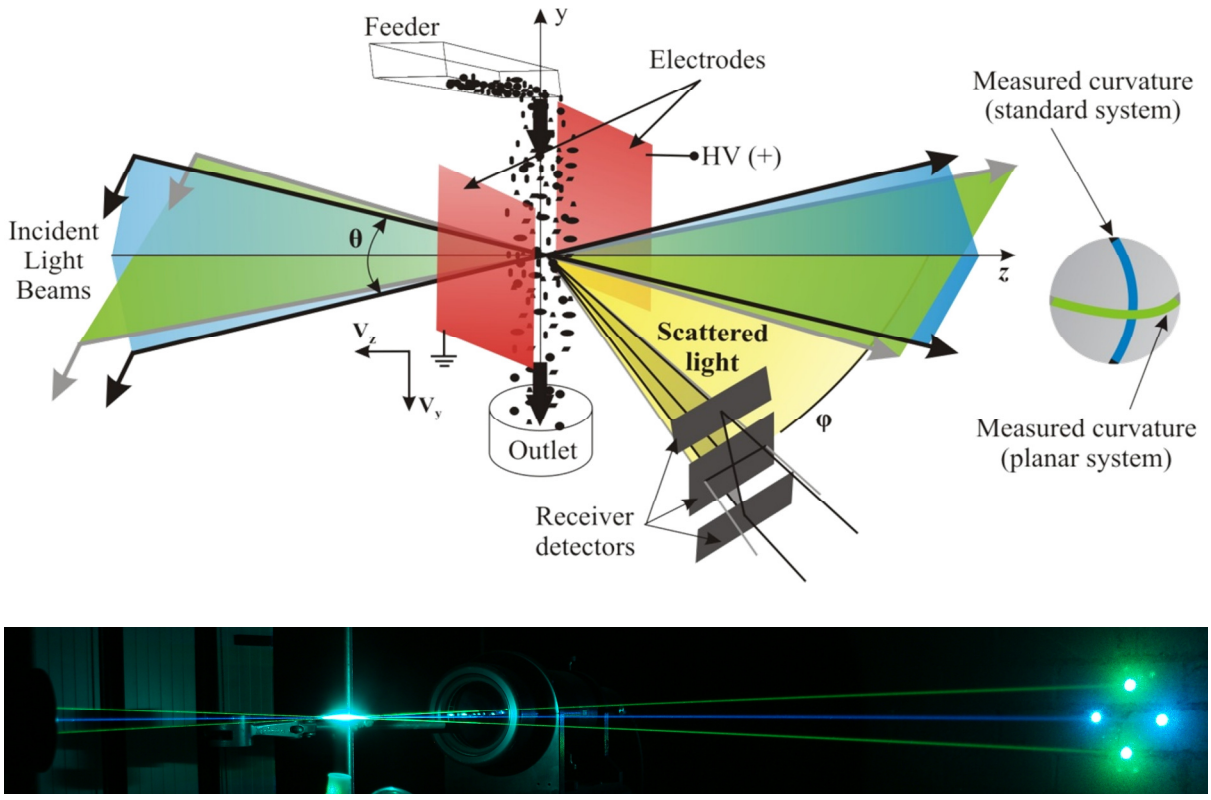

Fig. 4.13 Application of an auxiliary DC electric field within the measurement cell.

The frequencies of the scattered fields are Doppler shifted. Interference between scattered waves on the detector aperture leads to a beat signal (PDPA burst). The beat of the Doppler frequency is a measure of the particle velocity. A time phase shift between the three detectors in the receiving optics is determined by the size and the optical properties of the scattering particle. A linear relationship exists between the measured phase difference and particle

diameter only if the detector is positioned at a specific angle where a single light scattering mode dominates. The first-order refraction was selected as dominant scattering mode during the experiments with perpendicular polarization and an optimum scattering angle of 30º. No calibration of the method is required, as the PDPA system is calibrated at the factory (based on phase difference relative to particle diameter). A few measurements were conducted using standardized polystyrene microspheres 5, 10, 20, 60 & 80 μm in diameter (sourced from Duke Scientific Corporation) to check the PDPA calibration. These tests confirmed the overall applicability and accuracy of the technique in the expected size range of the measured dry powders.

The experimental investigation was performed on three samples of lactose grades (A, B, C), with size distributions in the range of 0.1 to 100μm. The micrograph below shows in detail the condition of lactose A samples used in experiments.

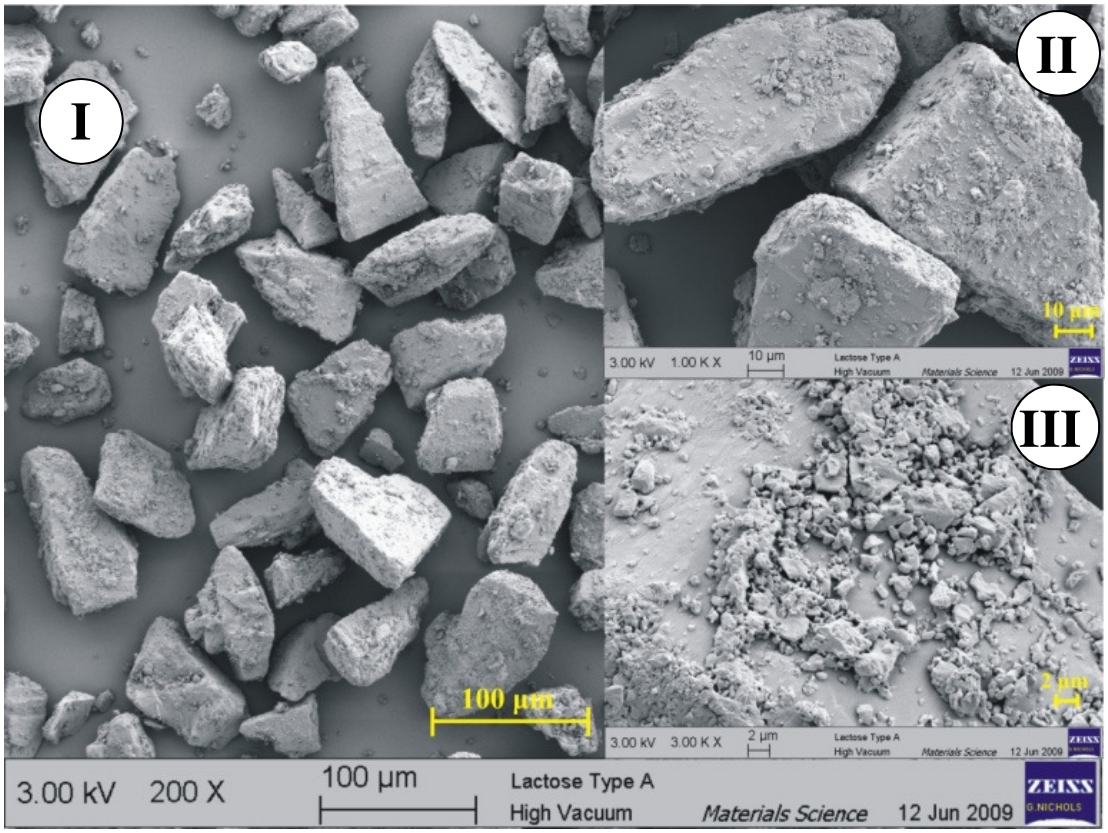

Fig. 4.14. Real-time view of a lactose sample under investigation: I: Sample 200x zoom, II: Detail 1000x zoom, III: Particle detail 3000x zoom.

The non-uniform bipolar charge distribution on individual particles is due to location of charge receptor sites (material physical and electrical properties) (Fig. 4.15). Each lactose sample has specific characteristics in particle morphology, hygroscopicity and electrical

charge, which made them very difficult to handle. Lactose B and C are very fine and proved to be highly cohesive while inter-particle forces enhanced agglomeration. In the case of agglomerated powder the speed and size measured by the PDPA will be of the whole agglomerate thus the charge on an individual particle cannot be determined.

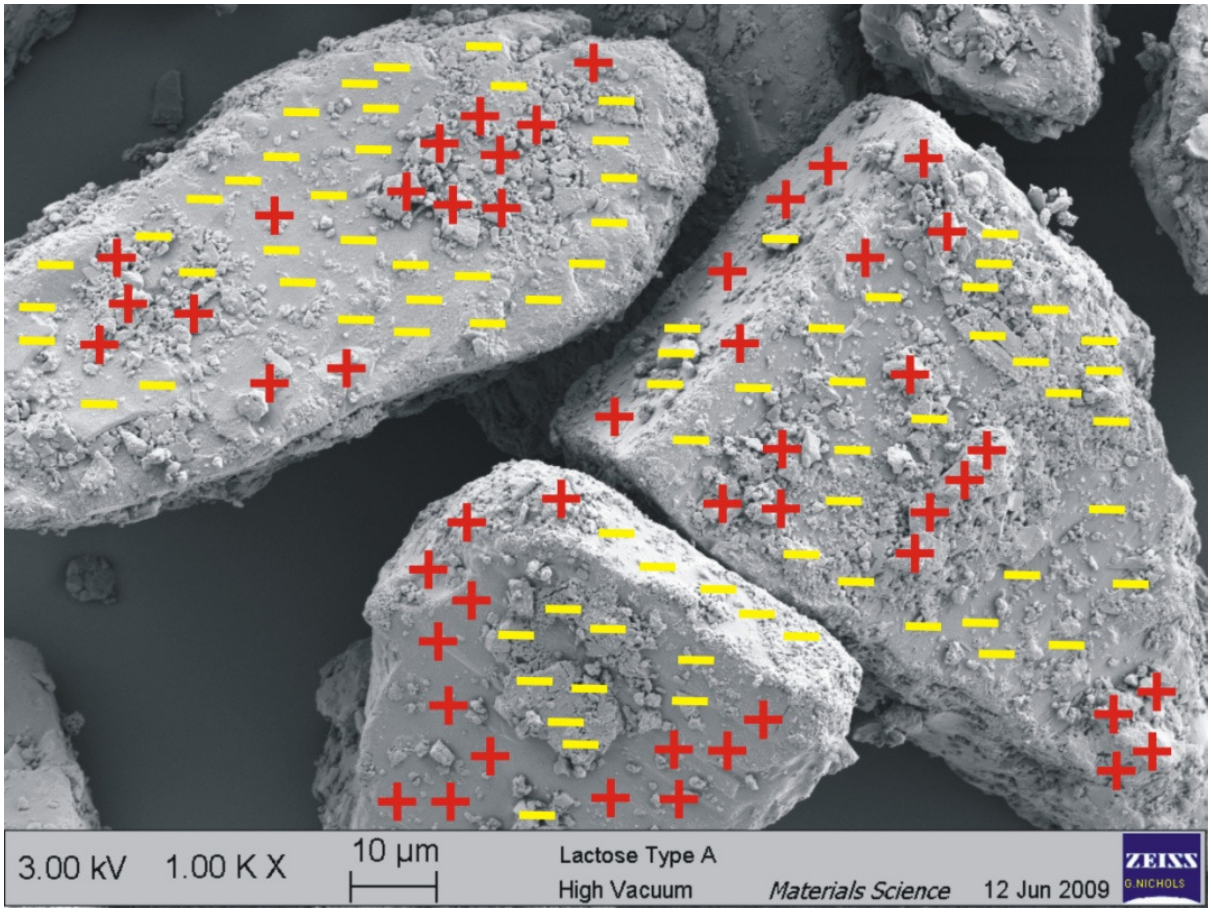

Fig. 4.15. SEM detail of a sample under investigation (hypothesis).

The specially designed feeder allows a curtain of dry powder test sample to enter the measurement cell, which is drawn out through a tube by a suction pump as seen in Fig. 4.13. The cell has a triangular shape with optical windows, incorporating two parallel-plate electrodes. The electrodes are placed 20 mm apart and a potential difference of 5kV is applied between them during the charge measurement. The electrodes have rounded edges to ensure field uniformity within the cell and a low flow rate of 0.06 L/min was maintained during measurements to ensure a laminar flow. When the lactose samples enter the measurement cell they are deflected towards the appropriate electrodes based on the polarity of charge associated with the particles. The measurement volume generated at the intersection of the four laser beams was maintained in a fixed position. The scattered light

signals were processed through a TSI-FSA 3500 8 bit signal processing unit connected via FireWire to a PC. The computer is equipped with an interface card and TSI FlowSizer 2.0.3.0 software for data acquisition and analysis.

4.3.2 Experimental results

Initial net charge measurements using a Faraday pail (see Table 4.2) revealed that the lactose powder samples were positively charged, while the *q/m* ratio increased with the finer lactose B and C. The feeder did not influence significantly the net charge of the lactose samples during transport. The measurements were performed at a temperature of 21ºC and a relative humidity of 48%. A quantity of 0.5 g lactose powder was used in each measurement. The difference between the values of the net charge obtained with lactose samples from the storage containers and the ones obtained from the feeder output are mainly due to powder handling.

TABLE 4.2 – NET CHARGE MEASUREMENTS

Faraday pail		
Lactose sample	*q* [nC/g]	*q* (using feeder) [nC/g]
A	1.59	1.30
B	3.63	2.17
C	3.95	3.30

A sample of each type of lactose powder was spread on an electrically isolated metallic plate (20×20 cm) and the surface charge was monitored using a JCI 140 Static monitor at several locations, which revealed the bipolarity of the lactose powder samples (see Fig. 4.16). The JCI 140 is a compact electric field mill instrument that allows one to determine the voltage of a surface at a given distance. It is an electromechanical device which measures the strength of a static electric field. The readings from the JCI 140 static monitor are not direct values of the surface potential, but proportional to the surface potential. To convert the readings into the surface potential, a calibration was carried out which gave a linear relationship between the readings and the applied voltage.

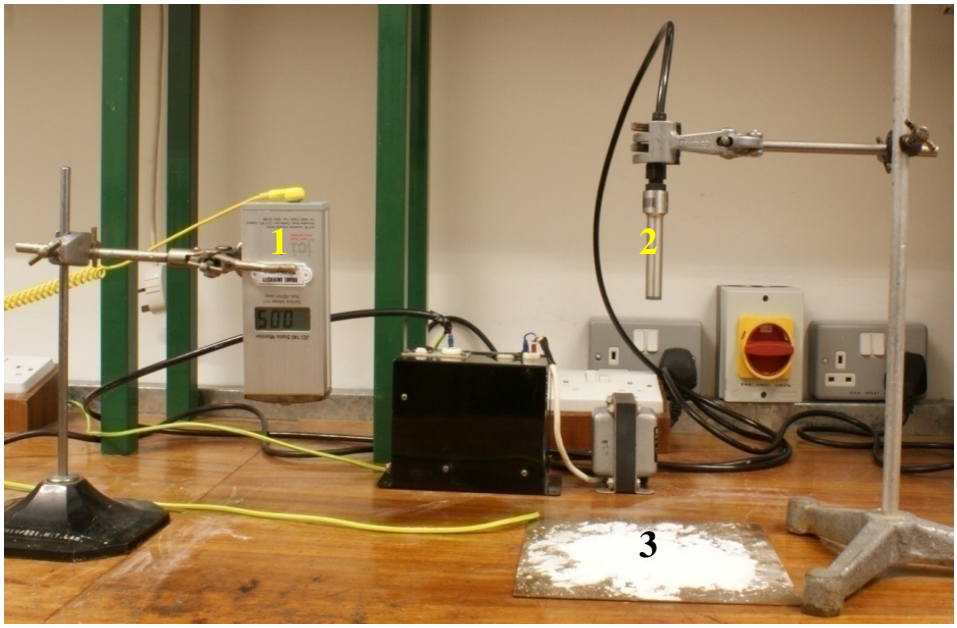

Fig. 4.16. Experimental set-up for Surface charge measurement and charge neutralisation of lactose powder samples: 1- JCI surface charge monitor; 2 – AC ionizer probe; 3- lactose sample under investigation.

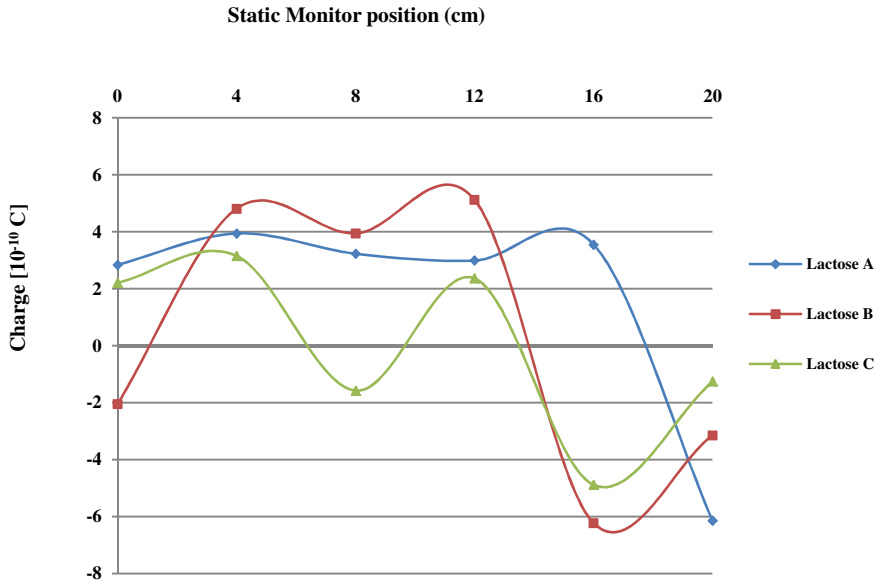

Fig. 4.17. Surface charge measurement of lactose powder samples under investigation.

The potential across the sample can then be estimated by:

$$V(t) = -\int_0^d E(x,t)dx \qquad (4.18)$$

where d is the thickness of the sample. The surface potential is related to the charge density distribution $\sigma(x)$ by Poisson's equation as:

$$\nabla E = \frac{\sigma(x,t)}{\epsilon_0 \epsilon_r} \qquad (4.19)$$

where ε_0 is the permittivity of vacuum and ε_r is the relative permittivity of the lactose sample. The charge levels can be obtained from the surface charge density which is defined as the total amount of charge q per unit area A: $\sigma = q/A$.

Tests were conducted with the modified PDPA system (see Fig. 4.12) to assess its performance and capability of measuring bipolar charge of powder particles. Figure 4.18 a. shows the particle size distribution of ambient airborne particles obtained from the PDPA, ranging from 0 to 5 μm. The bipolar charge distribution of the ambient airborne particles that passed through the measurement volume is presented in Fig. 4.18. b. These tests were conducted at a temperature of 24ºC and a relative humidity of 32%. A potential of 5 kV was applied between the electrodes (see Fig. 4.13). The majority of particles carry between -6×10^{-17} C to $+3\times10^{-17}$ C and a total of 20 000 particles have been analyzed in this run.

An experimental investigation of electrostatic properties of lactose A was performed using the modified PDPA system. A real-time capture of the particle size and velocity distributions of lactose A are shown in Fig. 4.19. The diameter and speed values obtained from Fig.4.19 a. & b. respectively are used to calculate the charge on a particle using equation (4.14).

The bipolar behavior of this type of lactose was investigated under three different experimental conditions. Firstly, the powder's inherent charge distribution was measured immediately after being dispersed from the feeder.

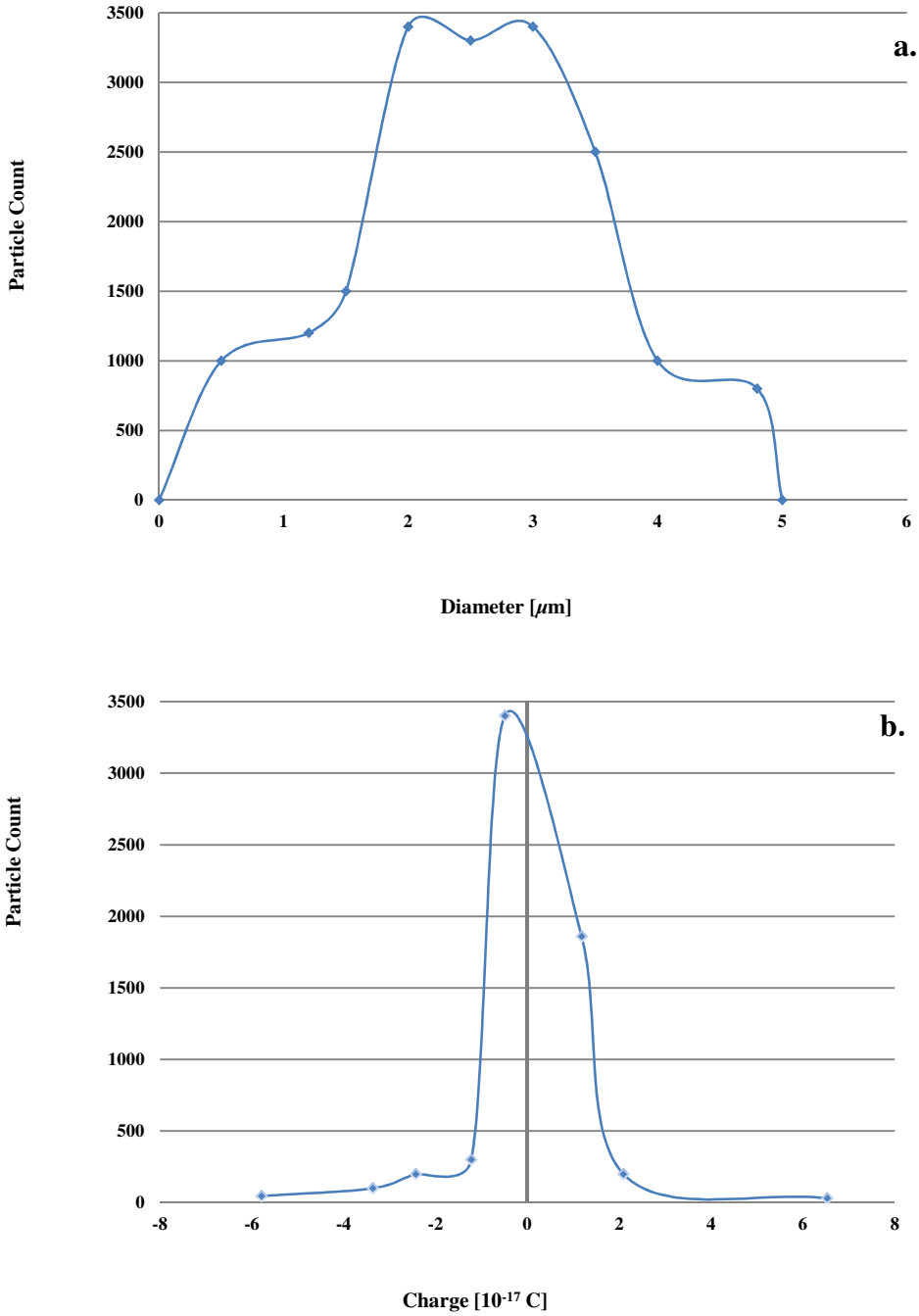

Fig. 4.18. PDPA test showing the diameter (a) and the bipolar charge (b) distributions of airborne particles in ambient air.

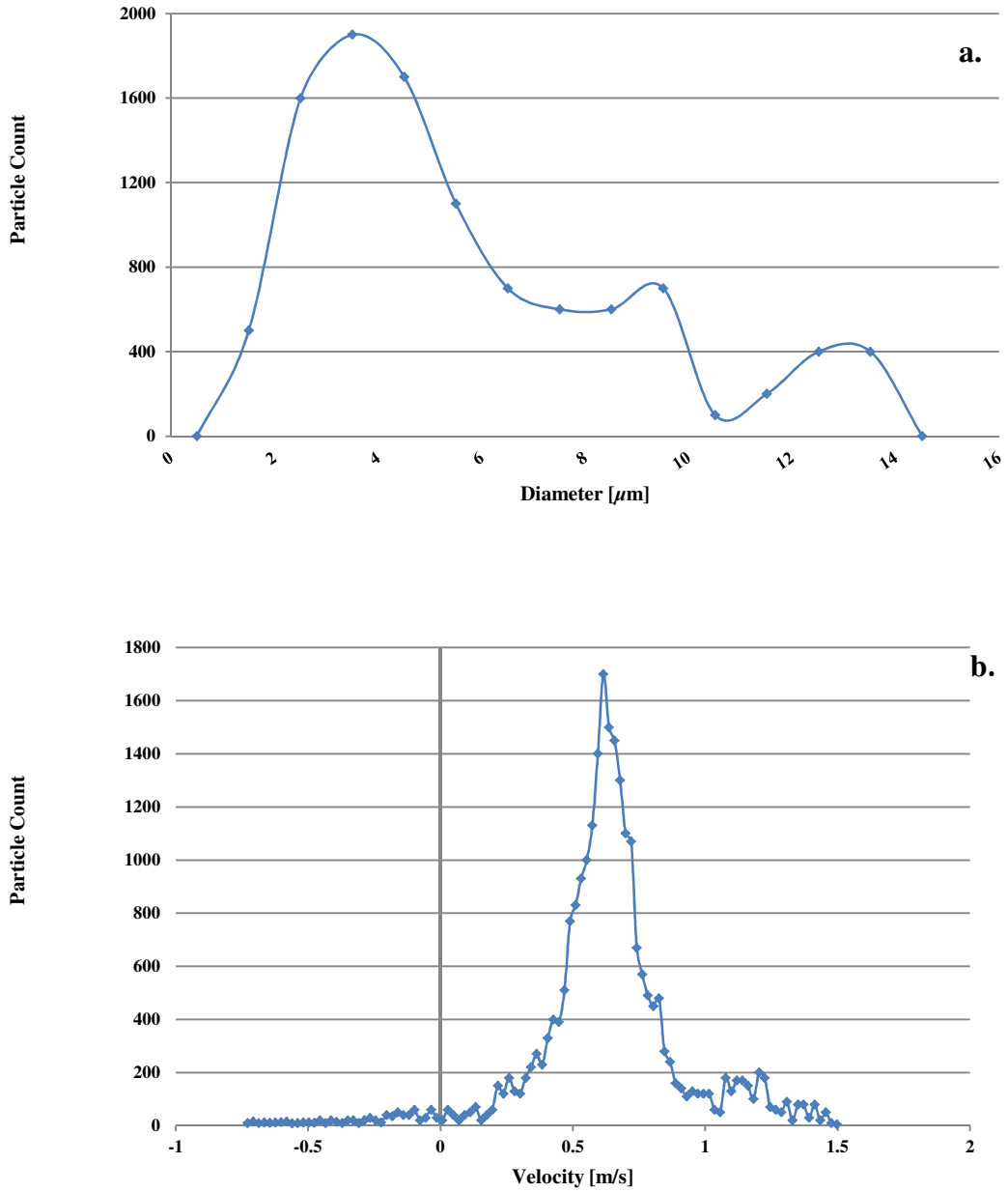

Fig. 4.19. Lactose A real-time diameter (a) and speed (b) distributions using PDPA system.

The measured values of the bipolar charge distribution are shown in Fig. 4.20.a. A total number of approximately 35 000 particles were analyzed per each run. The data was collected in the centerline of the electrode set-up as seen in Fig. 4.13. The charge distribution varies between -8×10^{-15} C and $+5\times10^{-15}$ C. For comparison purposes, the charge distribution on lactose particles precharged with positive or negative corona was examined. The corona charger used in the experiment employed a coaxial electrode arrangement. It comprises of a coaxial wire with the radius of 0.025 mm, maintained at high potential of 5 kV. Corona

charging has eliminated effectively one polarity of charge and produced predominantly unipolarly charged lactose particles.

The overall charge distribution (Fig. 4.20 b & c) for positive corona ranged from approximately 0 C to $+7\times10^{-15}$ C per particle, while for negative corona from 0 C to -10×10^{-15} C.

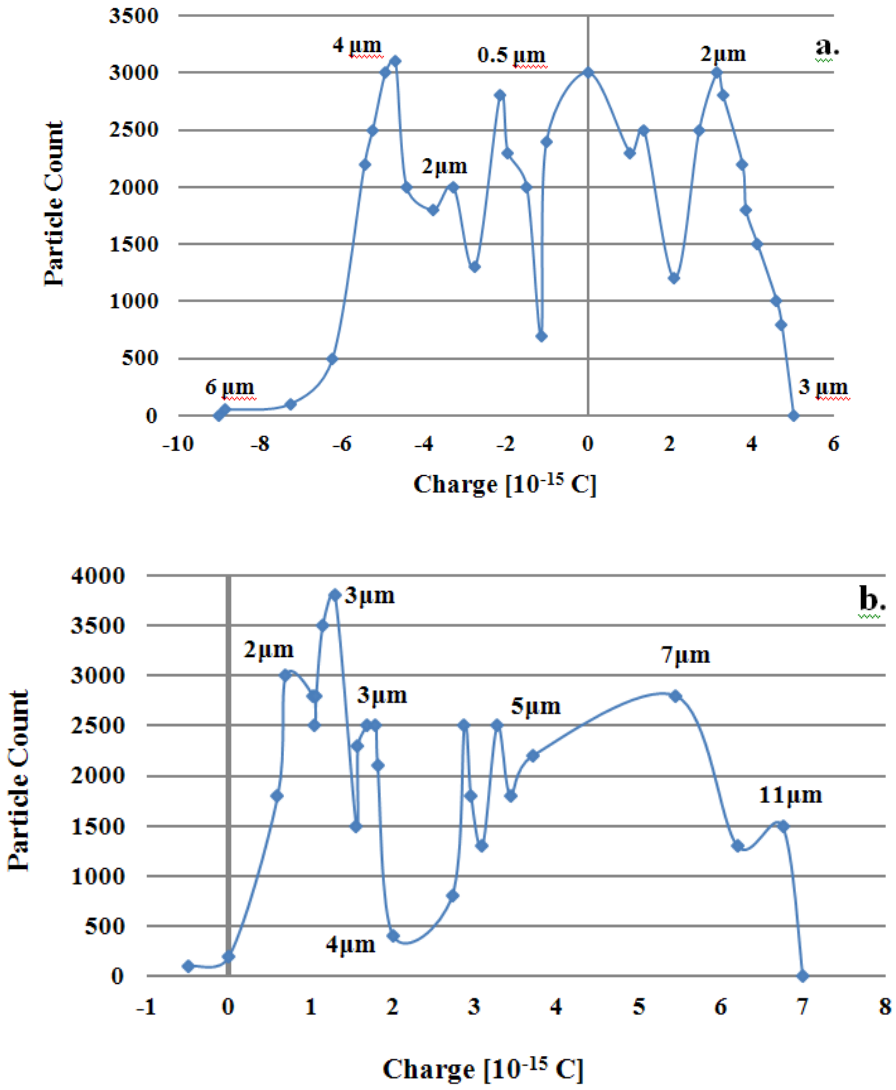

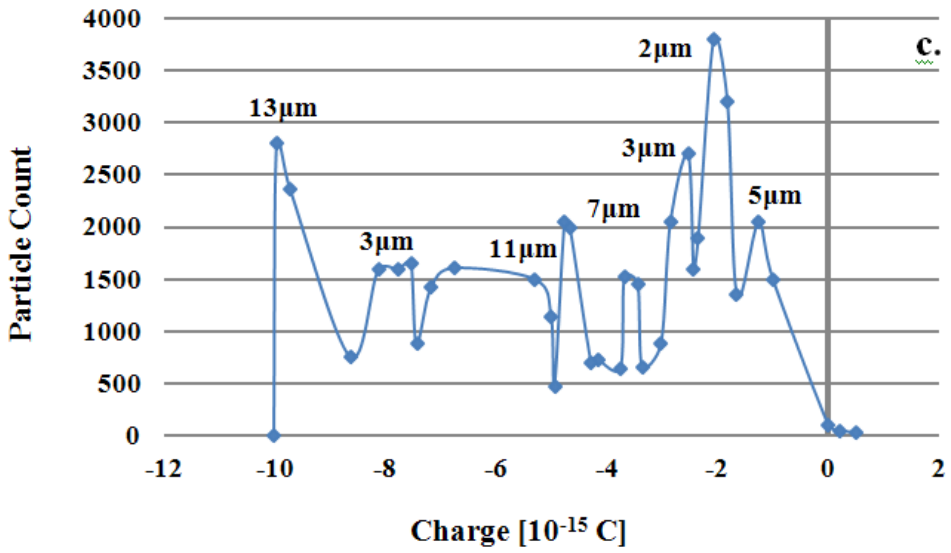

Fig. 4.20. Lactose A charge distribution. (a) Random lactose sample. (b) Positive corona discharge V=5 kV. (c) Negative corona discharge V= -5 kV.

The particle charging mechanism is probabilistic in nature, therefore, the charge accumulated by the particles is not uniform and shows a certain distribution. Figure 4.20 a., , reflects the most probable charge levels acquired by the majority of the particles. These charge levels depend on a number of factors such as the lactose particle size, particle residence time within the charging zone, the inter-particulate collisions, particle morphology, temperature, humidity, etc. It is difficult to correlate precisely the charge levels with the measured size of particles due to high complexity of inter-particulate interactions and sample's condition while passing throughout the PDA measurement volume. As shown in the paragraphs below size validation for solid particles is a true challenge when using optical sistems due to their non-sphericity. The finer lactose samples B and C proved to be highly cohesive in nature, which encouraged particle agglomeration and cohesion. This strongly influenced the ability to feed the test samples into the measuring cell by the feeder. Very few measurements for these samples were validated by the system, and the rest were discarded by the signal processing unit. The low data rate could not be used to calculate charge distribution for these samples, as the number of measurements were statistically insignificant (Beleca et. al, 2010).

4.3.3 Laser diffraction size validation performance

In order to understand the results which come from various particle size analysis techniques dispersion processes and the shape of materials makes particle size analysis a more complex matter than it first appears.

If we look at our particle under the microscope we are looking at some 2-D projection of it and there are a number of diameters that we can measure to characterise our particle. If we take the maximum length of the particle and use this as our size, then we are really saying that our particle is a sphere of this maximum dimension. Likewise, if we use the minimum diameter or some other quantity like Feret's diameter, this will give us another answer as to the size of our particle. Hence we must be aware that each characterisation technique will measure a different property of a particle (max. length, min. length, volume, surface area etc.) and therefore will give a different answer from another technique which measures an alternative dimension. Figure 4.21 shows some of the different answers possible for a single grain of sand. Each technique is not wrong – they are all right – it is just that a different property of the particle is being measured.

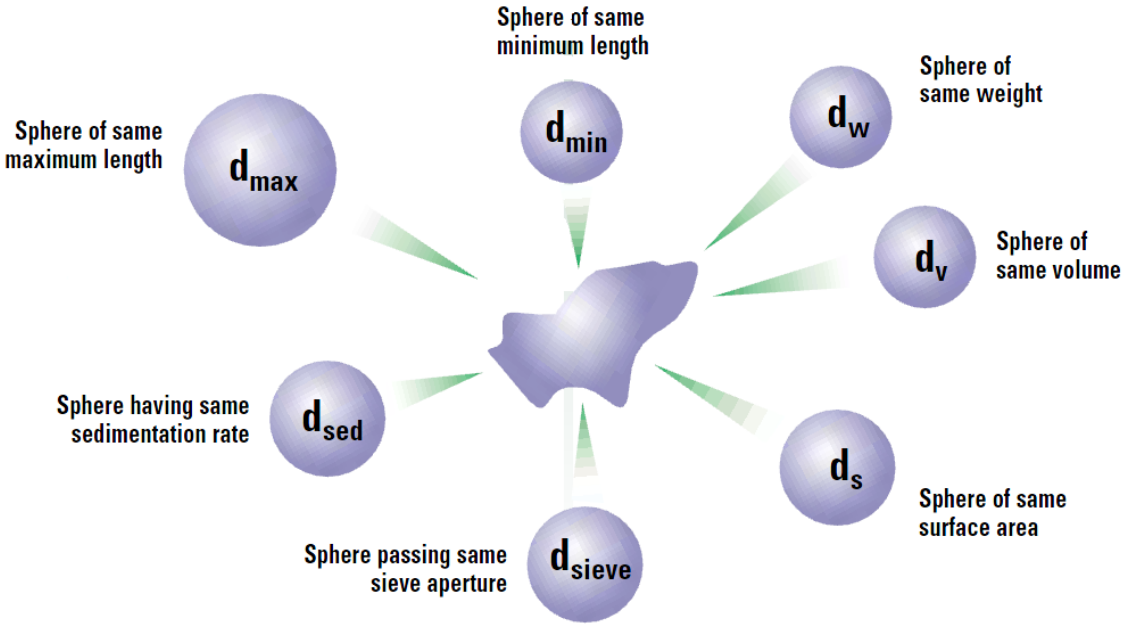

Fig. 4.21 Particle diameter characterisation methods (Malvern Instruments: www.malvern.com).

The main problem with the simple means, D[1,0], D[2,0], D[3,0], is that the number of particles is inherent in the formulae. This gives rise to the need to count large numbers of particles. The two most important moment means are the following:

- D[3,2] – Surface Area Moment Mean – Sauter Mean Diameter.
- D[4,3] – Volume or Mass Moment Mean – De Brouckere Mean Diameter.

These means are analogous to moments of inertia and introduce another linear term in diameter (i.e. surface area has a d^3 dependence and volume or mass a d^4 dependence as below):

$$D[3;2] = \sqrt{\frac{A_p}{\pi}}; \qquad D[4;3] = \left(\frac{6V_p}{\pi}\right)^{1/3}; \tag{4.20}$$

These formulae indicate around which central point of the frequency the (surface area or volume/mass) distribution would rotate. They are, in effect, centres of gravity of the respective distributions. The advantage of this method of calculation is obvious – the formulae do not contain the numbers of particles and therefore calculations of the means and distributions do not require knowledge of the number of particles involved. Laser diffraction initially calculates a distribution based around volume terms and this is why the D[4,3] is reported in a prominent manner.

- Pharmaceutical dry powder aerosols can be measured directly, although this may result in poorer dispersion than using a liquid dispersing medium. Due to this results using PDA system are not always clear. In order to test the precision of size validation we compared the PDPA size measurement with two other well established laser diffraction techniques: Sympatec and Malvern. The Sympatec measurement Figure 4.10 is presented as a size time sliced measurement (20 ms) of the dispensed aerosol cloud. The measured particle size is linearly dependent of the wavelength of the light source (HeNE Laser – 632.8 nm).

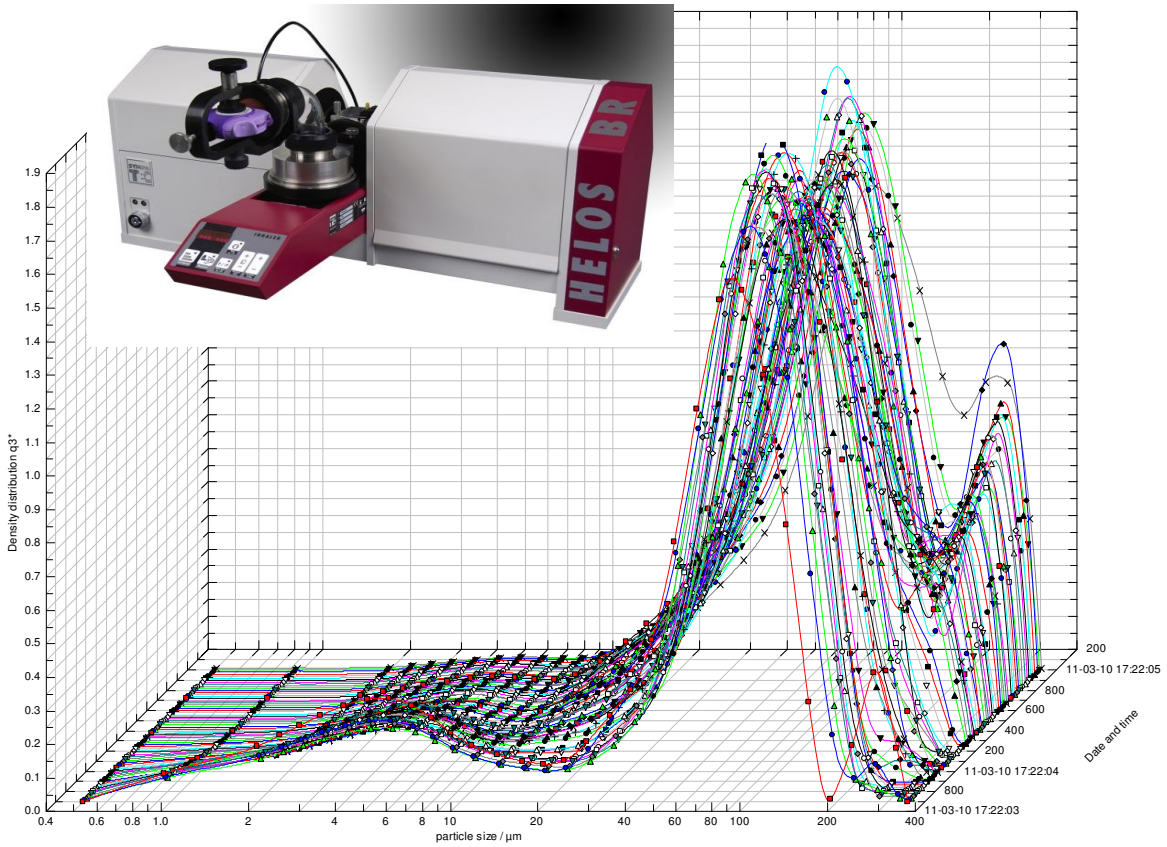

Fig. 4.22. Sympatec Helos System size distribution.

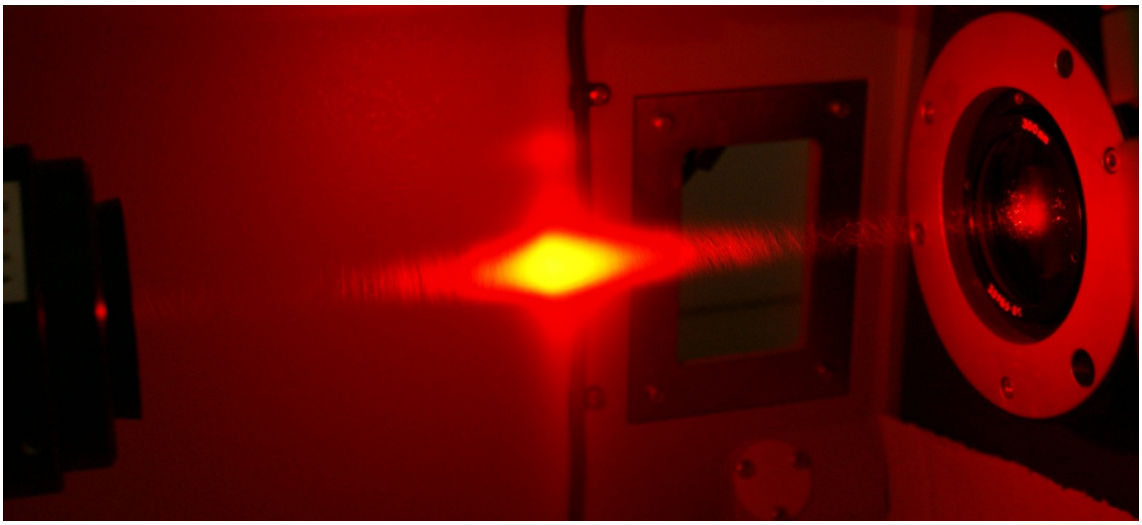

Fig. 4.23. Malver Mastersizer real time caption of dispersed pharmaceutical aerosol.

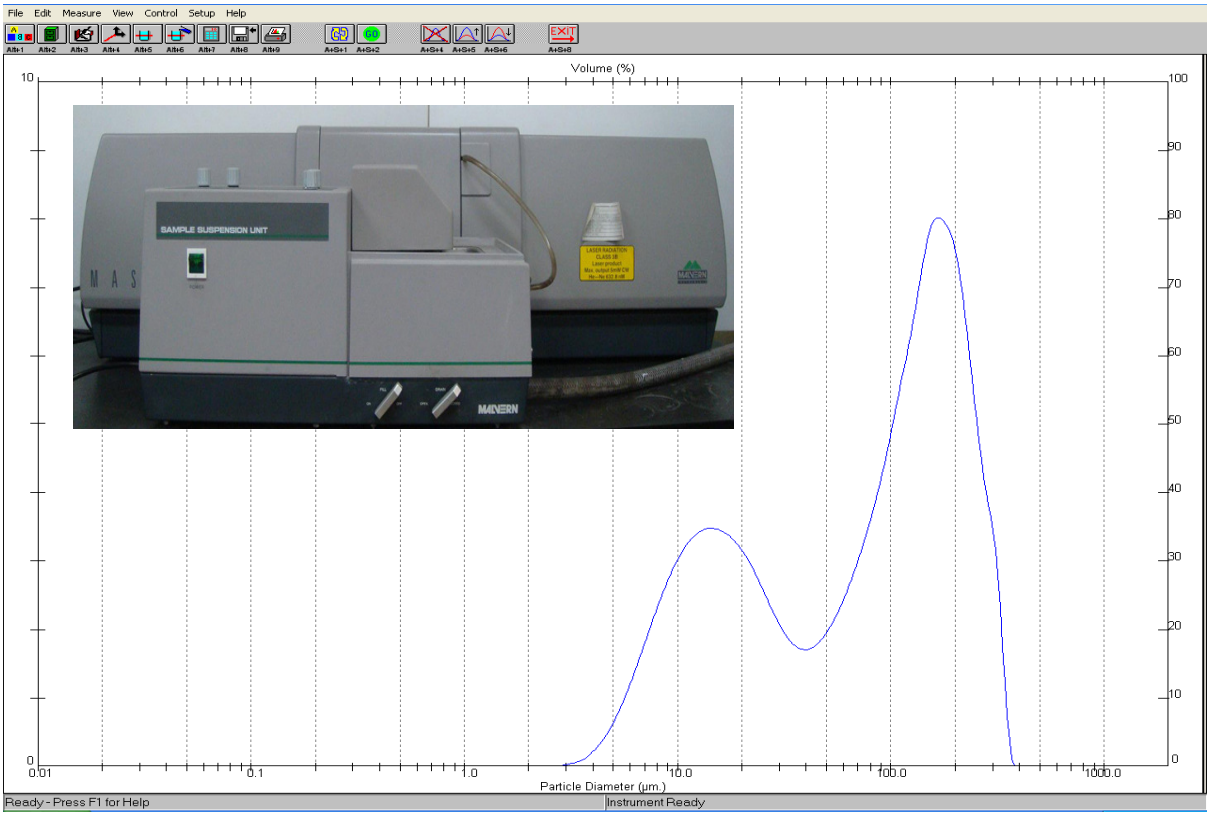

Fig. 4.24 Malvern Mastersizer size distribution of dispersed pharmaceutical aerosols.

The feasibility of the PDA system in determining correctly solid non-spherical particles has been successfully validated in conjunction with the measurements obtained using Sympatec Helos and Malvern Mastersizer optical systems as presented in figures 4.22 and 4.24. Correct size validation by such a system represents the crucial element in calculation of bipolar charge distribution of the pharmaceutical dry aerosols.

4.4 Electrostatic Properties of DPI Dispensed Drug Aerosols in a Human Upper Airway Model

Pharmaceutical aerosols, whether produced by atomisation of liquids or dispersion of dry powders, acquire a significant level of electrostatic bipolar charge on discharge from the inhaler device. Consistent dose delivery of inhaled particles along the respiratory tract depends mostly on control of particle characteristics such as morphology, crystallinity, particle density, area and size distribution, electrostatic charge and extrinsic factors including flow-rate and mouth position. The respirable fraction of an aerosol plume inhaled into the

lungs from a dry powder inhaler (DPI) increases in proportion to the airflow ability to break apart particle agglomerates and to the success of entrained, deaggregated particles to escape deposition in the DPI, mouth and throat. Due to filtering characteristics of the nasal tract, the aerosol is generally inhaled through the oral cavity, and then passes the pharynx, the larynx and the trachea before reaching the lung. This inhalation pathway mainly used to combat lung diseases it is becoming a preferred route for insulin delivery, pain management, cancer therapy and nanotherapeutics. Although the lung is the final target a significant part of the dose will deposit on the walls of the mouth-throat (extrathoracic) region, giving losses and departure from the ideal delivery. Electrostatic charge distribution of aerosols is likely to affect the efficiency of drug delivery by influencing both the transport and deposition of inhaled particles in the human airways due to space and image charge forces. This can result in a less efficient and more costly treatment in addition to unwanted side effects showing that deposition in the mouth-throat region itself becomes an important issue.

Dose-delivery efficiencies of the off-the-shelf inhalers have some serious shortcomings in drug effectiveness and inhaler efficiency. Studies showed that current asthma-drug inhalers efficiency for adults range from 10-30 % and 3-15 % for children (Kleinstreuer et al., 2008). Formulations are highly sensitive to electrostatic charge accumulation during manufacturing, storage and usage which may affect the ultimate delivery of 1 to 5 micron-sized, stable and reproductible aerosols into the lung. The mechanism of the charge generation in delivery devices has been neither well characterised nor fully understood. One reason for our present poor understanding of the electrostatic charge generation processes within the drug delivery systems is the complex fluid dynamics in these devices coupled with the effect of excipients (such as lactose or surfactants) and the blended drug particle properties including electrostatic charge. Second reason is the lack of systematic experimental studies as well as measurement equipment suitable for characterization of bipolar charge of rapidly evolving aerosols produced by dispensing devices. Despite the availability of a number of charge measurement techniques and instruments none of them is without serious disadvantages and practical limitations from the specific point of view of their application to the measurement of bipolar charge on pharmaceutical aerosols generated by drug dispensing devices.

The complicated geometry and physiology of the respiratory tract reduces our understanding of particle deposition in the lung and for this reason research into aerosol deposition is currently taking place both *in vivo* and *in vitro* in order to provide a better

understanding of the mechanisms involved in pulmonary deposition, improved routes of systemic drug administration, better treatments for lung diseases and increase protection from airborne toxic pollutants. During the past years due to continuous development in computing hardware and software, anatomically realistic airway models have been created. One technique to construct such models includes 3D reconstruction of the airways from 2D images obtained from CT and MRI, and cryosectioned images. Advanced computation fluid dynamics (CFD) models have been created to study airflow structures and predict aerosol deposition within the human respiratory system using visible human data sets, human casts and morphometric data. Balachandran *et al.* developed a numerical model of inhaled charged aerosol deposition in human airways with various lung deposition mechanisms such as inertial impaction, sedimentation, diffusion and electrostatic force (both image and space charge forces). However getting real time, non-intrusive data of bipolar charge levels on aerosols dispensed from DPI's within the human respiratory system represents a challenging issue. This chapter presents a simplified human upper airway model which combined with the modified Phase Doppler Anemometry (PDA) system is able to provide real time bipolar charge distributions of aerosols delivered from several commercially available DPI devices. This work constitutes the initial research that has been carried out in developing an improved and efficient system for bipolar charge distribution of aerosols. How the PDA measurement then relates to *in-vitro* impaction testing and/or *in-vivo* PK data may open up more pertinent debate as to the importance of charge and its control on an inhalation aerosol.

4.4.1 The anatomy of human respiratory system

The human respiratory system is an organ system that rhythmically takes in air and expels it from the body, supplying the body with oxygen and expelling the carbon dioxide that it generates. The gas exchange – allows oxygen from the air to enter the blood and carbon dioxide to leave the blood and enter the air. The cardiovascular system transports oxygen from the lungs to the cells of the body and carbon dioxide from the cells of the body to the lungs. Besides assisting the gas exchange the respiratory system performs other functions as well, but they are beyond the scope of this reprt.

The principal organs of the respiratory system are the external nose, the nasal cavity, the pharynx, the larynx, the trachea, the bronchi, and the lungs (Figure 4.25). The conductive division of the respiratory system consists of those passages that serve only for airflow,

essentially from the nostrils through the bronchioles. The respiratory division consists of the alveoli and other distal gas-exchange regions. The airway from the nose through the larynx is often called the upper respiratory tract and the regions from the trachea through the lungs compose the lower respiratory tract. Deposition of particles in the human extrathoracic airways, including the nose, mouth, pharynx and larynx, is an important protective mechanism for the lung and there isn't enough information available on airway dimensions and aerosol depositions in the oral passage for local therapeutic response, the factors that determine the absorption, clearance, and the role the bronchial circulation plays in the redistribution of the inhaled agents (Cheng et al., 1997; Labiris & Dolovich, 2003). Airway geometry, humidity, clearance mechanisms and presence of lung disease influence the deposition of aerosols and therefore influence the therapeutic effectiveness of inhaled medications.

The pharynx is a muscular funnel extending about 13 cm from the choanae to the larynx. It has three regions: the nasopharynx, oropharynx and laryngopharynx. The larynx or "voicebox" is a cartilaginous chamber about 4 cm long, and is located in the anterior part of the throat. It is connected by membranes and/or muscles superiorly to the hyoid bone and inferiorly to the trachea. The larynx performs three important functions:

- The thyroid (the largest of the cartilages) and cricoid (the most inferior cartilage) maintain an open passageway for air movement.
- The epiglottis (elastic cartilage) and vestibular folds (mucous membrane covering the superior ligaments "false vocal cords") prevent swallowed material from moving into the larynx.
- The vocal folds (mucous membrane covering the inferior cartilages "true vocal cords") are the primary source of sound production.

In the adult human, the larynx is about 3 cm in length in females and 4 cm in males, and it also changes size and shape with age. The laryngeal cross-sectional area varies and depends on the airflow rate passing through it (Cheng et al., 1997). The rapid expansion and contraction of this organ produce some degree of turbulence that could lead to significant deposition of inhaled particles. In addition, the larynx is a major resistive element to airflow and has been shown to create an inspiratory air jet that leads to particle impaction on the wall of the trachea (Kulon, 2003). Understanding the extrathoracic deposition and absorbtion

resulting from the intake of particles and gases is essential in assessing the potential biological effects to the entire respiratory tract.

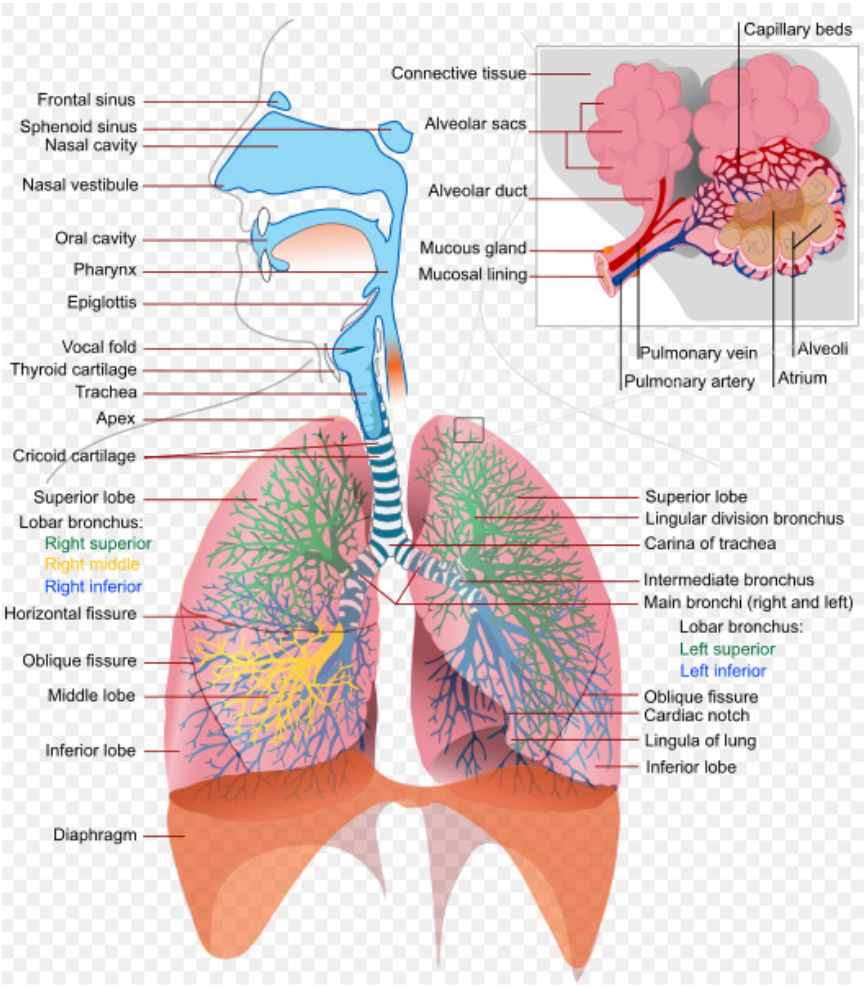

Fig. 4.25. The respiratory system (source: Wikimedia Commons, 2007).

The tracheobronchial or conductive airways region includes the airways from the larynx to the terminal bronchioles and can be subdivided into the conductive zone and the respiratory zone. The trachea or “windpipe” is a single tube 12 cm long leading from the extrathoracic environment of the neck, where it is anchored at one end at the larynx, into the intrathoracic environment containing the lungs where forks into right and left primary bronchi. It is the first of the conductive airways of the lungs, airways that conduct air to the respiratory airways where the exchange of gas that makes up the respiration takes place. The airways of the lungs are often referred as the bronchial tree. The trachea is the first and largest of about 23 generations. It is supported by 16 to 20 C-shaped rings of hyaline

cartilage. The open part of the C faces posteriorly where it is spanned by a smooth muscle, the trachealis witch contract or relax to adjust tracheal airflow. The inner lining of the trachea is a pseudostratified columnar epithelium composed mainly of mucus-secreting goblet cells, ciliated cells, and short basal stem cells. The mucus traps inhaled particles and the upward beating of the cilia drives the debris-laden mucus toward the pharynx, where it is swallowed. This mechanism is called mucociliary escalator. The airways of each generation arise from the previous one by a system of irregular dichotomus branching airways. Dichotomus because each `mother` airway gives rise to two `daughter` airways, and irregular because the daughters, although smaller than the mother, are not necessarily of equal size (Davies and Moores, 2003). Delivery of submicron drug particles of appropriate electrical charge to these lower alveolar regions is essential to dilate the constricted airways of the asthmatics. The model has also facilitated the understanding of pollen allergens reaching the lower alveolar regions, and in particular the thunderstorm initiated asthma. Progressive branching and narrowing of the airways encourage the impaction of particles. The larger the particle size, the greater the velocity of incoming air, the greater the bend angle of bifurcations and the smaller the airway radius, the greater the probability of deposition by impaction.

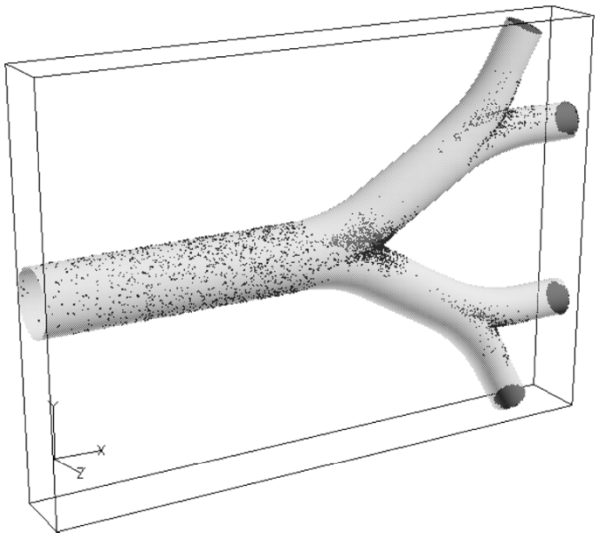

Fig. 4.26. Deposition pattern of charged particle on bifurcation model for steady inhaled flow. (Balachandran et al., 2004).

Respiratory diseases change the architecture of the lung through alterations in bifurcations angles and obstruction or the airways due to mucus accumulation, modifying the distribution and deposition patterns of aerosols. Also, drug particles are known to be hygroscopic and grow and shrink in size in high humidity, such as in the lung which has a

relative humidity of approximately 99.5%; increasing the total deposition (Xu & Yu, 1985). A decrease in the cross-sectional area of the lung caused by obstructions increases air velocities and turbulence in regions where normally the airflow is laminar, and so little drug is deposited in obstructed areas, where it is needed to reach to achieve optimal therapeutic effect.

For single breath devices such as MDI and DPI the inhaled volumes are normally between VC and IC. The flow rate during inhalation of this volume affects the uptake of the drug particles and deaggregation of powder from the drug dispenser as well as the aerosol deposition in the respiratory tract. Particles can be deposited by inertial impaction, gravitational sedimentation or diffusion (Brownian motion). While deposition occurs throughout the airways, inertial impaction occurs in the first 10 generations of the lung, where air velocity is high and airflow is turbulent. Most particles >10 µm are deposited in the oropharyngeal region with a large amount impacting on the larynx, particularly when the drug is inhaled from devices requiring a high inspiration flow rate (DPIs) or when the drug is dispensed from the device at a high forward velocity (MDIs). Flow rate affects the probability of particle impaction and the extent of turbulent flow, which enhances particle deposition in the upper airways. Deposition by gravitational sedimentation predominates in the last five to six generations of airways (smaller bronchi and bronchioles), where air velocity is low. In the alveolar region, air velocity is negligible, and the contribution to deposition by inertial impaction is nil. Particles in this region have a longer residence time and are deposited by sedimentation and diffusion. Deposition due to sedimentation affects particles down to 0.5 µm in diameter, whereas below 0.5 µm the main mechanism for deposition is by diffusion. The pattern of respiration during aerosol exposure influences regional deposition, since breathing volume and frequency determine the mean flow rates in each region of the respiratory tract, which, in turn, influence the effectiveness of each deposition mechanism. The combination of flow rate, tidal volume, breath-holding time, and lung volume affects particle residence time in each lung region and hence the probability of deposition by gravitational and diffusional forces (Kulon, 2003). Tidal volume and flow rate also influence the motion of the larynx and affect particle deposition there. Therefore, rapid breathing is often associated with increased deposition of larger particles in the upper respiratory tract, while slow, steady inhalation increases the number of particles that penetrate to the peripheral parts of the lungs.

4.4.2 Human Upper Respiratory Model

Anatomically realistic airway geometry is required for accurate biomechanical modeling particle deposition predictions and ultimately risk assessment and inhaled drug delivery protocols. Peripheral Systems Laboratory (Ecole Polytechnique Fédérale de Lausanne) offers a virtual anatomic construction kit on the web using the Visible Human Project® (VHP) from National Library of Medicine (U.S.A.) dataset.

The VHP digital image library of volumetric data represents complete, normal, healthy, adult male and female anatomy. The human male and female data sets consists of CT, MRI and photographic images from cryosectioning of cadavers. Cadavers with infections or metastatic disease, scars or physical distortions, surgery or any other condition that could have distorted the cadaver's anatomy were not used. If no abnormalities were found, radiographs of these cadavers were taken, CT and MRI's were obtained of each region of the body. After several freezing and sectioning procedures the cadavers were cut using a milling device and digital photographs were taken. MRI's and CT transverse images for the VHP were shot at 1mm intervals, CT images having a better resolution and a better air/tissue contrast compared to MRI images. However neither MRI nor the CT images had high enough resolution for accurate 3D reconstruction. The highest resolution was obtained from the cryosectioned images, unfortunately it limits reconstruction of the larger central airways. Another limitation is that the air passageway from the oral cavity to the throat superior to the glottis was not visible and could not be reconstructed.

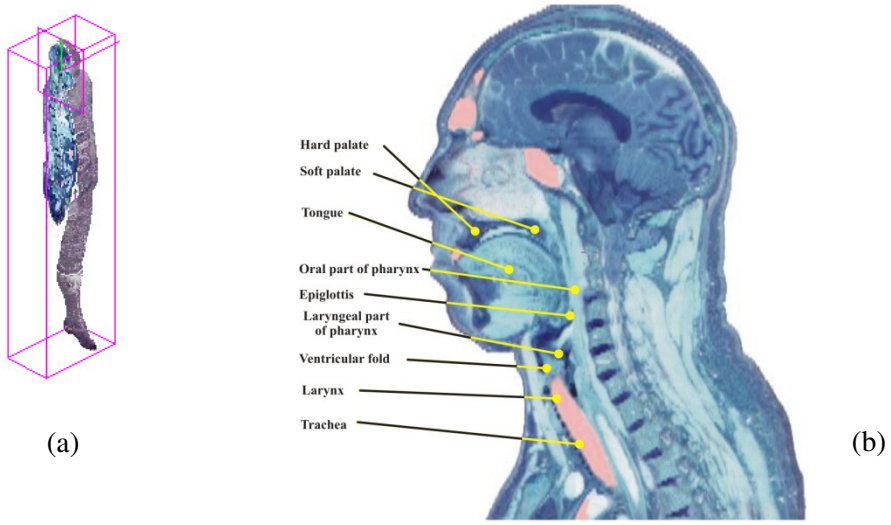

Fig. 4.27. Sagittal slice (b) with anatomical description of the upper human respiratory system obtained from the 3D Visible Human Model® (a).

This application offers to any web client the capability of interactively specifying the exact position and orientation of a desired slice and of requesting and obtaining that slice from a 3D tomographic volume, made of either CT, MRI of cryosection images (Fig. 4.27).
In order to reconstruct digitally the mouth and throat section from the multiple axial, sagittal and coronal medical photographs, several image processing and computer-aided design software (CAD) are used. The resulting 3D digital human upper respiratory model (Fig. 4.28.) has similar features and dimensions as other models reported in literature. Once such a design is obtained replica casts of human respiratory system can be built. Many CFD investigations of aerosols transport and deposition into the upper and lower human respiratory system have been developed. Numerical models of respiratory tract temperature, heat and water vapor exchange and intra-airway hygroscopic particle growth have been used to explore the etiology of cold-induced asthma and to take in consideration other factors that influence aerosol deposition. Also, numerical models of inhaled charged aerosol deposition in human airways have been developed, taking into account the effect of the space-charge and image-charge. These computer simulated models provided a better understanding of charged aerosol transport and deposition and helped improve control of drug delivery in human airways.

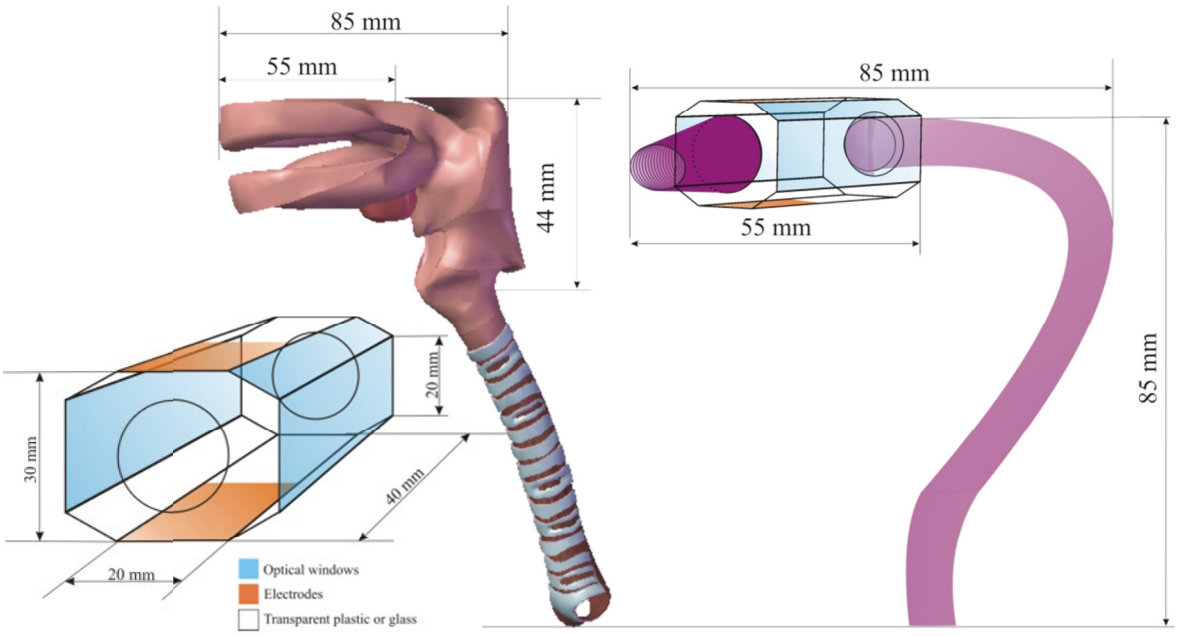

Fig. 4.28. 3D Digital Human Upper Respiratory Model (a) and BRUNEL concept of a simplified oral cavity and throat model for bipolar charge measurements using PDA system (b).

In order to be able to obtain real-time, non-intrusive data of bipolar charge levels of aerosol plumes dispensed by DPI's, a rigorous and precise experimental set-up needs to be built, that can be correlated with a human upper respiratory model and integrated with a PDA system. The resulting concept for the measurement chamber design (octagonal prism) is in close correlation with the size and volume of a human oral cavity at the moment of inhalation. The geometry of the chamber (Fig. 4.28), wall & optical windows thickness (1 mm) has been chosen in order to incorporate the PDA laser beams measurement volume and allow the aerosol scattered light to reach the detector. The throat section up to trachea was averaged with 20 mm diameter AuraOnce® Laryngeal tubes (Ambu UK Ltd.). The laryngeal tubes solution was preferred because of the fragility of the set-up and the benefits of these devices used in respiratory emergency management as they feature a special curve that carefully replicates natural human anatomy. Different types of mouthpieces can be incorporated with the chamber to allow any type of DPI inhaler to be tested.

4.4.3 Momentum transfer

The general formulation is based on the momentum equation for a small rigid sphere in an unsteady, non-uniform ow. The momentum equation relates the acceleration of the particle mass and its added mass to the sum of the various forces acting on the particle given by:

$$\rho_p V_p \left(1 + \frac{C_M}{\Psi}\right) \frac{du_p}{dt} = \sum F_k \tag{4.21}$$

where V_p is the particle volume, k is a summation index for all force components, C_M is the added mass coefficient, and Ψ is the ratio of particle density to continuous-fluid density.

The summation of forces are typically combined with the effects of drag (F_D), gravity (Fg), lift (F_L), uid stress gradients arising from the continuous-phase acceleration (F_S), Basset history term (F_H), wall interaction (F_W), and the other body forces (F_e & F_{img}) are the electrostatic force and image charge force , which are expressed as:

$$\sum F_k = F_D + F_g + F_L + F_S + F_H + F_W + F_e + F_{img} \tag{4.22}$$

However, the particle motion of aerosols for inhaled drug delivery mainly consider only drag, gravity, diffusion and body forces. For a non-turbulent Newtonian fluid Navier-Stokes equation for a compresible fluid is:

$$-\vec{\nabla}p + \mu\left(\vec{\nabla}^2 v\right) + \frac{1}{3}\mu\left(\vec{\nabla}\left(\vec{\nabla}v\right)\right) + \rho b = \rho\dot{v}$$

(4.23)

The Navier-Stokes equation is obtained by combining the fluid kinematics and constitutive relation into the fluid equation of motion, and eliminating the fluid stress and strain rate parameters. For a fluid at rest the equation reduces to:

$$-\nabla p + \rho b = 0 \tag{4.24}$$

Where the body of forces b is due to gravity only. All particle are described as a simple point moving at their own independent velocity. The trajectory of particle in Cartesian co-ordinate can be computed by integrating all the forces acting on particles (drag, gravity, space charge, and image charge forces).

$$\frac{dv_p}{dt} = F_D(v_p - v_f) + F_g + F_{spc} + F_{img} \tag{4.25}$$

4.4.4 Transport and Deposition of Pharmaceutical Aerosols

First step focuses on the uncharged particle case with mechanisms of impaction, gravitational sedimentation and diffusion. The transport of the pharmaceutical aerosols can be considered as a dispersed phase flow problem in which the dispersed phase does not materially connect with the continuous phase (e.g. gas-droplet, gas-particle and liquid-particle flows). The classification of dispersed phase can be divided into dilute and dense dispersed flows:

- The dilute dispersed phase flow is defined when the effects of particle-particle interaction are not significant. The particle motion is mainly dominated by the fluid forces.
- The dense flow represents the situation where particle motion is primary controlled by particle collision.

The simple criteria for classifying dilute or dense nature flow can be considered using the ratio of the momentum response time of particles to the collision time. The flow can be considered as dilute if:

$$\frac{\tau_v}{\tau_c} < 1 \tag{4.26}$$

Where τ_v is the relaxation time (momentum response time: $\tau_v = \frac{\rho_p d_p^2 C_c}{18\mu}$) and τ_c is the average time between particle-particle collisions. It means that the particles have sufficient time to respond to the local fluid force before the next collision. If the ratio is more than one, it can be considered a dense flow. Based on a study by Sommerfield, the maximum particle size for

dilute flow at the mass loading of unity with a standard deviation of the particle fluctuation velocity of 1.0 *m/s* would be about 20 μm, where the mass loading is defined as the particle mass per unit volume of mixture divided by the continuous-fluid mass per unit volume of mixture (Hidy and Brock, 1971):

$$\gamma = \frac{\beta \rho_p}{\rho_c} \tag{4.27}$$

Where β is the fraction of dispersed phase volume to the total mixed volume.

Due to the small particle size of pharmaceutical aerosols, the aerosol transport in the human respiratory system can be modelled as dilute dispersed phase flow.

The coupling between the continuous phase and the dispersed phase is important in flow analysis. The coupling can be divided in:

- One way coupling – it is assumed that the dispersed phase has no reverse effect on the continuous phase flow.
- Two way coupling – has effects between both phases and can be modelled through the inter-phase transfer of mass, momentum and energy. Mass coupling may involve the addition of mass to the continuous phase by evaporation or removal of mass by condensation. Momentum coupling is the result of drag forces between both phases. Energy coupling occurs through heat transfer between phases.

One criteria for defining coupling as one or two-way can also be the mass loading. The dispersed phase flow can be considered as one-way coupling if the mass loading is much smaller than unity ($\gamma << 1$).

Continuous phase simulation is commonly carried out in an Eulerian reference frame. The fluid characteristics (e.g. velocity, temperature, pressure) are represented by the different spatial discretization, e.g. constant linear and quadratic. Lagrangian manner is rarely used in this problems?

The continuous domain can be treated as either inviscid or a viscous formulation. The inviscid formulation does not take into account for the effect of viscosity to fluid motion. This formulation is not suitable for the application of potential flow, rotational flow and compressible rotational flow. The viscous formulation includes the effect of viscosity.

There are two viscous flow categories consisting of laminar and turbulent flows. The criteria of defining either laminar or turbulent flow often uses the Reynolds number.

Reynolds number gives a measure of the relative importance of inertia and viscous forces.

Turbulent flows can be characterized as unresolved-eddy (time-average flow) and resolved eddy (which predicts the individual spatio-temporal features of the turbulence eddy structure).

The unresolved eddy formation for turbulent flow is primarily based on Reynolds Average Navier-Stokes (RANS) equation, where all spatial velocity components are the combination of average and fluctuating componenets.

The main aim of RANS model is to represent the Reynold Stress term which appears in the flow transport equation.

There are many models for estimating the Reynolds stress : zero equation model, two equation model (k-ε, k-ω, q-ω model), Reynolds stress equation and Algebraic stress model.

- **Fluid governing equation**

The governing equations of fluid flow represent mathematical statements of the conservation law of physiscs:

- The mass of fluid is conserved.
- The rate of change of momentum equals the sum of forces on fluid particle (Newton second law).
- The rate of change of energy is equal to the sum of the rate of heat addition and the rate of work done by fluid particle (The first law of thermodynamics).

- **Mass conservation**

$$\frac{\partial \rho_c}{\partial t} + \nabla \cdot (\rho_c u) = 0 \tag{4.28}$$

Where u(x, y, z, t) is the velocity vector, and ρ_c is the density of the fluid.

For the incompressible fluid the density ρ_c is a constant and the equation becomes:

$$\nabla \cdot u = 0 \tag{4.29}$$

- **Momentum conservation**

The momentum equations along x-, y-, and z-directions with the body forces on fluid particles can be written as:

(x - momentum): $\frac{\partial(\rho_c u)}{\partial t} + \nabla \cdot (\rho_c u u) = -\frac{\partial p}{\partial x} + \nabla \cdot (\mu \nabla u) + S_{Mx}$

(y - momentum): $\frac{\partial(\rho_c v)}{\partial t} + \nabla \cdot (\rho_c v u) = -\frac{\partial p}{\partial y} + \nabla \cdot (\mu \nabla v) + S_{My}$

(z - momentum): $\frac{\partial(\rho_c w)}{\partial t} + \nabla \cdot (\rho_c w u) = -\frac{\partial p}{\partial z} + \nabla \cdot (\mu \nabla w) + S_{Mz}$ (4.30)

Where p is pressure, μ is a fluid viscosity, S_{Mx}, S_{My}, S_{Mz} are the body forces per unit volume.

- **Energy conservation**

The energy conservation is derived from the first law of thermodynamics. The energy of a fluid is often defined as the sum of internal (thermal) energy i per unit mass. Thus energy conservation can be written as:

$$\frac{\partial(\rho_c i)}{\partial t} + \nabla \cdot (\rho_c i u) = -p\nabla \cdot u + \nabla \cdot (k\nabla T) + \phi_d + S_i \qquad (4.31)$$

Where k is the thermal conductivity, S_i is the energy source term, ϕ_d is the dissipation function defined by:

$$\phi_d = 2\mu\left[\left(\frac{\partial u}{\partial x}\right)^2 + \left(\frac{\partial v}{\partial y}\right)^2 + \left(\frac{\partial w}{\partial z}\right)^2\right] + \mu\left(\frac{\partial u}{\partial y} + \frac{\partial v}{\partial x}\right)^2 + \mu\left(\frac{\partial u}{\partial z} + \frac{\partial w}{\partial x}\right)^2 + \mu\lambda(\nabla \cdot u)^2 \qquad (4.32)$$

Where λ is the second viscosity to describe stresses of volumetric deformation.

Fluid motion can be described by a system of five partial differential equations. Among the unknowns are included four thermodynamic variables: ρ_c, p, i, and T. At thermodynamic equilibrium, the state of a substance can be described by two state variable. If ρ_c and T are selected as state variables, the state equation for p and i can be expressed as:

$$p = p(\rho_c, T) \; and \; i = i(\rho_c, T) \qquad (4.33)$$

e.g.: perfect gas $p = \rho_c RT$ and $i = C_v T$; where R is a gas constant value, and C_v is a specific heat capacity at the constant value.

4.4.5 Aerodynamics Modelling

The measurement chamber mass transfer performance of a DPI dose is in direct link with the airflow pattern (laminar, laminar-to-turbulent, turbulent) inside the chamber at a 60l/min flow rate. In this situation numerical simulation is useful allowing to predict mouth-throat deposition. Typically Eulerian or Lagrangian approaches are considered to model aerosol transport in the human airways. In Eulerian approach particles are assumed to move towards the wall by turbulent diffusion and then reach the wall by a free flight mechanism, however Eulerian approaches have not been extended to more complex geometries such as mouth-throat deposition problem. In a Lagrangian approach, the primary flow is calculated by using direct numerical simulations (DNS), large Eddy simulation (LES) or Reynolds averaged Navier-Stokes (RANS) equations (e.g. the k-ε or k-ω turbulence model equations). Then individual particles are numerically released in the calculated flow, and move according to the particle equation of motion. When the particle concentration is very low, the primary flow is assumed to be unmodified by the presence of particles (e.g. one-way coupling), an

assumption that significantly facilitates the simulation of the motion of particles.

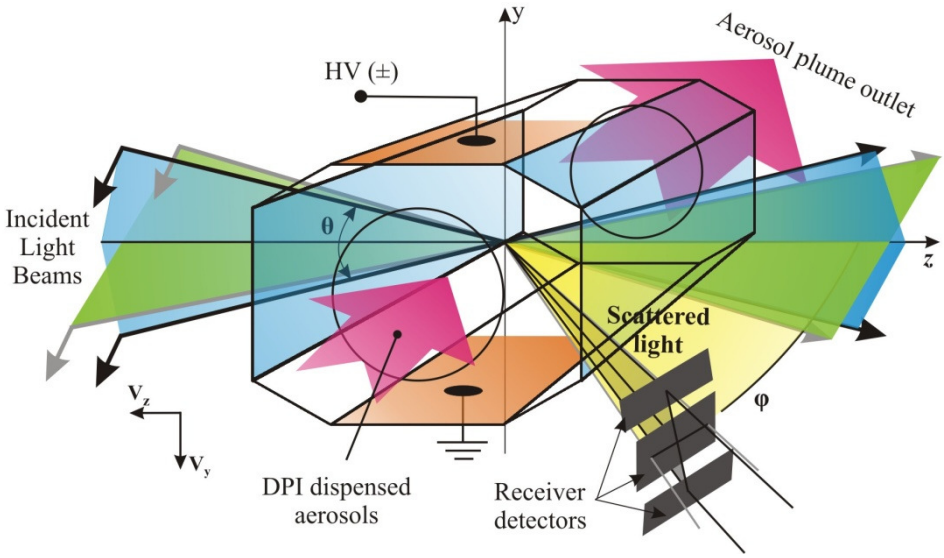

Fig. 4.29. Optical configuration of Phase Doppler dual-mode system and Measurement Cell.

On the other hand, when the particle concentration is not low, the mutual interaction between the primary flow and the particles must be incorporated into the simulation (e.g. two-way coupling). In this situation aerosol suspension in human mouth-throat section can be considered to be dilute due to low mass loading ratio at the oral inlet. As the flow pattern is influenced only by the Reynolds number one-way coupling is considered. Reynolds number calculated for various speeds of the airflow depending on the DPI used showed that the airflow pattern inside the chamber is mainly laminar and develops towards transient as it reaches the outlet of the chamber, becoming turbulent in the laryngeal tube. The steady-state airflow modelled using COMSOL is a Newtonian fluid in a steady incompressible laminar flow without considering the heat transfer between air and mouth-throat wall approach (adiabatic process). Because of the backstep geometry of the chamber the model implies a stream of functions to model incompressible flow in a divergence-free approach. Instead of conventional p2-p1 Lagrange elements, the model uses C1-continuous Argyris elements to discretize the incompressible Navier-Stokes equations. Formulating the flow equations in terms of a stream function eliminates the continuity equation altogether. The advantage of using Argyris elements in the discretization is that the continuity equation is always satisfied. The stream function Ψ is introduced through the following definition:

$$(u, v) = \nabla \times \Psi = \left(\frac{\partial \Psi}{\partial y}, -\frac{\partial \Psi}{\partial x}\right) \tag{4.34}$$

That is, the velocity field is the curl of the stream function. Therefore the divergence of the velocity field is identically zero wherever the stream function is smooth enough and the continuity equation is satisfied weakly everywhere in the domain.

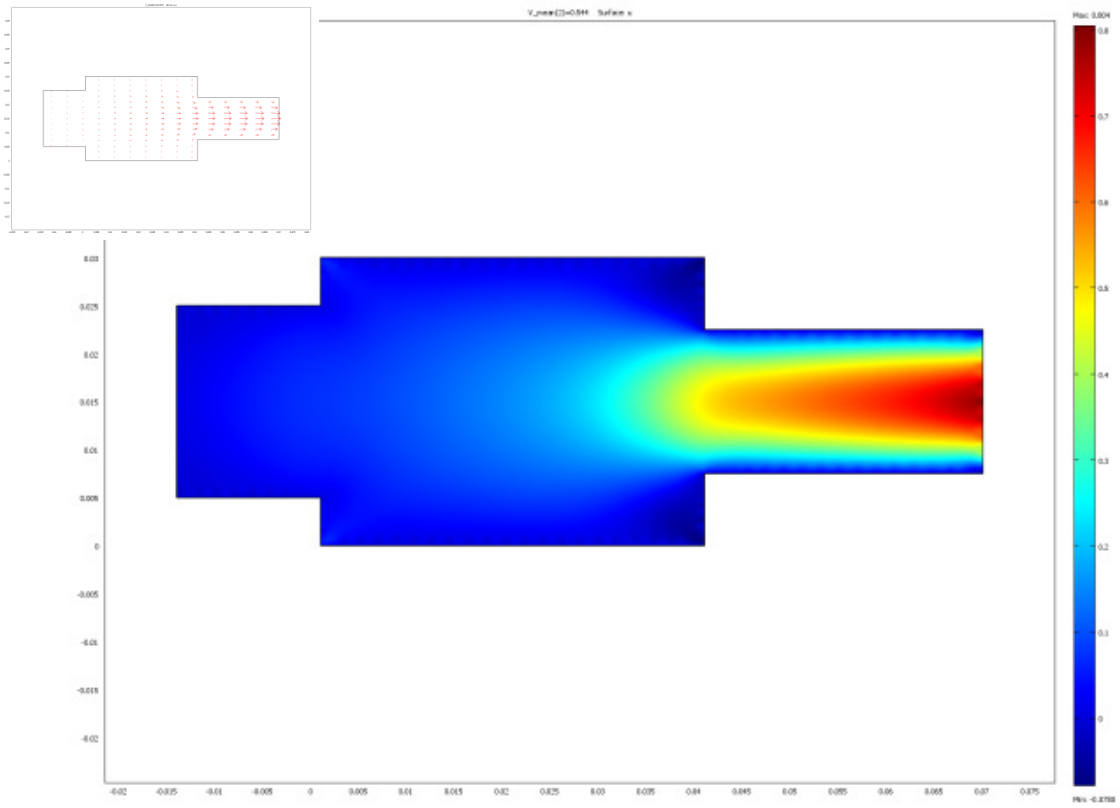

Fig. 4.30. Comsol modelling of the air pattern inside the Measurement Cell as the air is sucked through.

The coupling between the continuous phase and the dispersed phase is an important concept in flow analysis. The coupling can be divided into one-way coupling and two-way coupling. The continuous phase in many applications will effect the dispersed phase, but not vice versa. In one-way coupling, it is assumed that the dispersed phase has no reverse effect on the continuous phase ow. On the other hand, two-way coupling has effects between both phases. The coupling upon both phases can be modelled through the inter- phase transfer of mass, momentum, and energy. Mass coupling may involve the addition of mass to the continuous phase by evaporation or removal of mass by condensation. Momentum coupling is the result of drag forces between both phases. Energy coupling occurs through heat transfer between phases. One of the criteria for defining coupling as one or two-way can also be the mass loading. The dispersed phase flow can be considered as one-way coupling if the mass loading is much smaller than unity. Also to test the validity of the aerodynamic simulation smoke test experiments have been performed as shown in the figure below.

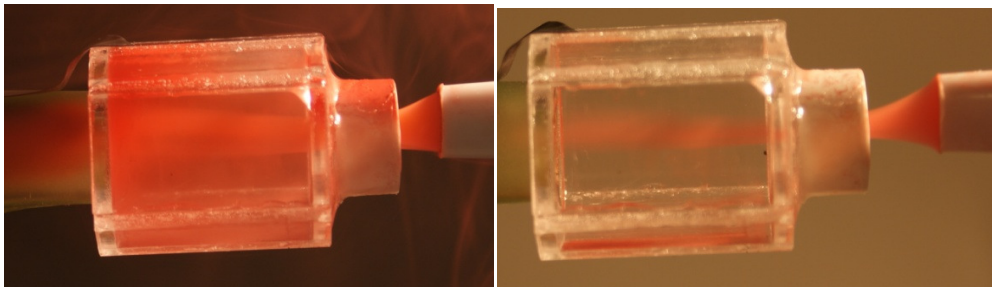

Fig. 4.31. Smoke experiments to test the air flow inside the designed test cell.

4.4.5 Experimental results using AC fields.

A second series of experiments was carried out with the measurement volume positioned in the middle of the cell, and the AC sin-waveform applied between the electrodes. In this experimental set-up several types of DPI's were tested and the bipolar charge distribution of their released plume is shown in Fig. 3.32 for the devices a, b & c. Because each device has a different operating mode the cell inlet was modified accordingly while the flow rate was maintained at 60 l/min using the Copley pump. The amplitude and the frequency of the sin-waveform electric field were: 4kV/m and 10Hz respectively. The sin-wave acoustic is valid in the whole range of acoustic frequencies and particle charges from 0 to saturation level. It is however less accurate for particles with low electrical mobility μ. The Doppler burst signal is more complex and requires sophisticated signal processing tools and is more susceptible to ambiguity noise. When particles are placed in a sinusoidal AC electric field the electrical force acting on a particle is given by:

$$F_e = qE_{ac}\sin(2\pi f_{ac}t) \tag{4.35}$$

The amplitude of the particle velocity can be written as:

$$|V| = \frac{\mu_p E_{ac}}{\sqrt{1+\omega^2\tau^2}} = \frac{qC_c}{3\pi\eta d_p}\cdot\frac{E_{ac}}{\sqrt{1+\omega^2\tau^2}} \tag{4.36}$$

Consequently, the amplitude of the particle displacement is equal:

$$A = \frac{\mu_p E_{ac}}{\omega\sqrt{1+\omega^2\tau^2}} = \frac{qC_c}{3\pi\eta d_p}\cdot\frac{E_{ac}}{\omega\sqrt{1+\omega^2\tau^2}} \tag{4.37}$$

Finally, the charge is calculated:

$$q = \frac{3\pi\eta d_p |V|}{C_c E_{ac}} \sqrt{1+\omega^2\tau^2} \tag{4.38}$$

The particle charging mechanism is complex in nature; therefore, the charge accumulated by the particles is not uniform and shows a different bipolar charge distribution in each sample and reflects the most probable charge levels acquired by the majority of the particles as seen in Fig 4.32.

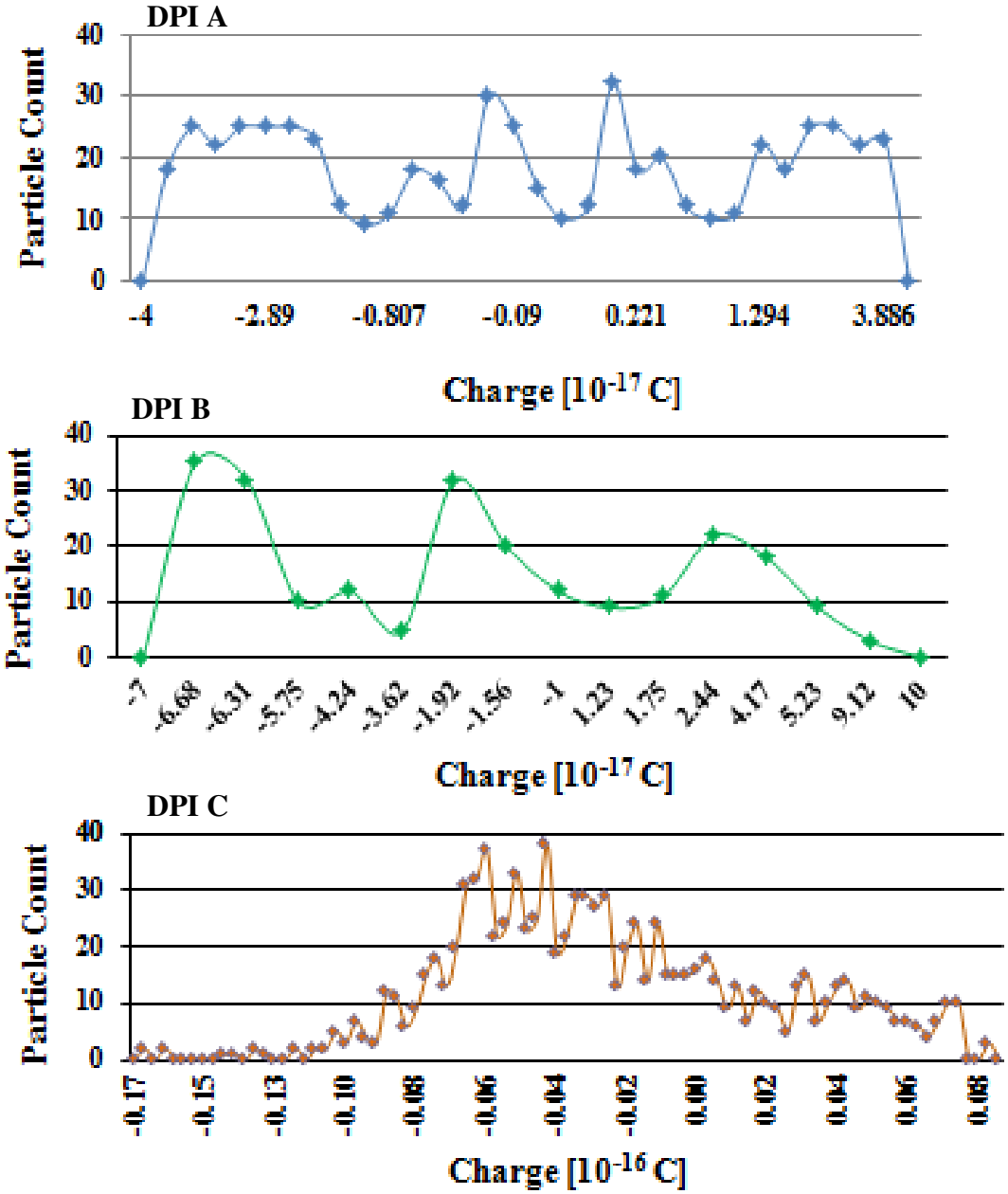

Fig. 4.32. Bipolar charge distributions of three dispersed samples from DPI devices a, b & c using AC fields.

We ended up with just a few hundred particles validate by the system per each run while the charge levels present a bipolar distribution within the dispersed aerosol plume. In the above experimental result we observe that in the DPI C aerosols have one order of magnitude higher charge levels (10^{-16}) that the other two (10^{-17}) for DPI A&B. This is mainly due it's complex fluid dynamics which allow the dry aerosols to acquire significant charge at actuation due to triboelectrification and also based on the bulk charge levels of the sample within. Some devices use capsules other blisters other small containers from which the dose is released to the patient. However the sample in the handling and manufacturing processes acquires charge levels which will remain within the bulk e.g. within the capsule. The capsules are also good insulators. For the flow rate used during experiments the resident time of the DPI released aerosol plume within the cell's PDA measurement volume area, was extremely fast (μs). This influenced significantly the data acquisition and mostly the size validation parameter crucial for charge calculation. However the validated particles have significant levels of charge mainly due to triboelectrification effect of the sample as it passed through the DPI system. Also the experimental procedure was quite tedious as the cell had to be cleaned and neutralized after each DPI actuation. Larger particles > 80μm ended up within the cell. In normal use these particles reach the stomach of the patient or dissolve in the mouth. If the DPI dispersion is not fully functional significant quantities of drug could be stuck to the carrier particles which will deposit within the cell. These experiments show how difficult is data collection and validation when actuating DPI's in a human mouth& throat models adapted for the PDA system. Another significant impediment constitutes the lack of information regarding the optical properties of the API's and Blends. This will reduce significantly the validation process within the PDA sensors. Thus for each DPI with its particular geometry, functionality and content (API&Lactose) we need to build a specialy designed measurement cell with optical windows at angles that favorize as much reflected light to be captured by the receiving sensors. Based on the flow rate the resident time will be the key factor in the number of particles validated as their main characteristic is non-sphericity. On the other hand the electrodes system has to be accommodated within the cell with each new design. Comsol modeling will be of great use in testing various electrode configurations and the electric field distribution in both presented cases AC&DC fields. The charge levels we measured are a combination of initial sample charge, triboelectrification between the particles and the device and particles at the moment of actuation. Device handling by the patient and the storage condition will also influence these charge levels.

4.4.5 Summary and Conclusions

Adapted phase Doppler anemometry has the potential to give bipolar charge distributions of aerosols - still issues around presenting raw powders i.e. APIs or blends, to the measurement cell without influencing intrinsic charge property of the materials.

The experimental results demonstrate the capability of the technique to determine in real-time particle size and charge distribution in the presence of AC fields of 50 Hz . The method does not require calibration, provided that the particle refractive index as well as PDA optical parameters are known accurately. Theoretically the instrument can measure the charge on particles from just a few electrons to almost a saturation level with an accuracy depending on the accuracy of velocity and particle size measurement, which is usually very high for PDA systems (±0.5%). The number of particles analyzed per second using the PDA system is limited by the coincidence loss and the requirement to maintain laminar-flow within the measurement cell. In the experiments presented in this chapter the particle count rate varied between 100 to 500 particles per second, which is still sufficiently large to provide good statistical representation.

It is clear from the analysis of previous simulations and other experimental work that device efficiency for respiratory drug delivery can be strongly influenced by critical powder attributes like electrostatic bipolar charge distribution. Therefore, the effort to develop valid charge measurement will be a significant benefit in controlling dry powder processes. Further research is underway to investigate bipolar charge distribution of a number of commercial DPI devices using the PDA measurement system. Data from these aerosol measurements can then be related to available *in-vitro* performance data and *in-vivo* scintigraphy or PK information to establish the likely influence of aerosol charge behaviour.

Chapter 5

Conclusions and Future Work

5.1 Conclusions

The Phase Doppler Anemometry (PDA) technique has become a well established, non-intrusive method, which offers not only an in situ measurement of size distributions but also a quantitative measurement of fluxes and particle-size/velocity correlations with a very high data rate at high particle concentrations. This technique is used for the measurement of spherical homogenous particles, a situation often encountered in sprays and it was also used successfully for some applications with rough inhomogeneous spherical particles (Durts et al., 1997; Jones, 1999; Webb & Jones, 2004). The system experienced a continuous development in precision and performances. Correction of some errors generating effects, such as the Gaussian beam defect (Durst et al., 1981; 1997), slit effect (Durst et al., 1981; Tropea et al., 1996; Qiu et al., 2000), was realized by using and developing masks and light filters; the measurement-volume effect by developing a four-detector PDA. Other research was focused on evaluating its response to non-spherical particles (Damaschke et al., 1998), and improving applications where instantaneous velocity and its correlations are important (Durst et al., 1981; 1997; Mishchenko et al., 2006). From this point of view Phase Doppler Anemometry proved to be a very useful tool in correlating instantaneous measurement of velocity and size with charge level measurement on a population of particles (Kulon & Balachandran, 2003). PDA extended the capabilities of Laser Doppler Velocimetry method, developed by Mazumder et al. (1991) offering very high accuracy without the need of calibration.

The optical properties of a medium are characterized by its refractive index and as long as this is uniform, light will pass through the medium undeflected. Whenever there is a discrete reorientation of the refractive index due to the presence of particles or because there are small scale density fluctuations, part of the radiation will be scattered in all directions. The scientific study of light scattering may be said to have commenced with the experiments on aerosols by Tyndall in 1869, which were followed from 1871 onwards by Lord Rayleigh theoretical work (Kerker, 1969). The problem is to relate the properties of the scatter – its shape, size and refractive index – to the angular distribution of the scattered light. The incident beam of known intensity and wavelength is usually taken to be parallel and linearly polarized. If the scatter is absorptive, part of the light will be absorbed within it as a heat,

another part will be scattered and the remainder will be transmitted unperturbed along the incident direction.

"Laser" is an acronym for light amplification by stimulated emission of radiation. If the electrons in special glasses, crystals or gases are energized, they will emit light photons in response to a weak laser pulse. The photons will all be at the same wavelength and will also be "coherent," meaning the light wave's crests and troughs are all in lockstep. In contrast, ordinary visible light comes in multiple wavelengths and is not coherent.

Phase Doppler technique as described by Durst et al. (1981) utilizes the wave nature of light to obtain information on velocity of small scattering particles suspended in a flow, by not disturbing the flow. As a scattering particle passes through an electromagnetic field it will also scatter an electromagnetic wave. If this wave is detected, it is possible to treat the scattering action of the particle as if it had penetrated the intensity field of the light beam and so combining the properties of particle and detection. Crossing two light waves results in interference patterns explained by the principle of superposition of oscillations and the resultant light intensity represents the sum of the two electromagnetic wave fields. These regions of maximum and minimum light intensity are referred to as “bright” and “dark” fringes. Generally if constant phase relations exist between two interfering light waves they are called “coherent” and the interference phenomena can be observed only with coherent light waves. Formation of the interference patterns allows the determination of particle velocity by measuring the transit time of the particle across a known number of interference fringes. Photo-detectors are employed to detect these intensity variations and result in electrical signals with frequency related to the velocity of a particle, its position relative to the light sources and photo-detector, and the frequencies of the sources. Interference patterns are formed for LDA purposes in three ways which are referred to as the dual-beam or fringe, reference-beam and two-scattered beam models.

Phase Doppler anemometers are among the most accurate instruments for measuring particle size and velocity. However, they are not immune to errors and, as with any other measurement technique, it is important to know the sources of error when making the PDA measurement. Broadening of spectrum is a one of the factors, which could potentially degrade the accuracy of the PDA velocity measurements, based FFT analysis (Tropea et al., 1996; Durst et al, 1997). Because of the linear relationship between the Doppler frequency and a velocity component the broadening of spectrum causes the particle velocity

measurement error. There are several sources of the power spectrum broadening such as finite transit time of particles crossing the measuring volume, velocity gradient, Brownian motion and the line width of the laser and the filter characteristics of the spectrum analyzer. Broadening form the laser and Brownian motion are considered as negligible. As already mentioned the finite transit time broadening arises because signals from individual particles last only for the time required to traverse the scattering volume. This spectrum broadening is related to the number of fringes in the measurement volume because, when processing a signal burst, we are trying to deduce a frequency from a limited number of cycles. Thus, increasing the number of fringes in the measurement volume minimizes the effect of finite transit time broadening. If the measurement is being made in a flow with a velocity gradient then successive particles passing through the measurement volume may have different velocities by virtue of their different positions in the gradient. So, even if the flow is completely steady, the LDA/PDA will measure a velocity fluctuation. To minimize gradient broadening the optical system should be arranged with a short dimension along the direction of the velocity gradient.

In addition to the spectrum broadening, the measurement error can be caused by the electric field induced by the space charge. Since the calculation of the charge is based on the accurate knowledge of the electric field inside the measurement cell any changes of the electric field will be directly reflected in charge values. This effect, however, may become significant only in the case of highly concentrated and highly unipolarly charged aerosols.

One of the inherent limitations of the PDA method is that it requires good sphericity of the analyzed particles as well as the homogeneity of the particle medium (although small inhomogeneity can be tolerated). Also, the process of taking measurements by traversing the measurement volume in some cases may not provide a representative picture of the aerosol charge distribution. Since the measurement volume can be positioned only in one region at a time the measurements will not reflect any rapid variation of particle concentration and therefore charge distribution in other measurement points. For example the arrival of the measurement volume at certain location may coincide with a lower concentration or higher concentration of particles of given mobility and the electrostatic charge, thus altering the overall picture of charge distribution within the aerosol cloud.

A comparison between the advantages and disadvantages of the PDA and PIV system is presented in Table 5.1.

Table 5.1. Advantages and disadvantages of the PDA & PIV measurement

Phase Doppler Anemometry (PDA)	Particle Image Velocimetry (PIV)
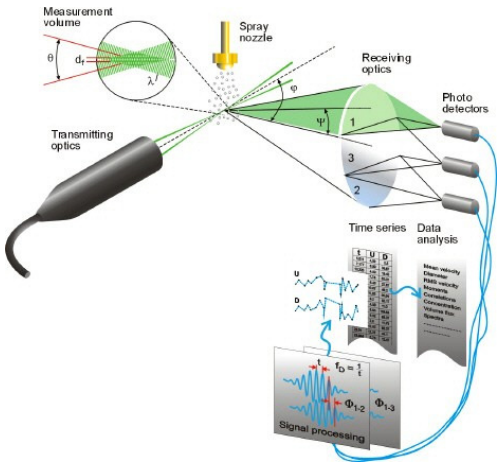 Source: Dantec Dynamics	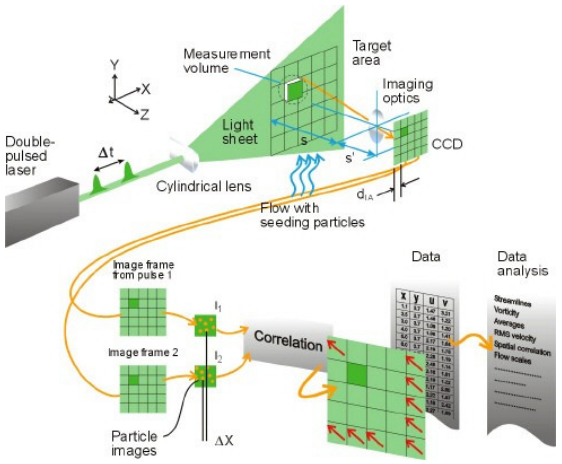 Source: Dantec Dynamics
• Optical Method – measures the speed and size of particles from a flow simultaneously. • Measures up to three speed components in a very small measurement volume. • The measurement volume is an ellipsoid formed at the intersection of two laser beams, has a light intensity (Gaussian) in three directions. • A non-intrusive method but it needs optical access. • Absolute measurement (it does not need calibration). • The laser light has to be coherent, monochromatic and linearly polarized. • Can detect spherical, cylindrical non-homogenic particles, 0.5-1000 µm diameter. • Index known or measurable. • Can be used in complex environments. • Seeding plays an important role, as LDA can detect only data from one particle at a time • Signal quality depends on laser power, particles and optical set-up. • Disadvantages: costly, discontinuous signals, bias, attention at the dynamics of the speed, detectors are difficult to align, very sensible to vibrations.	• Flow measurement technique used to obtain the time dependent full field velocity distributions of single and multi-phase flows • The components needed for PIV include: an illumination source, and optical system for illuminating the test section, digital imagers for capturing the flow field, and a system for image processing, particle identification, particle tracking, and vector field cleaning. • Procedure: the laser is synchronized with the digital imagers, the laser light is positioned to illuminate the test volume, the scattered light from the tracer particles is recorded with the digital cameras, and then image analysis is performed. • Usually, the approach requires seeding the flow with small tracer particles and illuminating with a sheet or volume of light from a pulsed laser. A single or multi-exposure image is recorded of the position of the particles as a function of time. The spacing between these particle images provides a measure of the local flow velocity. The spacing is determined through imaging techniques. • Can detect spherical, irregular particles, 5-1000 µm diameter.

PDA vs PIV

- The PDA can measure the size and speed of a particle simultaneously and is based on signal processing and interpretation while PIV measures speed of a whole flow and is based on imaging acquisition and treatment.
- PDA offers a 3D measurement volume at the intersection of two laser beams. In normal PIV systems, the third velocity component is "invisible" due to the geometry of the imaging. This third velocity component can be derived by using two cameras in a stereoscopic arrangement.
- PDA system can be used to detect and give required information on particles sizing less than 1 µm.
- PIV can detect speed in high speed flows (supersonic), while PDA depends highly on seeding and can measure only one particle at a time.
- PIV measurement set-up requires a large space and characteristic conditions for a proper usage while the PDA system can be used in smaller spaces and complex environments.
- Both systems are costly, sensible to vibrations, highly dependent on the optical arrangement.

5.2 Future work

Future work will concentrate on two areas. First area of research will be further development of the PDA technique in terms of the miniaturization of the instrument and development of the signal processing algorithms. Second area is the physical refinements to the cell design and detailed analysis (experimental and theoretical) of its physical behavior.

Therefore, one avenue of the future work will involve, construction of the particle charge and size analyser based on the miniature version of the PDA optics. In addition to that, by applying the AC excitation method rather then DC field, the measurement volume can have a fixed, stationary position in the centre of the cell. The main advantage of this approach is that it will eliminate expensive traversing mechanism and further reduce the complexity and the cost of the instrument. However, the advanced signal processing algorithms will have to be developed to derive the amplitude of particle velocity from the Doppler burst signal.

We face several major experimental challenges when testing DPI devices using the PDA system. First they require a closed system capable of providing the right pressure difference which will actuate the DPI devices in conjunction with powerful pumps. Refractive index of the materials used API's and lactose have to be known in order to set up the PDA's receiving probe at the appropriate angle. This will impose significant restrictions to cell design. Also each DPI has a different design and operating principles thus for each device a special cell has to be designed and constructed bearing in mind the optical angles of the PDA system. A cleaning and neutralization mechanism has to be integrated with the designed cell after each DPI actuation due to particle deposition and space charge. Electrode position and design would significantly improve aerosol charge detection. Appropriate optical windows have to be chosen for integration within the cell for a more accurate validation from the PDA system. This however proves to be costly.

We built a simplified human upper airway model which combined with the modified Phase Doppler Anemometry (PDA) system is able to provide real time bipolar charge distributions of aerosols delivered from several commercially available DPI devices. The three dimensional (3D) reconstruction of the upper respiratory system was performed from two dimensional (2D) images obtained from computerized tomography (CT), magnetic resonance imaging (MRI) and cryosectioned images available from Visible Human Server data set (Ecole Polytechnique Fédérale de Lausanne). The resulting dimensions of the model were consistent with morphometric data from the literature from which the simplified upper airway model consisting of two connected segments, i.e., the oral airways from the mouth to trachea

(Generation G0), was created. These results may be integrated with the existing lower airways models to obtain a full 3D design of the human airways which can be used by clinicians to predict the efficiency of prescribed medication. Also it would be of great use for the pharmaceutica industry in designing future generation DPI devices and a better understanding of aerosol transport and deposition efficiency within the human airways.

Realistic airway geometry is required for accurate electrohidrodynamical modelling, and particle deposition predictions as the ultimately risk assessment for inhaled drug delivery protocols. Morphometric studies to date provide data for specific anatomical locations or for more generational average data for the entire lung. The reconstructed human airway model extended from just mouth to the trachea down through the generation G0 of bronchial passageways. The resulting dimensions of the complete female model were consistent with morphometric data from the
literature, indicating that the model is a reasonable representation of an adult female that could be used for biomechanical modelling.

Bibliography

Agur, A.M.R., Dalley, A.F., 2009. Grant's atlas of anatomy, 12th edition. Hong Kong: Wolters Kluwer/Lippincott Wiliams & Wilkins.

Aldred, D.C., Howe, A.F., Wright, A., 1983. Size selective particle charge measurement. *Filtech. Conference*., pp.342-346.

Ali, F.S., Ali, M.A., Ali, R.A., Inculet, I.I., 1998. Minority charge separation in falling particles with bipolar charge. *Journal of Electrostatics*, 45, p. 139-155.

Anderson, P.J., 2005. History of Aerosol Therapy: Liquid Nebulization to MDIs to DPIs. *Respiratory Care*, 50(9), p. 1139-1150.

Bailey, A.G., 1997. The inhalation and deposition of charged particles within the human lung. *Journal of Electrostatics*, 42, p. 25-32.

Balachandran, W., Ahmad, C.N., Barton, S.A., 1991. Deposition of electrically charged drug aerosol in lungs, *Institute of Physics Conference Series* 118: Section 1, p. 57-62.

Balachandran, W., Machowski, W., Gaura, E., Hudson, C., 1997. Control of drug aerosol in human airways using electrostatic forces, *Journal of Electrostatics*, 40&41, p. 579-584.

Balachandran, W., Kulon, J., Koolpiruck, D., Dawson, M., Burnel, P., 2003. Bipolar charge measurement of pharmaceutical powders. *Powder Technology*, 135-136, p. 156-163.

Barnes, P.J., et al., 1994. Therapeutics in Respiratory Disease. Churchill Livingstone Medical Division of Longman Group UK Limited.

Beleca, R., Abbod, M., Balachandran, W., Miller, P.R., 2010. "Investigation of Electrostatic Properties of Pharmaceutical Powders using Phase Doppler Anemometry," *IEEE Transactions on Industry Applications*, 46 (3), pp. 1181 - 1187.

Booker, D.R., Griffiths, W.D, Lyons, C.P., Mark, D., Upton, S.L., Nichols, A.L., 1998. Aerosol sampling guidelines. Cornwall: MPG Books Ltd.

Born, M., Wolf, E., 1999. Principles of Optics: Electromagnetic Theory of Propagation, Interference and Diffraction of Light, 7th expanded Edition. Cambridge: Cambridge University Press.

Brown, R.C., 1997. Tutorial review: Simultaneous measurement of particle size and particle charge. *Journal of Aerosol Science*, 28(8), p. 1373-1391.

Beggs, P.J., Bambrik, H.J., 2005. Is the global rise of asthma an early impact on anthropogenic climate change? *Environmental Health Perspectives*, 113(8), p. 915-919.

Carveth, H.J., Kanner, R.E., 1999. Optimizing Deposition of Aerosolized Drug in the Lung: A Review, *Medscape General Medicine*, [online]. 1(3), Available at: http://www.medscape.com/viewarticle/408738 [accesed on 04/08/2008].

Chang, J.S., Kelly, A.J., Crowley, J.M., 1995. Handbook of electrostatic processes. New York: Marcel Dekker Inc.

Cheng, K.H., Cheng, Y.S., Yeh, H.C., Swift D.L., 1997. An experimental method for measuring aerosol deposition efficiency in the human oral airway. *American Industrial Hygiene Association Journal*, 58(3), p.207-213.

Cheng, K.H., Cheng, Y.S., Yeh, H.C., Swift D.L., 1997. Measurements of airway dimensions and calculations of mass transfer characteristics of the human passage. *Journal of Biomechanical Engineering*, 119, p. 476-482.

Chow, K.T., Zhu, K., Tan, R.B.H., Heng, W.S., 2008. Investigation of electrostatic behaviour of a lactose carrier for Dry Powder Inhalers. Pharmaceutica Research, 25(12), p. 2822-2834.

Clark, A.R., 1995. Medical aerosol inhalers: past, present, and future. *Aerosol Science and Technology*, 22, p. 374-391.

Corbett, R.P., Basset, J.D., 1971. Electric field measurements in ionic and particulate clouds. Proceedings of the Static Electrification Conference, London, England, May 1971, Institute of Physics, p. 307-319.

Cox, A.J., DeWeerd, A.J., Linden, J., 2002. An experiment to measure Mie and Rayleigh total scattering cross sections. *The American Journal of Physics*, 70(6), p. 620-625.

Crowder, T., Hickey, A., 2006. Powder specific active dispersion for generation of pharmaceutical aerosols. *International Journal of Pharmaceutics*, 327, p. 65-72.

Damaschke, N., Gouesbet, G., Gréhan G., Mignon, H., Tropea, C., 1998. Response of Phase Doppler Anemometer systems to nonspherical droplets. *Applied optics*, 37(10), p. 1752-1761.

Daniher, D.I., Zhu, J., 2008. Dry powder platform for pulmonary drug delivery. *Particuology*, 6, p. 225-238.

Dantec Dynamics, 2008. Laser Doppler Anemometry. Introduction to principles and applications. [online]. Available at http://www.dantecdynamics.com, [accessed on 18/03/2008].

Dantec Dynamics, 2008. Principles of Phase Doppler Anemometry. [online]. Available at http://www.dantecdynamics.com, [accessed on 20/03/2008].

Davies, A. & Moores, C., 2003. The respiratory system: Basis science and clinical conditions. London: Churchill Livingstone an imprint of Elsevier Science Limited.

Davis, E.J., 1997. A history of single aerosol particle levitation. *Aerosol Science and Technology*, 26, p. 212-254.

Davis, S.S., Hardy, J.G., Newman, S.P., Wilding, I.R., 1992. Gamma scintigraphy in the evaluation of pharmaceutical dosage forms. *European Journal of Nuclear Medicine*, 19, p. 971-986.

DiVito, W., Mazumder, M.K., Wilson, J.D., Sims, R.A., Louziu, P., Ojha, A., Grable, N., Chapman, S., 1998. Simultaneous analysis of particle size and electrostatic charge distribution of powder with high accuracy and precision, and its applications to electrostatic processes. Proceedings of the 33rd IEEE/IAS- Annual Meeting, Vol. 3, held at: St. Louis, Missouri, USA, 12-15 October, p. 1892-1897.

Durst, F., Melling, A., Whitelaw, J.H., 1981. Principles and practice of laser-doppler anemometry, 2nd Edition. London: Academic Press Inc.

Durst, F., Zaré, M., 1975. Laser Doppler measurements in two-phase flows. Proceedings LDA Symposium, Copenhagen, p. 403-429.

Durst, F., Brenn, G., Hu, T-H., 1997. A review of the developement and characteristics of planar Phase Doppler Anemometry. *Measurement Science and Technology*, 8, p. 1203-1221.

Eilbeck, J., Rowley, G., Carter, P.A., Fletcher, E.J., 1999. Effect of materials of construction of pharmaceutical processing equipment and drug delivery devices on the triboelectrification of size-fractionated lactose. *Pharmacy and Pharmacology Communications*, 7(5), p. 429-433.

Eilbeck, J., Rowley, G., Carter, P.A., Fletcher, E.J., 2000. Effect of contamination of pharmaceutical equipment on powder triboelectrification. *International Journal of Pharmaceutics*, 195, p. 7-11.

Engers, D.A., Fricke, M.N., Storey, R.P., Newman, A.W., Morris, K.R., 2006. Triboelectrification of pharmaceutically relevant powders during low-shear tumble blending. *Journal of Electrostatics*, 64, p. 826-835.

Engers, D.A., Fricke, M.N., Newman, A.W., Morris, K.R., 2007. Triboelectric charging and dielectric properties of pharmaceutically relevant mixtures. *Journal of Electrostatics*, 65, p. 571-581.

European Pharmacopeia, 2008. Section 2.9.18 - Preparations for inhalation: aerodynamic assessment of fine particles. *European Pharmacopeia*, Council of Europe, 67075 Strasbourg, France. Available at: http://www.edqm.eu/ [accessed on 05/07/2008].

Farzan, S., 1978. A Concise handbook of respiratory diseases. Reston, Virginia: Reston Publishing Company Inc.

Fink, J.B., 2000. Metered-Dose Inhalers, Dry Powder Inhalers, and transitions. *Respiratory Care*, 45(6), p. 623-635.

Flagan, R.C., 1998. History of electrical aerosol measurements. *Aerosol Science and Technology*, 28(4) , p. 301-380.

Gard, P., 2001. Human Pharmacology. London: Taylor & Francis.

Global Initiative for Asthma (GINA). 2007. *Global Strategy for Asthma Management and Prevention,* [online]. Available at: http://www.ginasthma.com [accessed on 25/07/2008].

Glover, W., Chan, H-K., 2004. Electrostatic charge characterization of pharmaceutical aerosols using low-pressure impaction (ELPI). *Journal of Aerosol Science*, 35, p. 755-764.

Gotoh, K., Masuda, H., Ko, H., 1997. Powder Technology Handbook, 2nd edition revised an expanded. New York: Marcel Dekker, Inc.

Haken, H., 1981. Light, vol. 1, Waves, Photons, Atoms. Amsterdam: North-Holland Physics Publishing.

Haken, H., 1985. Light, vol. 2, Laser Light Dynamics. Amsterdam: North-Holland Physics Publishing.

Honeywell International Inc., 2008. *Water content calculation*. Available at: http://www.honeywell.com [accessed 25/09/2008]

Hickey, A.J., Mansour, H.M., Telko, M.J., Hu, Z., Smyth, H.D.C., Mulder, T., Mclean, R., Langridge, J., Papadopoulos, D., 2007. Physical characterization of component particles included in dry powder inhalers. I. Strategy review and static characteristics. *Journal of Pharmaceutical Sciences*, 96(5), p. 1282-1301.

Hickey, A.J., Mansour, H.M., Telko, M.J., Hu, Z., Smyth, H.D.C., Mulder, T., Mclean, R., Langridge, J., Papadopoulos, D., 2007. Physical characterization of component particles included in dry powder inhalers. II. Dynamic characteristics. *Journal of Pharmaceutical Sciences*, 96(5), p. 1302-1319.

Hidy, G.M., and Brock, J.R., 1971. *Topics in current aerosol research 1st ed.,* Pergamon Press in Oxford.

Hinds, W.C., 1999. Aerosol Technology, 2nd Edition. New York: John Wiley & Sons, Inc.

Horvath, T., Berta, I., 1982. Static Elimination. New York: Research Studies Press.

Hrabar, S., Machowski, W., Balachandran, W., 1998. A bipolar charge measurement system for aerosol characterization. Proceedings of the IEEE Industry Application 33rd Annual Meeting, St. Luis, Missouri, USA, 12-15 October, pp. 1967-1972.

Inculet, I.I., Castle, G.S.P., 1992. Faraday pail with self regulating ion repulsion. Proceedings of the IEEE Industry Application Annual Meeting, Huston, Texas, USA, 4-9 October, pp. 1502-1505.

Inculet, I.I., 2005. Measuring techniques in industrial applications of electrostatic forces: Plenary Lecture at Electrostatics 2005, Helsinki, Finland. *Journal of Electrostatics*, 63, p. 523-531.

Inculet, I.I., Castle, G.S.P., Aartsen, G., 2006. Generation of bipolar electric fields during industrial handling of powders. *Chemical Engineering Science*, 61, p. 2249-2253.

Islam, N., Gladki, E., 2008. Dry powder inhalers (DPIs)-A review of device reliability and innovation. *International Journal of Pharmaceutics*, 360, p. 1-11.

Jones, A.R., 1999. Light scattering for particle characterization. *Progress in Energy and Combustion Science*, 25, p. 1-53.

Kerker, M., 1969. The scattering of light and other electromagnetic radiation. New York: Academic Press.

Khorasani, M.T., MoemenBellah, S., Mirzadeh, H., Sadatnia, B., 2006. Effect of Surface Charge and Hydrophobicity of polyurethanes and silicone rubbers on L929 cells Response, *Colloids and Surfaces: Biointerface*, 51, p. 112-119.

Kleinstreuer, C., Zhang, Z., Donohue, J.F., 2008. Targeted Drug-Aerosol Delivery in the Human Respiratory System, *Annual Review of Biomedical Engineering*, 10, p. 195-220.

Koolpiruck, D., Prakoonwit, S., Balachandran, W., 2004. Numerical modelling of inhaled charged aerosol deposition in human airways. *IEEE Transactions on Industry Applications*, 40(5), p. 1239-1248.

Kulon, J., Balachandran, W., 2001. The bipolar charge aerosol classifier. *IEEE Industry Applications 36th Annual Meeting*, Vol. 4, p. 2241-2248, 30 Sept- 4 Oct., Chicago, USA.

Kulon, J., Balachandran, W., 2001. The measurement of bipolar charge on aerosols. *Journal of Electrostatics*, 51-52, p. 552-557.

Kulon, J., Hrabar, S., Machowski, W., Balachandran, W., 2001. A bipolar charge measurement system for aerosol characterization. *IEEE Transactions on Industry Application*, 37(2), p. 472-479.

Kulon, J., Malyan, B.E., Balachandran, W., 2003. Simultaneous measurement of particle size and electrostatic charge distribution in DC electric field using Phase Doppler Anemometry. *IEEE Transactions on Industry Applications*, 39(5), p. 1522-1528.

Kulon. J., 2003. Real-time measurement of bipolar charge distribution on pharmaceutical aerosols and powders using phase doppler anemometry and a bipolar charge measurement system. PhD Thesis, Dept. Systems Engineering, Brunel University, London, UK.

Kulvanich P, Stewart PJ. 1987. An evaluation of the air stream Faraday cage in the electrostatic charge measurement of interactive drug systems. *International Journal of Pharmaceutics*, 36, p. 243–252.

Labiris, N.R., Dolovich, M.B., 2003. Pulmonary drug delivery. Part I: Physiological factors affecting therapeutic effectiveness of aerosolized medications. *British Journal of Clinical Pharmacology*, 56 (6), p. 588-599.

Labiris, N.R., Dolovich, M.B., 2003. Pulmonary drug delivery. Part II: The role of inhalant delivery devices and drug formulations in therapeutic effectiveness of aerosolized medications. *British Journal of Clinical Pharmacology*, 56 (6), p. 600-612.

Lavorini, F., Fontana, G., Postolesi, M., 2006. Drug delivery to the lungs – effects of spacer devices. *European respiratory disease* [online]. Available at: http://www.touchrespiratorydisease.com/, [accesed on: 12/08/2008] .

Macdonald, G., 2008. Injectables to drive growth in US drug delivery market to 2012. [online]. Available at: http://www.in-pharmatechnologist.com [accesed on 04/08/2008].

Machowski, W., Balachandran, W., 1998. Dispersion and transport of cohesive lactose powder using travelling wave field technique. *Powder Technology*, 99, p. 251-256.

Malyan, B., Balachandran, W., 2001. Sub-micron sized biological particle manipulation and characterization. *Journal of Electrostatics*, 51-52, p. 15-19.

Marjamäki, M., Virtanen, A., Moisio, M., Keskinen, J., 1999. Modification of electrical low pressure impactor for particles below 30 nm. *Journal of Aerosol Science*, 30, Suppl. 1, p. S393-S394.

Mazumder, M.K., Ware, R.E., Yokoyama, T., Rubin, B.J., Kamp, D., 1991. Measurement of particle size and electrostatic charge distribution on toners using E-SPART analyzer. *IEEE Transactions on Industry Application*, 27(4), p. 611-619.

Mazumder, M.K., Grable, N., Tang, Y., O'Connor, S., Sims, R.A., 1999. Real-time particle size and electrostatic charge distribution analysis and its applications to electrostatic processes. *Institute of Physics Conference Series,* No. 163.

Mazumder, M.K., Ware, R.E., 2000. Aerosol particle charge and size analyser, *United States Patent 4,633,714*.

Mie, G., 1908. Contributions to the optics of turbid media, particularly of colloidal metal solutions. *Annalen der Physic*, 25(3), 377-445.

Mishchenko, M.I., Travis, L.D., Lacis, A.A., 2006. Multiple scattering of light by particles. Radiative transfer and coherent backscattering. Cambridge: Cambridge University Press.

Mitchell, J.P., Nagel, M.W., 2004. Particle size analysis of aerosols from medicinal inhalers. *KONA Powder and Particle*, 22, p. 32-65.

Molina, M.J., Rowland, F.S., 1974. Stratospheric sink for chlorofluoromethanes: chlorine atom-catalyzed destruction of ozone. *Nature*, 249, p. 810-812.

Morton, D., Staniforth, J., 2006. Systemic pulmonary delivery: success through integrated formulation and device development. [online]. Available at: http://www.ondrugdelivery.com. [accessed on 04/08/2008].

Moyle, B.D., Hughes, J.F., 1984. Particle charging and absolute measurement of charge to mass ratio. *IEEE Transactions on Industry Applications*, IA-20(6), p. 1931-1635.

Murtomaa, M., Laine, E., 2000. Electrostatic measurements on lactose-glucose mixtures. *Journal of Electrostatics*, 48, p. 155-162.

Murtomaa, M., Ojanen, K., Laine, E., 2002. Effect of surface coverage of a glass pipe by small particles on the triboelectrification of glucose powder. *Journal of Electrostatics*, 54, p. 311-320.

Murtomaa, M., Harjuen, P., Mellin, V., Lehto, V.P., Laine, E., 2002. Effect of amorphicity on the triboelectrification of lactose powder. *Journal of Electrostatics*, 56, p. 103-110.

Murtomaa, M., Mellin, V., Harjunen, P., Lankinen T., Laine, E., Lehto, V., 2004. Effect of particle morphology on the triboelectrification in dry powders inhalers. *International Journal of Pharmaceutics*, 282, p. 107-114.

Murtomaa, M., Pekkala, P., Kalliohaka, T., Paasi, J., 2005. A device for aerosol charge measurement and sampling. *Journal of Electrostatics*, 63, p. 571-575.

Naqwi, A., Ziema, M., 1992. Extended phase Doppler anemometerfor sizing particles smaller than 10 μm. *Journal of Aerosol Science*, 23, p. 613-621.

National Ignition & Photon Science, 2008. Lawrence Livermore National Laboratory, University of California, USA. How Lasers work, [online]. Available at: https://lasers.llnl.gov/education/. [accessed on 04/05/2008].

Noakes, T., 2002. Medical aerosol propellants. *Journal of Fluorine Chemistry*, 118, p. 35-45.

Olympus Corporation, 2008. Fluoview resource center, Japan. Helium-Neon Lasers, [online]. Available at: http://www.olympusfluoview.com. [accessed on 04/05/2008].

Pawankar, R., Baena-Cagnani, C.E., Bousquet, J., Canonica, G.W., Cruz, A., Kaliner, M.A., Lanier, B.Q., 2008. State of World Allergy Report 2008: Allergy and Chronic Respiratory Diseases. *World Allergy Organization Journal*, 1(6), Supplement S1-S3.

Peart, J., Byron, P.R., 1999. Electrostatic Properties of Metered Dose Inhalers. Proceedings of the10th International Conference on Electrostatics, held at: Cambridge, United Kingdom, 28-31 March 1999, p. 77-80.

Pedersen, S., 1996. Inhalers and nebulizers: which to choose and why. *Respiratory Medicine*, 90, p. 69-77.

Philip, V.A., Mehta, R.C., DeLuca, P.P., Mazumder, M.K., 1997. Electrostatic charge and particle size analysis of poly (D, L-lactide-co-glycolide) microspheres formulated for dry powder aerosols. *Particulate Science and Technology*, 15, p.245–261.

Philip, V.A., Mehta, R.C., DeLuca, P.P., Mazumder, M.K., 1997. E-SPART Analysis of Poly (D, L-lactide-coglycolide) microspheres formulated for dry powder aerosols. *Particulate Science and Technology*, 15, p. 303–316.

Pitcairn, G.R., Hooper, G., Luria, X., Rivero, X., Newman, S.P., 1997. A scintigraphic study to evaluate the deposition patterns of a novel antiasthma drug inhaled from the Cyclohaler dry powder inhaler. *Advanced Drug Delivery Reviews*, 26, p. 59 –67.

Psivida Corp., 2008. News. [on line]. Available at http://www.psivida.com/ [accessed on 04/08/2008].

Qiu, H-H., Jia, W., Hsu, C.T., Sommerfeld, M., 2000. High accuracy optical particle sizing in Phase Doppler Anemometry. *Measurement Science and Technology*, 11, p. 142-151.

Saini, D., Gunamgari, J., Zulaloglu, C., Sims, A., Mazumder, M.K., 2004. Effect of electrostatic charge and size distributions on respirable aerosol deposition in lung model. Industry Application Conference, 39th IAS Annual Meeting, Vol. 2, 3-7 October 2004, p. 948-952.

Saladin, K.S., 2007. Anatomy and physiology: The unity of form and function, 4th edition. New York: McGraw-Hill international edition.

Seeley et al., 2006. Anatomy and Physiology, 7th edition. New York: McGraw-Hill.

Smith, I.J., Parry-Billings, M., 2003. The inhalers of the future? A review of dry powder devices on the market today. *Pulmonary Pharmacology & Therapeutics*, 16, 79-95.

Staniforth, J.N., Rees, J.E., 1981. Powder mixing by tribolectrification. Powder Technology 30, p.255–256.

Taylor, D.M., Secker, P.E., 1994. Industrial electrostatics – fundamentals and measurements. Exeter, United Kingdom: Research Studies Press Ltd.

Taylor, D.M., 2001. Measuring techniques for electrostatics. *Journal of Electrostatics*, 51-52, p. 502-508.

Terzano, C., 2001. Pressurized Metered Dose Inhalers and Add-on Devices. *Pulmonary Pharmacology & Therapeutics*, 14, p. 351-366.

Tropea, C., Xu, T-H., Onofri, F., Gréhan, G., Haugen, P., Stieglmeier, M., 1996. Dual-mode Phase Doppler Anemometer. *Particle & Particle Systems Characterization*, 13, p. 165-170.

United Nations Environment Programme, 2000. Montreal Protocol on substances that deplete the ozone layer, [online]. Available at: http://www.unep.org/ozone [accesed on 18/07/2008].

USP 28-NF 23, 2005. Chapter 601 - Physical tests and determinations: Aerosols. *United States Pharmacopeia*, Rockville, Maryland, USA, Available at: http://www.usp.org/ [accesed on 10/07/2008].

Vanbever, R., 2005. Performance-driven, pulmonary delivery of systemically acting drugs. *Drug Discovery Today: Technologies*, 2(1), p. 39-46.

Virtanen, A., Marjamäki, M., Ristimäki, J., Keskinen, J., 2001. Fine particle losses in electrical low-pressure impactor. *Journal of Aerosol Science*, 32, p. 389-401.

Waldman, G., 1983. Introduction to light. The physics of light, vision and color. Englewood Cliffs: Prentice-hall, Inc.

Webb, C.E., Jones, J.D.C., 2004. Handbook of laser technology and applications. Volume III: Applications. London: Taylor & Francis.

Wilson, I.B., 1947. The deposition of charged particles in tubes with reference to the retention of therapeutic aerosols in the human lung. *Journal of Colloid and Interface Science*, 2, p. 271–276.

World Health Organization Regional Office for Europe. 2007. *Prevalence of asthma and allergies in children*, International Study of Asthma and Allergies in Childhood, Fact Sheet: 3.1, [online]. Available at: http://www.euro.who.int, [accessed on 15/07/2008].

Xu, G.B., Yu, C.P., 1985. Theoretical Lung Deposition of Hygroscopic NaCl aerosols. *Aerosol Science and Technology*, 4, p. 455-461.

Young, P.M., Traini, D., Coates, M., Chan, H.K., 2007. Recent advances in understanding the influence of composite-formulation properties on the performance of dry powder inhalers. *Physica B*, 394, p. 315-319.

Yu, C.P., Chandra, K., 1977. Precipitation of submicron charged particles in human lung airways. *Bulletin of Mathematical Biology*, 39, p. 471-478.

Yurteri, C.U., Mazumder, M.K., Grable, N., Ahuja, G., Trigwell, S., Biris, A.S., Sharma, R., Sims, R.A. 2002. Electrostatic effects on dispersion, transport, and deposition of fine pharmaceutical powders: Development of an experimental method for quantitative analysis. *Particle Science and Technology*, 20, p.59–79.

Zhao, H., Castle, G.S.P., Inculet, I.I., Bailey, A.G., 2000. Bipolar charging in polydisperse polymer powders in industrial processes. *IEEE Transactions on Industry Application*, p. 835-841.

Zhao, H., Castle, G.S.P., Inculet, I.I., 2002. The measurement of bipolar charge in polydisperse powders using a vertical array of Faraday pail sensors. *Journal of Electrostatics*, 55, p. 261-278.

Zhu, K., Tan, R.B.H., Ng, W.K., Shen, S., Zhou, Q., Heng, P.W.S., 2008. Analysis of the influence of relative humidity on the moisture absorption of particles and the aerosolization process in a dry powder inhaler. *Journal of Aerosol Science*, 39, p. 510-524.